Fiber Optic Sensors for PEM Fuel Cells

by

Nigel David
B.Sc., Simon Fraser University, 2004
M.Sc., Simon Fraser University, 2007

A Dissertation Submitted in Partial Fulfillment of the
Requirements for the Degree of

DOCTOR OF PHILOSOPHY

in the Department of Mechanical Engineering

Fiber Optic Sensors for PEM Fuel Cells

by

Nigel David

B.Sc., Simon Fraser University, 2004

M.Sc., Simon Fraser University, 2007

Supervisory Committee

Dr. Peter Wild, Co-supervisor

(Department of Mechanical Engineering)

Dr. Ned Djilali, Co-supervisor

(Department of Mechanical Engineering)

Dr. David Sinton, Departmental Member

(Department of Mechanical Engineering)

Dr. Tom Fyles, Outside Member

(Department of Chemistry)

Supervisory Committee

Dr. Peter Wild, Co-supervisor

(Department of Mechanical Engineering)

Dr. Ned Djilali, Co-supervisor

(Department of Mechanical Engineering)

Dr. David Sinton, Departmental Member

(Department of Mechanical Engineering)

Dr. Tom Fyles, Outside Member

(Department of Chemistry)

ABSTRACT

Fibre-optic sensing techniques for application in polymer electrolyte fuel cells (PEMFC) are presented in this thesis. Temperature, relative humidity (RH) and air-water two-phase flow sensors are developed and demonstrated based on optical fibre Bragg gratings (FBG). Bragg gratings offer the following characteristics that warrant their development for application in PEMFCs: small size, environmental compatibility and the possibility of multiplexed multi-parameter sensing. Contributions of this work are in novel sensor development and implementation strategies. Important installation design considerations include the sensor proximity to the catalyst layer, sensor strain relief and minimal bending of the fibre. With these considerations, the dynamic and steady-state performance of FBG temperature sensors distributed throughout the flow-field of a single cell PEMFC was validated with a co-located micro-thermocouple. In the development of FBGs for *in situ* measurement of relative humidity, a polyimide-coated FBG based RH sensor is presented with significantly improved response time and sensitivity over previously reported designs. The RH inside a PEMFC under transient operating conditions is monitored. Step increases in current induce significantly larger increases in RH near the outlet than near the inlet of the cell, and associated transients within the fuel cell are found on a time scale approaching the sensor response time. Finally, to complete the suite of FBG sensors for water management in PEMFCs, an evanescent field based FBG sensor embedded in a microchannel for the measurement of two-phase flow dynamics is presented. Using high speed video for validation, it is established that the novel sensor enables the measurement of droplet average velocity and size in flow regimes representative of an operating fuel cell.

Contents

List of Tables

List of Figures

Acknowledgements

First and foremost I would like to thank my supervisors, Dr. Peter Wild and Dr. Ned Djilali, for their guidance and support throughout this research. Their technical expertise in the fields of sensor development and fuel cells, respectively, combined to make this project a continuing success. I am also very appreciative of their understanding of my responsibilities as a father while being a graduate student.

I would also like to thank my coworkers. Without their help this work would not have been nearly as productive and enjoyable as it was. I would like to thank Dr. Chris Dennison, who, as Peter's pioneering grad student in fibre optics, introduced me to the exciting research field that was entirely new to me. When not discussing sensor design with Chris, we could discuss other important matters like hunting and fishing. Other past and present members of Dr. Wild's sensing group with whom I have shared in the pleasures and pitfalls of sensor development work include Dr. Dustin Olender, David Singlehurst, Juan Botero, Devan Bouchard and Chris Bueley. From Dr. Djilali's fuel cell research group, I would like to thank Dr. Slava Berjnov, Dr. Amy Bazylak, Dr. Jingwei Hu and T.C. Wu. Many thanks also goes to Dr. David Sinton and members of his microfluidics group for access to their equipment and expertise.

I would like to thank Sue Walton and Peggy White from the Institute for Integrated Energy Systems (IESVic) office. During my years of studies at IESVic, Sue and Peggy have provided constant support to our research groups creating an environment for them to thrive.

Finally, I would like to thank my family for their love and support during this seemingly endless journey of school.

Dedication

This thesis is dedicated to my mother and stepfather; without their help it simply would not have been possible.

Chapter 1

Introduction

This dissertation describes the development and implementation of optical in-fibre Bragg grating (FBG) sensors for monitoring temperature, relative humidity, and the liquid water phase in polymer electrolyte fuel cells (PEMFCs). In PEMFCs, these coupled parameters have significant impact on performance and degradation. For optimal performance it is well understood that a water balance must be maintained, which ensures good hydration of the membrane without flooding the electrodes [7–10]. Furthermore, accumulation of liquid water in the electrodes can initiate and exacerbate degradation of the membrane electrode assembly (MEA), which functions as the core of a PEMFC. Currently there is a lack of diagnostics tools for the parameters of interest in water management, particularly tools that can provide non-invasive distributed measurements.

Fibre optics and, in particular, FBG sensors, are well suited to *in situ* monitoring of PEMFCs due to their small size, inherent electrochemical resistance and the possibility of multiplexing several sensors on a single fibre. The FBG-based sensors described in this thesis rely on different underlying mechanisms that span the thermal, mechanical and optical properties of the FBGs. These mechanisms are described in Chapter 2 of this thesis. Chapter 3 gives a summary of the experiments and results that were obtained in the development of the FBG sensors for temperature, RH and liquid water. A more detailed account of the research undertaken for this thesis is provided in Appendices A-D, which comprise published and submitted manuscripts that have resulted from this work.

This introductory chapter provides context for the measurements and sensor development, beginning with an overview of PEM fuel cells and the associated water management issues.

1.1 Overview of PEMFCs and Water Management Issues

PEM fuel cells have been seen for decades as a promising source of clean power for stationary and transportation applications. Delay in their widespread usage can be attributed to high materials costs (e.g., membranes and platinum catalyst), lack of hydrogen infrastructure, and inadequate performance and durability. Improvements in performance and durability, particularly in relation to water management issues, continues to be an area of active research within industry and academia.

The operation of a fuel cell depends on the optimized regulation of the flow of reactants, products, heat, and charged species in conjunction with reaction kinetics. These strongly coupled processes take place over a large range of length and time scales and in structures with very different characteristics. These include micro-channels, porous electrode layers, and polymer electrolytes. See Figure1.1.

There are various structures and transport processes that form the basis of PEMFC operation [11]. The anode and cathode micro-channels carry hydrogen and oxygen gases, respectively. The micro-channels are typically grooved into graphite plates,

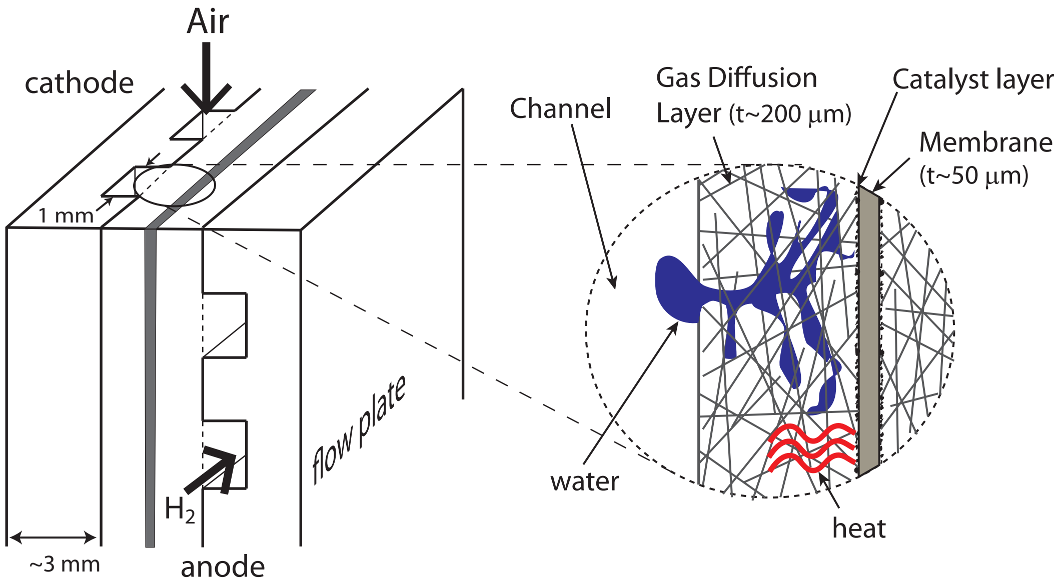

Figure 1.1: Schematic of a PEMFC showing the main components and their relative scales.

which offer good mechanical, thermal and electrical properties. The gas diffusion layers (GDL) consist of an anisotropic fibrous structure, typically in the form of carbon paper, that allows distribution of the reactant gases to the catalyst layers. In addition to gas distribution, the GDLs and the graphite bipolar plates transport electrons. Simultaneously, proton transport takes place across the membrane between the catalyst layers, byproduct heat is transferred through the GDL, and evaporation and condensation of water takes place.

The byproduct water and heat created from the electrochemical operation of a PEMFC (Figure 1.1) can impact negatively on performance if not properly managed. MEA flooding and membrane drying are two of the main performance degradation mechanisms that occur when water management is not adequate. A thorough review of these phenomena, their causes, characterization methods, and mitigation strategies, is given in [3, 9, 11].

The effects of water management issues on cell performance are depicted schematically on the polarization curve shown in Figure 1.2. In general, optimum cell performance is achieved when the cell temperature is held at ∼80°C and the membrane is well hydrated. This combination ensures adequate reaction kinetics (i.e., low activation losses) and good proton conductivity (i.e., low ohmic losses) [12].

At higher currents, or when local water and heat management is inadequate, water condensation can lead to "flooding" within the GDL and catalyst layer. Flooding of these structures, typically occurring on the cathode side, inhibits the gas from reaching the reaction sites within the catalyst layer and results in transport or concentration losses. See Figure 1.2.

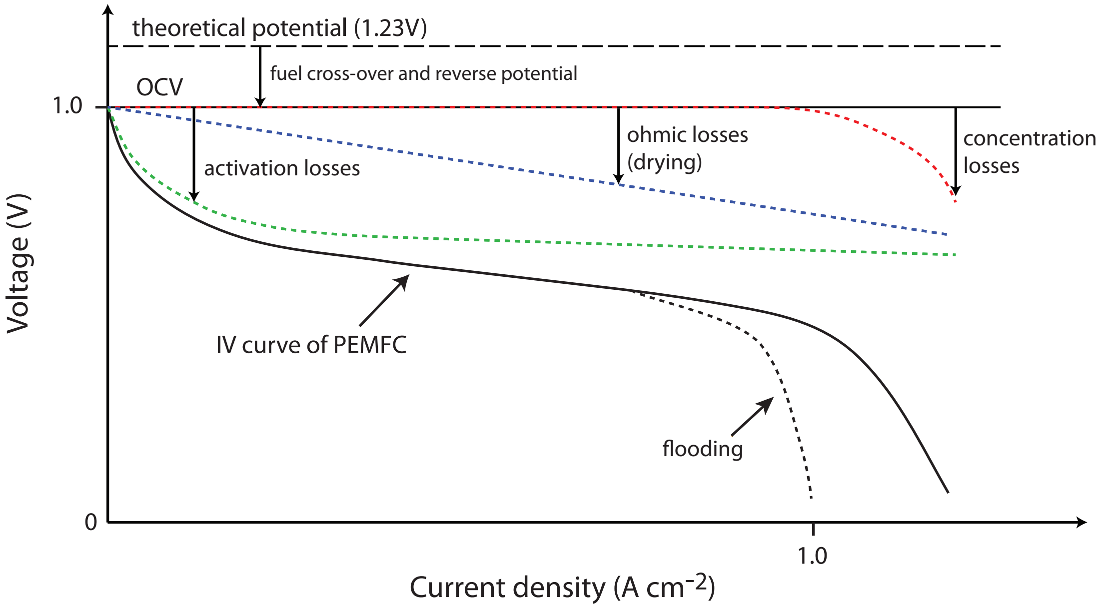

Figure 1.2: Typical polarization curve for a PEMFC showing the different loss mechanisms.

Liquid water and the resulting "two phase-flow" often propagate from the microstructure of the GDL to the gas channels where small droplets join together to form "plugs" of water, blocking the entire flow channel. Due to local reactant starvation and the associated transient pressure surges, water plugs can cause large and sudden perturbations in the voltage of the cell. Such voltage perturbations are operationally undesirable and can induce degradation mechanisms. *In situ* techniques for the localized detection of liquid water are likely to be part of mitigation strategies for flooding.

Conversely, membrane dehydration is caused by excessive water removal and/or high local temperatures. This leads to an increase in ohmic losses since the ionic conductivity of the membrane is strongly dependent on its hydration level, or relative humidity (RH) of the gas [7].

Increased ohmic losses also occur in regions where membrane thinning is present. Membrane thinning is thought to be caused by manufacturing defects or chemical attack. A region of thinner membrane will have a lower through-plane ionic resistance, promoting higher current densities, and increased ohmic heating in that region. This mechanism results in a local area of high temperature known as a hotspot. If left unchecked, the temperature at the hotspot can reach the glass transition temperature of the membrane material (∼135°C), causing irreversible damage to the membrane in the form of pinholes.

In current fuel cell stack technology, the regulation and control of these complex processes is based on elaborate design and material features (*e.g.* flow-field design and hydrophobic GDLs) in conjunction with water management strategies. Water management strategies rely on *global* performance indicators and bulk measurements (*e.g.* stack voltage and current, outlet relative humidity and temperature, and pressure drop), which are relatively insensitive to *local* changes in conditions that are believed to be the precursors to performance drop and degradation. *In situ* measurements of these local changes in the parameters that affect water management are essential for better understanding of the associated mechanisms and, ultimately, improved stack performance.

1.2 Overview of Diagnostic Techniques For Water Management in PEMFCs

The inability of bulk characterization methods such as polarization curve, electrochemical impedance spectroscopy, membrane resistance and pressure drop to spatially resolve phenomena associated with water management has led researchers to develop new techniques. The techniques that have been used to measure temperature, RH, and the presence of liquid water inside operating fuel cells, either by visualization, or with sensors are reviewed here with emphasis on their suitability for application to PEMFC stacks. The limitations of such techniques, which are also discussed, served to motivate and guide the FBG sensor techniques developed in the course of this thesis work.

1.2.1 *In situ* temperature measurement techniques

It has been noted that the temperature inside a PEM fuel cell impacts its performance. The temperature has an effect on electrochemical activation of the reactants, and the relative humidity in the flow field, which affects membrane drying and flooding. If the temperature of the membrane becomes too high at a hot spot, excessive degeneration and potential failure of the MEA can occur. In addition to information relevant to water management and failure diagnostics, the local determination of temperature throughout the cell can provide information on the distribution of other parameters such as current density and relative humidity.

Temperature measurements inside an operating PEMFC have been made using a variety of techniques including infra red camera [1], thermocouples [13–17], resistance temperature detectors (RTDs) [18–27], bandgap sensor [2], optical fibre sensors [28–32], and tuneable laser diode absorption spectroscopy [33–36].

The infrared imaging technique requires a window for optical access and, therefore is clearly not feasible in a commercial FC. The infrared imaging technique of Wang *et al.* [1] was nonetheless important in demonstrating the spatially resolved distribution of temperature in an operating fuel cell. The most notable feature in their thermal images were the gradients of up to 5°C across the active area of the small single cell. See Figure 1.3. The temperature gradients were attributed to current density gradients caused by self humidification of the membrane, which increased from inlet to outlet.

Using miniaturized electronic sensors (thermocouples, RTDs, and silicon bandgap) researchers have resolved in-plane temperature gradients in the flow channels [15], on the landings [13], between the catalyst layer and the GDL [17], and within the membrane [18]. Thermocouples have the advantage of off-the-shelf availability and small size ($\sim$250 μm). Thermocouples have good temperature resolution capabilities and, as a result of their size, have a short response time.

Micro-scale RTDs have the added advantage over thermocouples of the possibility of thin film device fabrication techniques, which is good for mass production of these sensors. These thin film RTD sensors are inherently thin and can be as small as $\sim$100 μm on a side. They are typically surface mounted and, therefore, take on the temperature of the substrate on to which they are mounted. For this reason, they are well suited for experimental measurements within membranes, as shown by He *et al.* [18]. Also for this reason, however, they are not well suited for the measurement of gas temperature within the flow channels of a fuel cell.

A silicon bandgap temperature sensor was used by Hinds *et al.* [37] to measure the gas temperature in a diverted flow channel just outside the active area of a PEMFC.

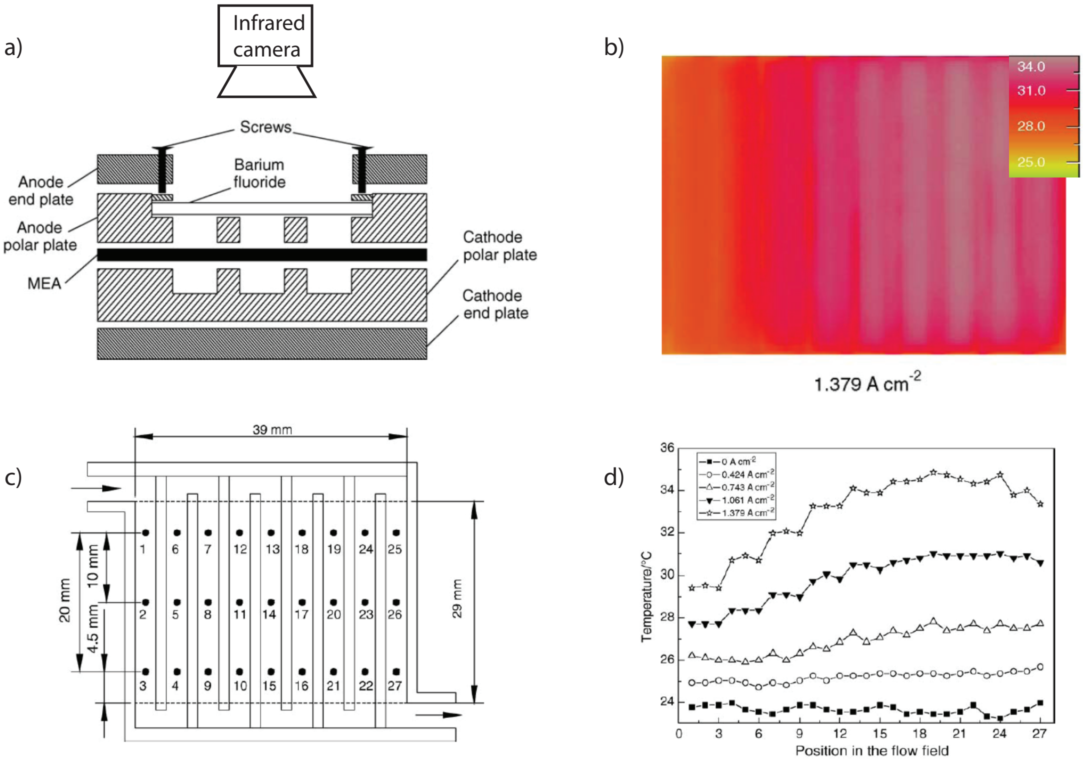

Figure 1.3: (a) Schematic of test cell for infrared imaging technique used by Wang *et al.* to measure the temperature profile across the active area. (b) Infrared image of active area during high current operation. (c)Detailed drawing of flow field of the PEMFC. (d) Temperature plotted against location along the flow field for different current densities. Reproduced with permission from the Journal of Power Sources [1].

This sensor, which was part of the commercial RH sensor they were using for *in situ* RH measurements discussed in the following section, yielded good results, but was too large to be located within the active area of a PEMFC. Furthermore, these sensors cannot be multiplexed.

In general, the limitations of electronic sensors for application to PEMFC stacks lie in their lack of robustness, both mechanically and electrochemically and in their inability to be multiplexed for spatially resolve distributed measurements. With the small size that is necessary for minimal impact on performance, the wire leads become delicate and the sensors prone to failure [13]. Careful consideration of the wire materials is necessary since the environment within a fuel cell promotes corrosion due to the constant presence of humidity and electrochemical activity. Separate installation of many sensors, each with at least two leads, would be necessary to obtain any sort of spatially resolved measurements. This would not only require modifications to the fuel cell, but an interrogation system with sufficient separate channels for each sensor.

Optical approaches that have been used for temperature measurement include tuneable diode laser absorption spectroscopy (TDLAS) and optical fibre sensors. TDLAS was first demonstrated in PEMFCs by Basu *et al.* [33]. The technique is based on the absorption of light emitted from a tuneable laser as it passes along the length of a flow channel. The spectrum of the laser diode can be tuned to the absorption band of water vapour or other species. The spectrum of light that is detected on the side opposite the laser can give information on the temperature and partial pressure of the gas species within the channel. The technique is limited in that it is only operational if the channel is free of liquid water to achieve a line-of-sight between the laser and the detector. Other drawbacks to this technique are the low temperature resolution (±2°C) and that the measurements are based on an average over the channel length, which yield limited spatial resolution.

Optical fibre sensors reported for *in situ* temperature measurements include phosphorescence based sensors [28], fluorescence based sensors [29], and as presented in this thesis, FBG sensors [31]. The former two sensors rely on the temperature dependent decay of light emitted from a photo-luminescent substance on the distal end of an optical fibre. Due to the inherent small size of optical fibres, these techniques have good spatial resolution potential. The main drawback of these fibre-end techniques, as compared to FBGs, is the inability to multiplex several sensors on a single fibre. FBG sensors are wavelength encoded, which means they can be multiplexed. The main characteristics of these optical techniques, and the others that have been used for in

Table 1.1: Summary of the *in situ* temperature techniques in PEMFCs

	Spatial resolution	**Temporal resolution**	**Temperature resolution**	**Cost**	**Merits**	**Drawbacks**
Thermocouples	250 μm [13]	Good	±0.19°C [15]	Low	Small size; Commercially available	Non-multiplexing (many wires needed for distributed sensing in stack); Trade off: robustness vs. size; May be affected by e.m. noise
RTDs	110 μm [19]	Good	±0.3°C [27]	Medium	Thin; Commercially available	Non-multiplexing; Substrate may block ions for membrane measurements
TDLAS	Low (average over channel length)	4 s [35]	±2°C in 80-100°C [35]	High	Allows detection of species; Does not disturb fuel operation	Cannot be used with condensation in channel; Complex optical alignment; Require complex signal processing or reference signal;
fibre optics	700 μm (Phosph) [30]; 1 mm (FBG) [31]	Good	±0.2°C [32]	High (Equipment)	Multiplexing (FBG); Immune to e.m. noise; Chemically inert	Brittle ; FBGs require careful strain isolation

situ temperature measurements are summarized in Table 1.1 for easy comparison.

1.2.2 *In situ* relative humidity measurement techniques

It has been mentioned that the ionic conductivity of a polymer electrolyte membrane is strongly dependent on its water content [7]. Attempts to regulate the hydration level of the membrane, and minimize ohmic losses, are made by controlling the inlet RH of the gas streams and the fuel cell temperature. During cell operation, however, a combination of water generation, water transport phenomena, and temperature gradients cause inhomogeneities in RH and membrane water content. These inhomogeneities are likely to cause localized concentration and ohmic losses within the fuel cell. *In situ* distributed measurement of RH is necessary to quantify these losses and improve cell design and mitigation strategies. Prior to a discussion of the *in situ* RH measurement techniques that have been demonstrated, some background on the physical parameter of RH is given.

The most commonly used units for humidity measurement are relative humidity

(RH), dew point and parts per million. Dew point is the temperature (above 0 °C) at which the water vapour in a gas condenses into liquid. Dew point depends on the pressure of the gas, but is independent of temperature and is therefore defined as an absolute humidity measurement. Part per million is also an absolute measurement, and represents the water vapour content in a given volume of gas. Absolute humidity measurement is typically used for trace amounts of moisture, whereas RH is most common for higher humidity ranges, such as would often be the case in a PEMFC.

Most humidity sensors that could potentially be installed into a PEMFC are RH sensors [38]. RH is the ratio of the partial pressure of vapour to saturated vapour pressure: [39].

$$RH = \frac{P_{H_2O}}{P^*_{H_2O}(T)} \times 100\% \tag{1.1}$$

Where P_{H_2O} is the partial pressure of water vapour, and $P^*_{H_2O}$ is the saturation pressure of water vapour. The saturation pressure is a function of pressure and temperature and, therefore, so is the relative humidity. There are several empirical relations for the saturation pressure of water vapour. A relatively simple relation that provides a reasonable balance between usability and accuracy is given by [8],

$$P^*_{H_2O}(T) = -2846.4[\mathrm{Pa}] + 411.24[\mathrm{Pa}^\circ\mathrm{C}^{-1}]\mathrm{T} - 10.554[\mathrm{Pa}^\circ\mathrm{C}^{-2}]\mathrm{T}^2 + 0.16636[\mathrm{Pa}^\circ\mathrm{C}^{-3}]\mathrm{T}^3, \tag{1.2}$$

where T and P are the temperature and pressure of the water vapour, expressed in degrees Celsius, and Pascals, respectively. This curve fit is accurate from 15°C to 100°C.

The electronic sensors used for *in situ* RH measurements have all been capacitive. The most successful demonstration of one was reported by Hinds *et al.* [37] using small commercially available capacitive RH sensors (Sensirion, Inc., SHT75). These combined RH and temperature sensors were installed around the outside of the flow-fields of the anode and cathode plates of a single cell PEMFC (Figure 1.4a and b). Steady state results for different temperatures and inlet humidities were presented. Representative results for the cathode dew point as a function of position along the flow-field side for under-humidified inlet gases are shown in shown in Figure 1.4c. From this plot, a positive gradient from inlet to outlet is evident, becoming more pronounced with increasing current density. The temperature measurements yielded the same positive gradients. These results support the mechanism of self humidification causing current density gradients proposed by Wang *et al.*.

The transient RH measurements made by Hinds *et al.* provided useful information on the dynamics of the RH in the flow-field. Measurements acquired during a sudden change in cell current showed RH transients on the timescale of the SHT75 response time ($\tau_{63} = 8s$) [40]. This information serves to guide the use of other sensors, putting an upper limit on the response time necessary for meaningful measurements.

The main limitations of the miniature capacitive RH sensor from Sensirion is their size, inability to recover quickly from saturation, and inability to multiplex. Despite being small, the sensor footprint of 3 x 7 mm [40] prohibits their installation *within* the flow-field for truly localized measurements and requires significant modification to the fuel cell plate.

Significantly smaller capacitive RH sensors based on MEMS fabrication techniques were developed by Lee *et al.* specifically for in situ measurements in PEMFCs [19,20, 22–24]. Despite the potential of minimally invasive sensors, their *in situ* performance was either drastically reduced upon installation in the PEMFC, or not reported.

An electrochemical technique for failure diagnostics using micro-sensing electrodes was reported by Herrera *et al.* [41]. The technique is based on the use of 50μm platinum wire sensing electrodes located at the inlet and outlet of the cell. The potentials of the reference electrodes were correlated with relative humidity and the onset of flooding of the fuel cell. Despite the clear benefit presented in this technique for detecting flooding, drying and low fuel stoichiometry, calibration specifications of the response of the electrodes to RH was not provided, and will likely depend on the electrode location within the cell.

Rather than installing micro-sensors in the PEMFC, Mench *et al.* and Partridge *et al.* used micro-tubes to extract small samples of gas for analysis by chromatography and mass spectrometry, respectively [42, 43]. These techniques were used to measure water vapour concentration at multiple locations in the serpentine flow filed of an operating PEMFC. The authors suggest that in combination with spatially resolved temperature measurements, the transient RH distributions could be measured, however, data for such measurements were not presented. The main drawbacks for these techniques are the need for co-located temperature sensors and, in the case of the work of Partridge *et al.* [43], a prohibitively expensive mass spectrometer.

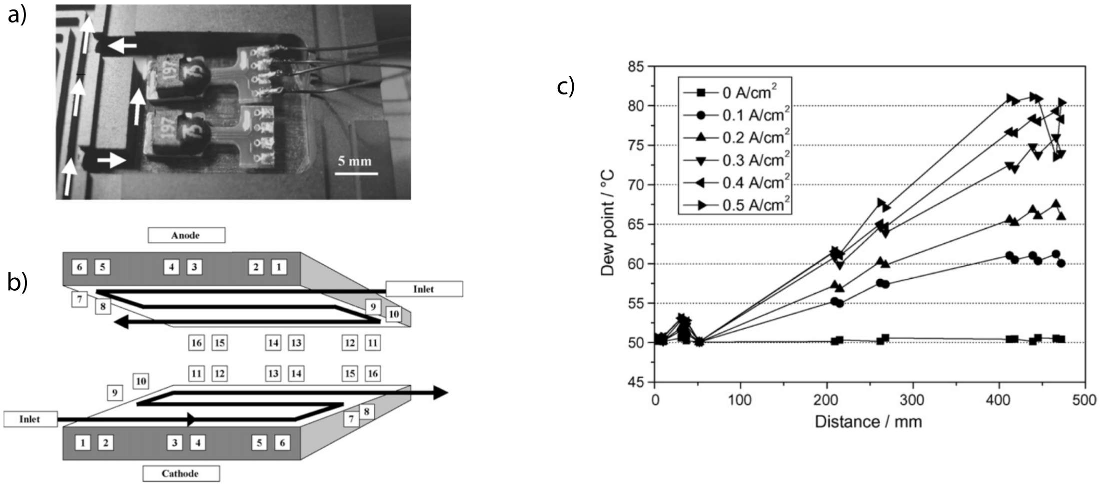

Figure 1.4: (a) Miniature capacitive RH sensors (Sensirion, Inc.) used by Hinds *et al.* for *in situ* measurements. (b) Diagram of single cell showing sensor locations. (b) Results from cathode side showing positive gradient in RH from inlet to outlet. Reproduced with permission from the Journal of Power Sources [2]

Optical techniques reported for *in situ* RH measurement include TDLAS and fibre-optics. As mentioned previously TDLAS can be used to measure the partial pressure of water vapour as well as temperature. With this technique, Basu *et al.* claimed the first simultaneous non-intrusive measurements of the partial pressure of water vapour and temperature inside a PEMFC under steady state and transient operations [33]. Two channels in the serpentine flow path of a collector plate were extended to allow optical access into the test cell. One sensing channel was located near the inlet and one was located near the outlet. The partial pressure was measured to increase linearly with cell current and was higher towards the outlet. These measurements agreed with the calculated production of water at the cathode side and were not significantly affected by electro-osmotic drag.

The main drawbacks of TDLAS for RH measurements lie again in its temperature resolution and spatial resolution. To obtain RH from the partial pressure measurements, conversion is made using Equation 1.1, which contains the temperature dependent saturation pressure of water vapour. Examining Equations 1.1 and 1.2, it is clear that limitations in temperature resolution put limitations on the RH resolution of the technique. Also, locally resolved measurements are not possible, as the measurements are taken as an average over the channel.

Using a U-bent optical fibre coated with a silica-gel solution Tao *et al.* [30] demonstrated an RH sensor based on the principle of spectroscopic absorption. The reported range of measurement and response time at 90% of the total signal of this sensor were 4-95 %RH and 3 minutes, respectively. This sensor response is slow compared to the transient RH measurements made by Hinds *et al.* [2]. In addition, the U-bent design constrains spatial requirements and multiplexing is not possible.

A fibre optic RH sensor with a significantly faster response (10s) than the one reported by Tao *et al.* [30] was demonstrated by David *et al.* for *in situ* measure-

Table 1.2: Summary of the *in situ* humidity measurement techniques in PEMFCs

	Spatial resolution	**Temporal resolution**	**Best RH resolution**	**Cost**	**Merits**	**Drawbacks**
Capacitive	100μm [19]	8 s (63%) [37]	±0.25%RH [19]	Medium	Small size (non-commercial); Easy to mass produce; Easy placement inside fuel cell	Non-multiplexing
TDLAS	Low (average over channel length)	4 s [35]	±2.5%RH [35]	Medium	Does not interfere with F.C. operation	Limited range (40-90%RH)
Fibre optics	1 mm (Length of FBG) [32]	10 s (90%) [32]	±2%RH [32]	High (Equipment)	Small size; Multiplexing possible; Immune to e.m. interference and corrosion	Brittle; Complex installation (strain isolation)
Reference electrode	High (50μm) [41]	not reported	not reported	Low	Commercial; Easy to instrument, Multi-parameter sensing	Location specific response, Non-multiplexing

ments [32]. In addition to having a short response time and good sensitivity, the sensor has the potential for multiplexing. This development and demonstration of this work is presented in detail in Appendix B and C. The main characteristics of the electrical and optical techniques that have been used for in situ RH measurements are summarized in Table 1.2 for easy comparison.

1.2.3 Liquid water detection in PEMFCs

As previously discussed in this chapter, electrode flooding and air-water two-phase flow in the gas channels are common during fuel cell operation and have been linked to a variety of performance and material degradation mechanisms. Due to the complex nature of these two-phase flow phenomena, *in situ* diagnostic tools are necessary to gain better understanding of the phenomena and to suggest effective mitigation strategies [3, 5, 44]. So far, various visualization techniques and pressure drop measurements have been used to detect liquid water in operating fuel cells, however, due to their limitations, there is still a need for spatially distributed information of the hydrodynamics within the flow channels of a commercial fuel cell [3].

Pressure drop measurements are typically made across the cathode flow plate of a PEMFC. The pressure drop across the flow field increases as liquid water builds up in the porous GDL and in the flow channels, impeding the flow of gas. Increasing pressure drop is, therefore, an indication of electrode flooding and two-phase flow. These measurements can be used as feedback for the control of operating parameters to mitigate flooding; however, pressure drop measurements typically lack the spatial resolution required to obtain distributed two-phase flow information [44]. Visualization techniques on the other hand generally offer good spatial resolution, which allows for accurate flow regime characterization; however, the results often depend on the specific materials used for the transparent plate, which are dissimilar to those in a typical graphite bipolar plate fuel cell.

Despite the limitations of pressure drop and visualization techniques, numerous *in situ* and *ex situ* experiments have been carried out using them. These experiments were recently reviewed by Anderson *et al.* [3]. Results from these studies highlighted the importance of flow maldistribution across the flow field and two-phase flow patterns within the channels for water management of PEMFCs. Knowledge of the common flow regimes (see Fig. 1.5) can help guide the design and placement of micro sensors such that they can be utilized for system control and for flow field development. For example, all of the flow regimes shown in Fig. 1.5 indicate liquid flow on the sidewalls of the channel, whether two-phase flow (slug flow, transition flow) or film flow (wavy stratified, stratified annular). These flow patterns suggest that a sensor located on the sidewall of a micro channel would be most useful. Such a sensor design could, potentially, differentiate between types of stratified flow adjacent to the sidewalls.

As mentioned, most techniques developed for liquid water detection in operat-

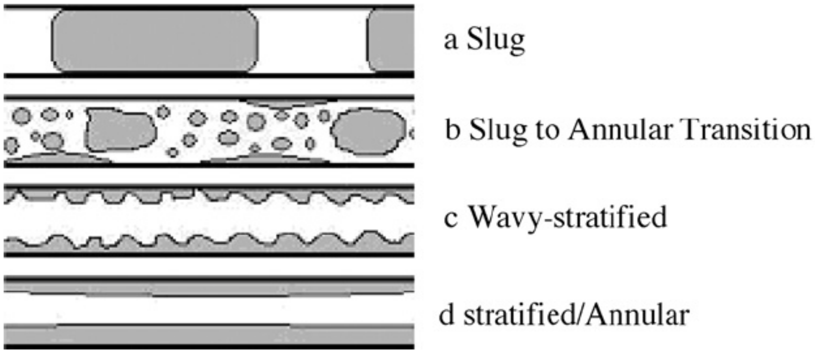

Figure 1.5: Flow patterns in PEM fuel cell operation. (a) slug flow, (b) transition flow from slug to annular, (c) wavy stratified flow, and (d) stratified annular flow. Reproduced with permission for the Journal of Power Sources [3].

ing PEMFCs have involved visualization techniques of varying degrees of complexity. These include optical imaging, X-ray imaging, magnetic resonance imaging and neutron imaging. These techniques were recently reviewed by Bazylak *et al.* [5]. Due to the need for optical access or a custom fuel cell design for the particular technique, none of the visualization techniques would be feasible on commercial PEMFC stacks; however, the information that visualization techniques can provide on the fundamentals of water transport through the micro-structures of a PEMFC is important.

Droplet formation on the surface of the GDL and water transport within the flow channels has become a key area of research that can guide sensor development. Real time optical imaging of these phenomena is routinely carried out using transparent cells, where a standard conductive collector plate has been replaced with a custom plate, usually made of plexiglass and metal. Studies using these cells have correlated local two-phase flow regimes with local current density and pressure drops. Some of the most striking correlations were made in a recent study by Dillet *et al.* [4]. Figure 1.6 shows two images of the flow-field of their test cell taken in sequence. This study clearly shows the existence of water slug flow in the flow channel and the consequences it has on the current density distribution across the cell. From the images they measured the average speed of the slugs to be 190 mms^{-1}, which is a useful benchmark for sensor development. Optical visualization techniques are limited to single cells, or the end cell of a stack where full optical access can be gained.

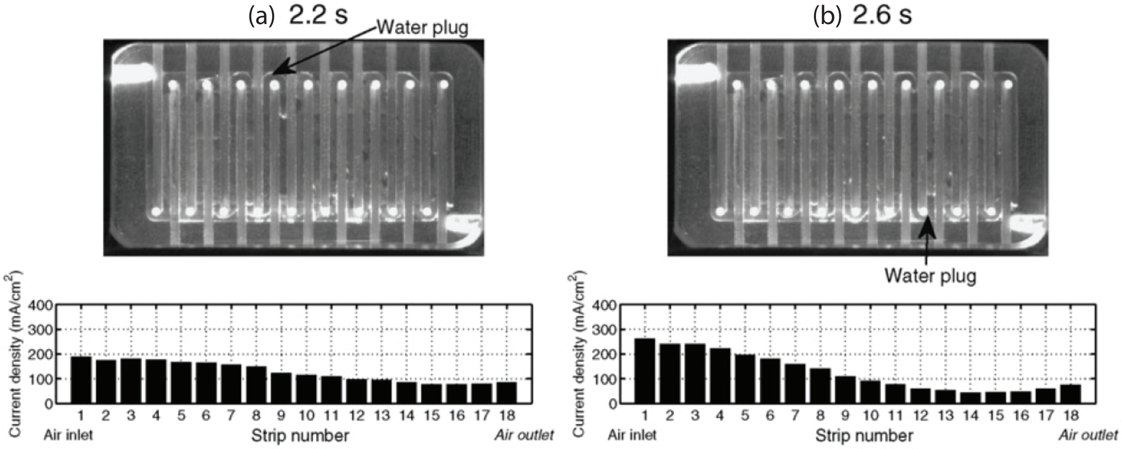

Figure 1.6: Sequence of flow-field images with corresponding voltage data showing the effect of a water plug. Reproduced with permission from the Journal of Power Sources [4].

The more advanced imaging techniques of magnetic resonance imaging, neutron imaging, and X-ray imaging have been used to resolve through-plane water distribution in the MEA [45–47]. Investigation of water generation, transport and accumulation in the micro-structures of the MEA, including the membrane, the micro-porous layer and the GDL, is critical to gaining understanding of flooding phenomena and, ultimately, water management. The impact of these imaging techniques on commercial stack design is likely limited because they require modified fuel cells, as well as costly and sophisticated large-scale equipment that is not widely available. However, for the development of novel micro-sensors, such as optical fibre sensors, that could potentially be embedded into these micro-structures, use of these advanced imaging techniques could prove essential for their validation. The spatial and temporal resolution capabilities of the visualization techniques suitable for use in a PEMFC are summarized in the table shown in Figure 1.7.

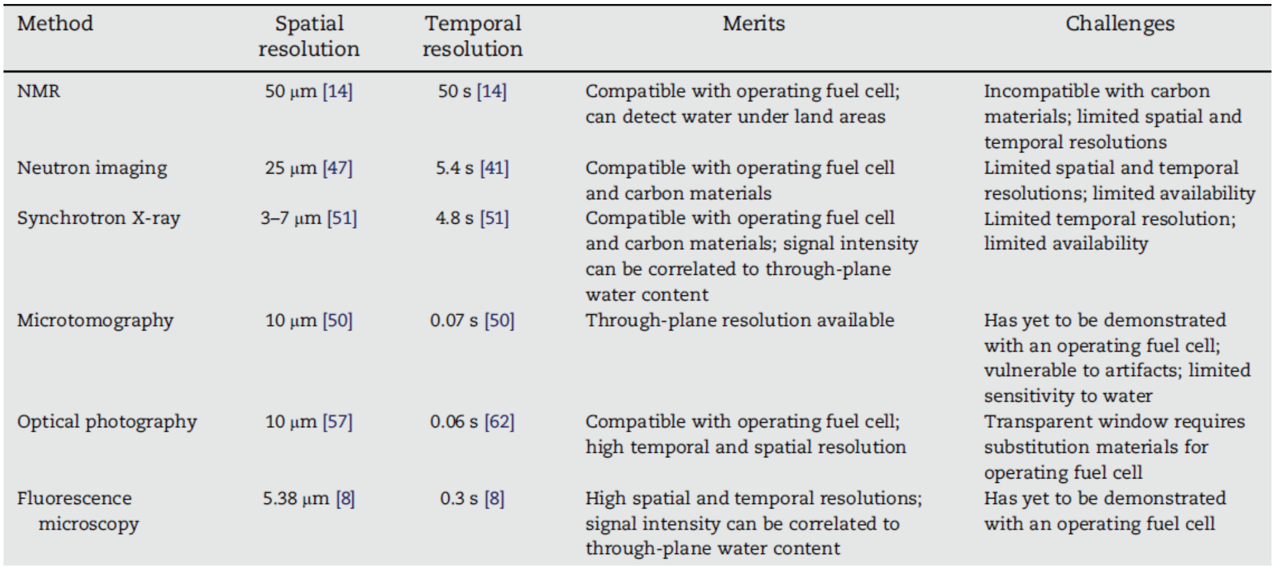

Method	Spatial resolution	Temporal resolution	Merits	Challenges
NMR	50 μm [14]	50 s [14]	Compatible with operating fuel cell; can detect water under land areas	Incompatible with carbon materials; limited spatial and temporal resolutions
Neutron imaging	25 μm [47]	5.4 s [41]	Compatible with operating fuel cell and carbon materials	Limited spatial and temporal resolutions; limited availability
Synchrotron X-ray	3–7 μm [51]	4.8 s [51]	Compatible with operating fuel cell and carbon materials; signal intensity can be correlated to through-plane water content	Limited temporal resolution; limited availability
Microtomography	10 μm [50]	0.07 s [50]	Through-plane resolution available	Has yet to be demonstrated with an operating fuel cell; vulnerable to artifacts; limited sensitivity to water
Optical photography	10 μm [57]	0.06 s [62]	Compatible with operating fuel cell; high temporal and spatial resolution	Transparent window requires substitution materials for operating fuel cell
Fluorescence microscopy	5.38 μm [8]	0.3 s [8]	High spatial and temporal resolutions; signal intensity can be correlated to through-plane water content	Has yet to be demonstrated with an operating fuel cell

Figure 1.7: Table of comparison of the various visualization techniques used for liquid water in PEMFCs. Reproduced from Bazylak *et al.* [5] with permission from the International Journal of Hydrogen Energy

Only a single micro-sensor for water measurement in a PEMFC flow-field has been reported to date. Conteau *et al.* [48] recently developed and demonstrated an electrochemical sensor for detecting water droplets within the flow channel of an emulation fuel cell. The sensor was based on an impedance measurement between two electrodes on either side of a graphite micro-channel. Simulated dynamic droplet conditions were created within the channel, and the sensor data was correlated with high-speed digital camera footage. The sensor proved capable of detecting the small and fast droplets that occur in real PEM fuel cells under operation.

As with the other electronic sensors discussed in the previous sections, the electrode based sensor developed by Conteau *et al.* will require particular attention to electrical isolation, which, inside a fuel cell can prove difficult due to the conductive materials. For distributed measurements using these sensors, multiplexing will require several electrically isolated leads, which poses another significant instrumentation challenge. As has been mentioned, many of the limitations of electronic sensor techniques can be overcome with the use of fibre optic sensors.

1.3 Fibre optic sensors

Fibre optic sensors have certain advantages which include immunity to electromagnetic interference and corrosion, lightweight, small size, high sensitivity, high bandwidth, and, in the case of Bragg gratings, ease of multiplexing for distributed measurements. These properties combine to make fibre optic sensors an attractive solution for in situ diagnostics relating to water management in PEMFCs. In the previous sections, the discussion of fibre optic sensors was limited to temperature and humidity sensors, as there have not been any reported techniques for *in situ* detection of liquid water using fibre optics. In addition to other optical fibre-based techniques for temperature and humidity, there are techniques for detection of phase (i.e., liquid or gas) and refractive index that could be implemented in PEMFCs. These techniques are surveyed in the following sections.

1.3.1 Temperature

For temperature, the fibre-end photoluminescence techniques [28,29] and fibre Bragg grating sensors [31,32] discussed above represent the most common types of fibre optic temperature sensors, and the progression towards multiplexing that FBGs can offer. Multiplexing is an attractive feature for distributed measurements in PEMFC stacks. Multiplexed FBG temperature sensors have been proven in similarly challenging environments such as those found in down-hole (oil and gas well) applications [49] and biomedical applications [50]. An additional benefit of the combined temperature sensitivity and multiplexing capability of FBGs is that the temperature compensation of sensors for other parameters can be done on a single fibre [32].

1.3.2 Humidity

The fibre optic techniques that have been demonstrated for humidity measurement in PEMFCs [30, 32] also represent a progression towards FBGs, which enable multiplexing and multi-parameter measurements. There are, however, several other optical fibre based sensors that have been reported for humidity. These were reviewed recently by Yeo *et al.* [51]. All of the sensors rely on the application of a sensing layer on to the optical fibre, and are categorized in terms of the basic sensing principles. The fibre optic humidity sensing principles include spectroscopic, evanescent wave, interferometric, and fibre Bragg gratings.

Spectroscopic based techniques typically rely on the deposition of a reagent on to the tip of an optical fibre. The sensitive layer on the tip of the fibre elicits a spectral response to humidity either by absorbing light or fluorescing in the presence of moisture. Despite being widely used for chemical sensing, the main drawback with spectroscopic humidity sensors is the lack of multiplexing capability that would be required for distributed sensing in a fuel and the slow response of the sensors reported in the literature ($\sim$2mins) [51].

Evanescent wave sensors operate by accessing the evanescent field that penetrates from the core into cladding of the fibre. Coatings that exhibit a change in refractive index in the presence of moisture can be applied to a region of exposed core to achieve a modulation in the transmitted or reflected power as a function of the surrounding RH. The use of such a configuration gives flexibility in terms of the interaction length, response time and distributed sensing capability [51].

Among the sensors reviewed by Yeo *et al.*, the polyimide-coated FBG stands out with a large reported measurement range (10-90% RH) [52] combined with the potential for multiplexing. These sensors rely on the moisture induced swelling of the polyimide coating. This hygroscopic property of the polyimide transfers strain into the FBG, which is then detected as a shift in the Bragg wavelength. A more detailed discussion of this FBG sensing mechanism is given in Chapter 2.

1.3.3 Liquid water

Despite not having been applied to PEMFCs, techniques using optical fibre-ends, without FBGs, as reflectometers to detect two-phase regimes have been demonstrated [53, 54]. Multi-point probes were used to measure bubble size and velocity with time resolved intensity-based measurements that were binary, depending on the phase of the fluid; gas or liquid. Two-phase flow occurs in the gas channels of PEMFCs, and the measurement of droplet size and velocity using this technique could be very useful. An advantage of the technique is that it requires fairly rudimentary equipment, but there is no multiplexing capability.

One technique that could be used to detect water droplets and has multiplexing capabilities like FBGs, but requires expensive interrogation equipment is optical time domain reflectometry (OTDR). This technique is typically used to locate defects along long spans of fibre, and works by measuring the backscattered light intensity from a fibre following a light pulse. Defects in the fibre show up as irregularities in the time trace, and can be located along the fibre simply by using the time of flight and the velocity of light in the silica fibre. “Defects” can be created along the fibre and made sensitive to water by etching to the core. Expense of interrogation equipment increases with desired spatial resolution and examples of OTDR being done on length scales found inside a PEMFC are not reported in the literature.

A promising FBG technique that can be used to detect liquid water, and could equally well be applied to study flooding phenomena in PEMFCs, involves etching away the fibre cladding to allow interaction of the evanescent field. The reflected spectrum of the FBG becomes sensitive to the refractive index of the surrounding medium. A more detailed discussion of evanescent field based sensing with FBGs is provided in the following chapter, as it is the basis for the sensor presented in Appendix D.

1.4 Objectives

The overall objective of this research is to develop and demonstrate optical fibre measurement techniques for temperature, RH and liquid water in PEMFC. For the temperature technique, the objective is to install multiple FBG temperature sensors into the active area of an operating fuel cell and compare data to a co-located micro-thermocouple for validation. For relative humidity, the objectives include *ex situ* validation of an improved polymer-coated FBG sensor design followed by *in situ* demonstration of the improved sensor design. The objective for the liquid water detection is to develop an evanescent field based FBG sensor to measure droplet speed and size in a micro flow channel without perturbing the two-phase flow.

1.5 Organization of Dissertation

This dissertation is presented in the manuscript format, where the most detailed aspects of the research are contained in published and submitted manuscripts that are included in the appendices. The chapters leading up to the appendices serve to provide context and a framework that links the manuscripts in terms of background, motivation and objectives.

Much of the background presented in Chapter 1 has focused on PEMFCs to provide the design space for the sensors developed during this thesis work. Also in

Chapter 1, it became clear that optical fibre Bragg grating sensors are a potentially feasible platform on which to develop a suite of sensors for temperature, humidity and liquid water. The manuscripts presented in Appendices A-D are in fact individual proof-of-concept studies on the development or implementation of FBG sensors for these three parameters in PEMFCs. FBGs being the common thread between the manuscripts, Chapter 2 is devoted to optical fibre and FBGs with emphasis on the sensing mechanisms behind the FBG techniques for each parameter. In Chapter 3 the contributions presented in the manuscripts are summarized, which includes a brief discussion of the objectives, methods, and results for each paper. In the fourth, and final chapter of the thesis, the key conclusions and future considerations for this work are discussed.

Chapter 2

In-fibre Bragg Gratings

The potential of fibre-optics for *in situ* diagnostics in PEMFCs was highlighted in Chapter 1. This chapter is focused on the properties of optical fibre and in-fibre Bragg gratings for this application. Before discussing the specific sensing mechanisms for temperature, RH, and liquid water, the basic principles of optical fibre and FBGs are presented. Related techniques reported in the literature are cited to establish the feasibility and novelty of the sensors developed in the present work.

2.1 Optical fibre and FBGs

The geometry of an optical fibre typically comprises two concentric solid glass cylinders . The inner cylinder is called the core, and the outer cylinder the clad. The core has an index of refraction, n_1, that is slightly higher than the cladding index, n_2 (Figure 2.1a). This is achieved with the addition of dopants to the silica used in the core. This slight difference in index is sufficient to guide light in the core by total internal reflection, provided the cladding is thick enough to contain the evanescent waves associated with total internal reflection [55].

The most common type of optical fibre for telecommunications and for commercial FBG sensors is asingle-mode fibre. A typical single-mode fibre has a cladding diameter of ~125 μm and a core diameter of ~8 μm. These dimensions allow only single mode waves (solutions to Maxwell's equations) to propagate along the fibre. Single mode propagation ensures low modal dispersion, which is particularly important for information transfer over long distances. Wavelengths in the near infrared (1.3-1.5 μm) are typically used in single-mode fibre, since this bandwidth corresponds to minimal absorption in silica glass [55].

Due to low power requirements and high data transfer rates, optical fibre began replacing copper wire for telecommunications soon after the fibre was developed in the 1970s. Since then, numerous sensing techniques covering a broad range of applications have emerged based on fibre optics [56, 57]. The proliferation in sensing applications can be attributed to optical fibre being inherently small, chemically resistant and immune to electromagnetic interference. Despite these useful properties of optical fibre, it is in general more challenging than copper wires to work with because of the small diameter and brittle nature of the fibre. Furthermore, in contrast to the mechanical contact or soft solder connections that can be made easily with wires, optical fibres require close tolerance mechanical or fusion splicing for their connection. To make the fibre easier to handle during installation, polymer coatings are often applied to strengthen the fibre and make it more flexible.

Among the many types of optical fibre sensors is the FBG. The FBG is unique in that it offers the possibility of spatially distributed multi-parameter measurements on a single fibre [58]. Because of these capabilities, FBGs have found numerous applications as single-point sensors or as distributed sensors. They have become particularly important in the the field of structural health monitoring [58, 59].

An FBG occupies a short length (typically 1mm-10mm) of optical fibre and is comprised of a periodically modified index of refraction along the core (Figure 2.1a

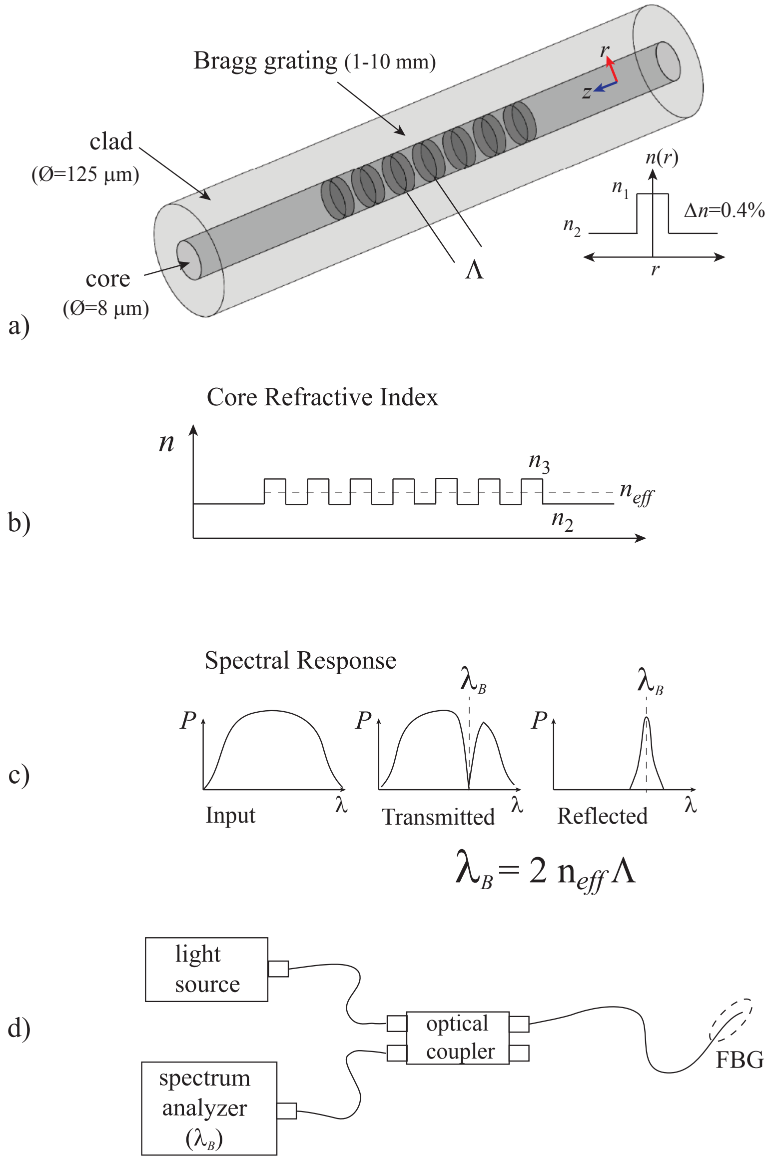

Figure 2.1: (a) Schematic (not to scale) of an FBG sensor written in single mode optical fibre. (b) Refractive index profile along the length of the FBG created by patterned UV exposure. (c) Typical spectral response of FBG sensor when illuminated with broadband light. (d) Basic optical setup for measuring FBG spectra.

and 2.1b). This pattern of modified indices is typically photo-induced by UV laser, using either interference or phase mask techniques. The original profile of the fibre is unaffected by the grating so that it is indistinguishable from other regions of the fibre.

When light transmitted along an optical fibre encounters a grating, a narrow band of wavelength is preferentially reflected (Figure 2.1c). In accordance with Bragg's law, the center-wavelength of this narrow band (i.e., the Bragg wavelength) is given by

$$\lambda_B = 2n_{eff}\Lambda, \tag{2.1}$$

where Λ is the spatial period of the grating and n_{eff} is the effective index of refraction in the core. The effective index of refraction is approximated by the average index along the grating. See Figure 2.1b. Due to the evanescent field that penetrates into the cladding, however, n_{eff} also depends partly on n_1, the index of the clad. If the cladding is etched down into the region of evanescent field penetration, n_{eff} becomes dependent on the refractive index of the surrounding medium. This is the principle behind evanescent field or wave sensors, which are discussed later in the chapter.

The shape of the reflected FBG peak is largely determined by the length of the grating, L, and the magnitude of the index difference in the grating,

$$\Delta n = n_3 - n_2. \tag{2.2}$$

This is expressed quantitatively in the following equations for maximum reflectivity [58]:

$$R_{max} = tanh^2\left[\pi\left(\frac{\Delta n}{n_2}\right)\left(\frac{L}{\Lambda}\right)\right] \tag{2.3}$$

and the full width half maximum (FWHM) bandwidth, $\Delta\lambda_W$, of the peak [58]

$$\Delta\lambda_W = 2\lambda_B\left[\left(\frac{\Lambda}{L}\right)\left(\frac{\Delta n}{2n_2}\right)\right]^{1/2}. \tag{2.4}$$

The typical Bragg wavelength of commercially available FBGs is around 1550 nm. Other commonly used Bragg wavelengths for FBGs are 800 nm and 1300 nm. Maximum reflectivity values are typically 90% of the peak intensity of incident light. The FWHM of the peak typically varies from as narrow as 0.2 nm for 10 mm long gratings to 1 nm for 1 mm gratings [58].

The reflected spectrum of an FBG can be measured by a number of techniques [58], an example of a common method is shown in Fig. 2.1(d). The FBG is illuminated with a broadband light source, and the reflected light is coupled into an optical spectrum analyzer for measurement. From this spectral data, the centre of the peak can be calculated to obtain the Bragg wavelength of the sensor. For the detection of several FBGs with different Bragg wavelengths on a single fibre, interrogation units that employ wavelength division multiplexing are commonly used [60].

2.2 Thermal and mechanical influence on FBGs

Because of the Bragg condition (Eq.2.1), FBGs are able to measure both strain and temperature. Both the refractive index, n_{eff}, and the spatial period of the grating, Λ, are functions of applied strain and temperature. The difficulty of using FBGs as strain or temperature sensors, therefore, is often in the decoupling of these parameters.

Assuming the refractive index, $n_{eff}(\varepsilon, T)$, and the grating spacing, $\Lambda(\varepsilon, T)$, are linear functions of strain and temperature, a Taylor expansion of Eq. 2.1 wavelength about a reference state of temperature and strain yields [58]

$$\frac{\Delta\lambda_B}{\lambda_B} = \varepsilon_z - \frac{n_{eff}^2}{2}(\varepsilon_z p_{12} + \varepsilon_r(p_{11} + p_{12})) + \xi\Delta T \tag{2.5}$$

The first term, ε_z, is the thermally and mechanically induced axial strain in the grating, which changes the grating pitch. The second term represents the strain-optic effect, where p_{11} and p_{12} are the principal components of the strain-optic tensor and ε_z and ε_r are the corresponding axial and radial strains, respectively. The third term represents the thermo-optic effect, where ξ is thermo-optic coefficient.

For a Bragg grating written in single mode optical fibre subjected only to axial strain the following simplified version is often used [61],

$$\frac{\Delta\lambda_B}{\lambda_B} = (1 - P_e)\varepsilon_z + ((1 - P_e)\alpha + \xi)\Delta\mathrm{T}, \tag{2.6}$$

where

$$P_e = p_{12} - \nu(p_{11} + p_{12}) \tag{2.7}$$

represents the effective strain optic coefficient in which the radial strain is accounted for by the Poisson effect.

Equation 2.6 is a superposition of the mechanical and thermal response of the FBG; α is the coefficient of thermal expansion (CTE) of the fibre; and ξ is the thermo-optic coefficient. The temperature sensitivity of a bare fibre is primarily due to the thermo-optic effect [62].

The temperature response of an FBG written in standard single mode fibre is linear up to 85 °C with a typical sensitivity of $\sim$10 pm$^\circ$C^{-1} for bare fibre [62]. At higher temperatures the sensitivity increases and becomes slightly non-linear [62]. In the operating range of a PEMFC (20-90°C) the FBG response to temperature can be assumed to be linear.

The UV induced change in refractive index that forms the grating decays over time at a rate that increases with temperature due to thermal excitation of trapped electrons [63]. Edrogan *et al.* [63] used experimental data to develop a model for accelerated aging of UV induced Bragg gratings at various temperatures. The model suggests that at a temperature of 400K (higher than in PEMFCs), the decay in reflectivity of an FBG starting at 90% reflectivity is expected to be negligible over the lifetime of a fuel cell.

A typical value for the sensitivity of an FBG in a bare fibre to applied axial strain is ~1.2 pm$\mu\varepsilon^{-1}$ at λ_B=1550 nm [64]. The sensing of many parameters (e.g. pressure, electromagnetic fields, chemicals, humidity) relies on the strain sensitivity of the FBG. Transducing layers or structures can be used to convert these measurands into strain in the fibre. For an FBG humidity sensor, for example, the glass fibre has been coated with a hygroscopic polymer that expands in the presence of moisture [52,61,65]. This expansion induces strain in the fibre, which is detected as a shift in the Bragg wavelength.

With the sub-picometer resolution of current multiplexing interrogators [66] precise measurement of strain (and other parameters) and temperature is possible, with resolution comparable to conventional strain gauges and thermocouples ($<1\ \mu\varepsilon$,<0.1°C). Due to the co-sensitivity of FBGs to strain and temperature, temperature compensation of sensors is often necessary. This can be done using a co-located FBG with a different Bragg wavelength [32, 67].

2.2.1 FBG humidity sensing

Of particular interest in this research is humidity sensing using FBGs, which, as mentioned can be achieved by applying hygroscopic polymer coatings to the fibre. The polymer coating acts as a strain transducer, transferring strain into the fibre as it absorbs moisture. The first polymer reported as a transducing layer for FBGs was polyimide. Polyimide is a commonly used polymer for protective coating on optical fibre due to its thermomechanical stability. Polyimide is also hygroscopic. In 2001, it was demonstrated by Giaccarri *et al.* that commercial FBGs recoated with polyimide for protection produced a linear, reversible shift in Bragg wavelength with changes in

RH [68].

Soon after demonstration of the sensitivity of polyimide-recoated commercial FBGs by Giaccarri *et al.*, the FBG humidity sensor concept was investigated further by Yeo et al. and Kronenberg et al. [52, 61]. In their studies they systematically tested the steady state response of FBGs on standard single mode fibre coated with varying thicknesses of polyimide. They found that a simple 1-D axial strain model could be used to predict experimental results for sensitivity as a function of coating thickness.

Achieving sufficient sensitivity to enable 1% RH resolution with the sensor design of Yeo et al. and Kronenberg et al., polyimide coatings of ∼10 μm were required. With coatings if this thickness, however, it was shown by Yeo *et al.* that the response times are prohibitively long (τ_{63} ∼5 min) for dynamic measurements within PEMFCs [37, 61]. An improved sensor design that enables high resolution and fast response measurements was presented by David *et al.* [31,32]. The sensor is based on an etched single mode optical fibre with thinner polyimide coatings. The details of this sensor are discussed in Appendices B and C.

2.3 Evanescent field sensors

Another sensing mechanism for optical fibre and FBGs is based on evanescent field interaction. The evanescent field describes the part of the electromagnetic wave solution for an optical fibre that decays exponentially into the cladding region of the fibre. See Figure 2.2. Sensing is achieved by reducing the thickness of the cladding so that the evanescent field interacts with the surrounding medium. With this interaction, the index of refraction of the guided mode in the core becomes influenced by the refractive index of the surrounding medium. Based on this principle, numerous optical fibre and FBG chemical [67, 69], biological [70] and liquid refractive index sensors [6, 71, 72] have been developed in recent years.

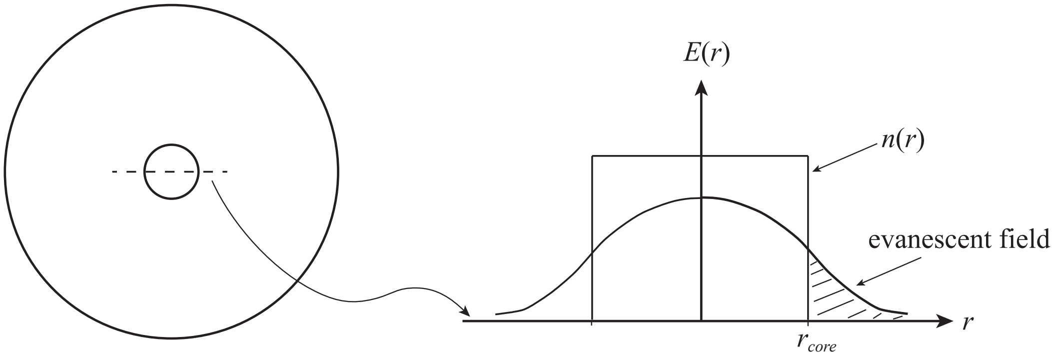

Figure 2.2: Schematic showing the refractive index profile n(r) of a standard single mode optical fibre and the associated electric field profile E(r) of the lowest propagation mode. The part of the electric field that extends beyond the core is the evanescent field.

For FBGs with sufficiently reduced cladding thickness, the change in refractive index of the surrounding medium is detected as a shift in the Bragg wavelength. The dependence of the Bragg wavelength on the index of its surrounding medium can be written as

$$\Delta\lambda_B = 2\Delta n_{eff}(n_s)\Lambda \tag{2.8}$$

where n_{eff} has simply been written as a function of n_s, the refractive index of the surrounding medium. The dependence n_{eff} on n_s for an FBG written in standard single mode fibre and operating at 1550 nm was solved numerically by Iadicicco *et al.* [6] for different cladding diameters. See Figure 2.3. This dependence was verified experimentally by testing the response of an FBG that was progressively etched to smaller diameters using hydrofluoric (HF) acid until the cladding was fully removed, leaving only the 8.3 μm diameter core.

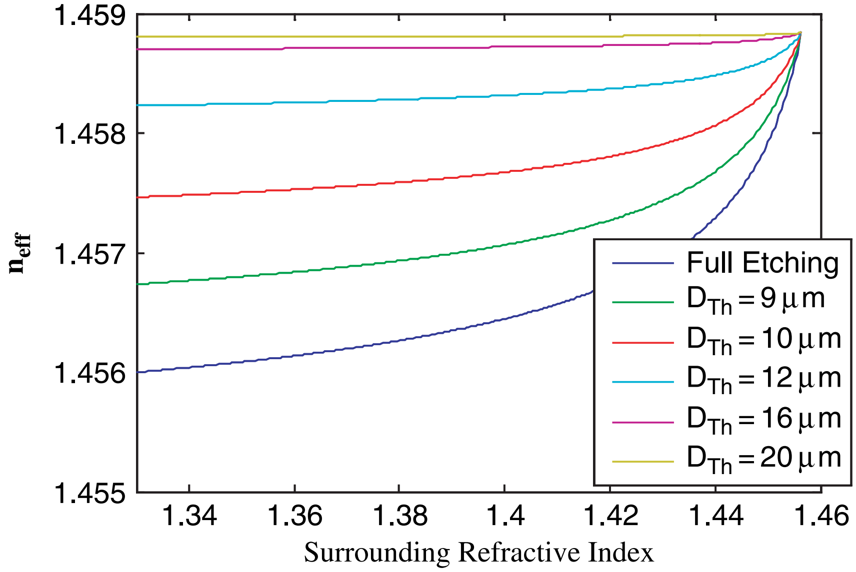

Figure 2.3: Numerical results of Iadicicco *et al.* showing the sensitivity of the effective refractive index to the surrounding refractive index for different cladding diameters. Reproduced with permission from IEEE [6]

Figure 2.3 shows that the sensitivity of n_{eff} to changes in n_s is low for n_s=1.33 (water) and increases to a maximum when the surrounding medium has the index of glass (n_s ~1.45). This increase in sensitivity is due to a larger penetration depth of the evanescent field for higher index surrounding media. The penetration depth is the distance it takes for the field intensity to drop to 1/e of its value at the core cladding interface. The penetration depth depends on the refractive index of the core and the cladding or, in the case of a fully etched cladding, the index of the surrounding medium [73]. For low index surroundings, as is the case with water (n_s ~1.33) and more so with air (n_s ~1.0), the light is well confined within the core leading to a weaker dependence of n_{eff} on n_s.

This low response of an etched FBG in low index media such as air and water is a design consideration for detecting two-phase flow in a PEMFC. Based on the above discussion, and extrapolation of the sensitivity curve shown in Figure 2.3, an FBG in standard single mode fibre needs to be etched close to the core to elicit a strong response to phase for water. Such a reduction in fibre diameter, however, leaves the fibre prone to breakage and difficult to work with during sensor construction. The difficulty of accessing the evanescent field in standard single mode optical fibre has lead researchers to design FBG evanescent field sensors based on novel methods of accessing the core and special types of fibre. Rather than uniform chemical etching of the cladding with HF, alternative methods of accessing the core in standard fibre have included femtosecond laser micro-machining [74, 75] and side polishing of the cladding [67]. Starting with a specialty D-shaped fibre on the other hand, which has a flat side that is in close to proximity (~14μm) to the core (Fig. 2.4, less cladding removal is required to access the core, leaving substantially more fibre to work with in sensor fabrication.

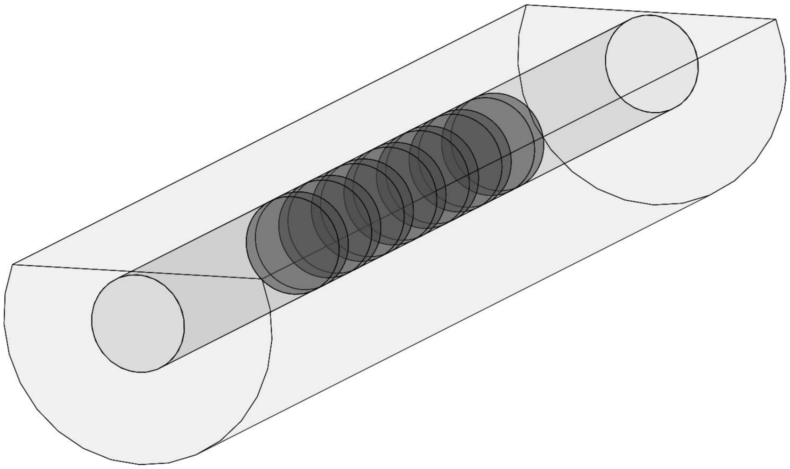

Figure 2.4: Schematic of D-shaped fibre with FBG (not to scale). Use of this fibre requires less etching for evanescent field based sensors.

The side-polished technique was demonstrated by Shroeder *et al.* [67] in an FBG evanescent field sensor for hydrogen gas. An FBG written in standard single mode fibre was embedded into a glass block and then polished leaving a residual cladding thickness of less than 2 μm. The authors show that the sensitivity to refractive index of evanescent field FBG sensors can be improved by applying thin layers of high refractive index dielectric materials or metals. In their sensor they applied a thin layer of palladium, the refractive index of which changes with hydrogen concentration. Shroeder *et al.* also demonstrated the use of a co-located full cladding FBG for temperature compensation in their sensor.

Although the technique of mechanical side-polishing used by Schroeder *et al.* was effective in the demonstration of their sensor, the ability to uniformly polish the length of the FBG with sub-micron tolerance could prove challenging to reproduce. An alternative approach to side-polishing is the use of D-shaped optical fibre which, as mentioned, requires minimal chemical etching to access the core. Chemical etching ensures uniform exposure of the evanescent field along the length FBG and is easily reproducible. An evanescent field FBG refractive index sensor based on D-shaped fibre was demonstrated by Meltz *et al.* [76]. For this sensor, the cladding on the flat side of the D-fibre was etched with HF to within an estimated 0.5 of the core. The sensor response from air to water was measured as a shift in the Bragg wavelength of approximately 200 pm, which would give a signal to noise ratio of ~200 when using current FBG interrogation systems. Implementation of this sensor into a microchannel to measure droplet speed and size is one of the objectives of the work presented in this thesis. Development of such a sensor is discussed in Appendix D.

2.4 FBGs in PEMFCs

The mechanisms for the measurement of temperature, RH, and liquid/gas phase transitions have been presented. From the above discussions, FBGs emerge as a feasible solution for measurement of these parameters in the PEMFC environment.

In the context of distributed monitoring of temperature, RH and water in PEMFC stacks for research, and potentially commercial applications, FBGs possess promising characteristics that warrant further development and investigation:

- *Small size*: optical fibres are nominally 125μm in diameter, and as small 10 μm when etched [6]. The small size of FBGs allows for installation into the flow channels of PEMFC plates and possibly into the other structures comprising the MEA. Installation of current capacitive RH sensors is limited by their relatively large size.

- *Environmental compatibility*: glass fibre is chemically inert and immune to electromagnetic interference. In the high humidity, high temperature and electrochemically active environment of a PEMFC, corrosion resistance and electromagnetic interference are significant barriers to the use of wired electronic sensors in this application. In addition, glass fibre is tolerant to high temperatures, much higher than occur inside a PEMFC.

- *Multi-parameter and multiplexed sensing*: FBG sensors for temperature, RH and refractive index (water) have been demonstrated in the literature and in the research presented in this dissertation [31,32,76]. One of the primary motivations for using FBGs for this application is that they are wavelength encoded and, therefore, can be multiplexed. This leaves open the possibility of combining sensors for all three parameters on a single fibre for distributed measurements. With other techniques seen in the literature, such integrated measurement of multiple parameters is not possible.

Despite their clear benefits for this application, as listed above, optical fibre and FBGs present themselves with inherent challenges for sensor development. In working with optical fibre, the challenges are mainly due to its fragility when not coated and the restriction on bending of the fibre. The minimum suggested bend radius of standard single mode optical fibre is ∼15 mm. Excessive bending of the fibre causes light loss and the possibility of breakage. This limitation is a major consideration for implementation of FBGs into the low-profile planar structures of a PEMFC.

As discussed above in this chapter, the sensitivity of FBGs to strain and temperature is the basis for many FBG sensors. It is this co-sensitivity that poses a significant challenge in sensor design. For an FBG used strictly as a temperature or RH sensor for example, isolation from extraneous strain must be incorporated into the design so only the desired measurand is being measured. For FBG sensors that are based on strain, like the polymer coated RH FBG sensor for example, co-sensitivity to temperature is unwanted and requires temperature compensation. This adds an element of design challenge, but fortunately can be accomplished using a co-located FBG that is isolated form strain.

2.4.1 Techno-economics of FBG sensing system

Based on the discussions of the previous sections and the work presented in the manuscripts found in the appendices of this thesis, FBG based techniques for the in situ monitoring of temperature, RH and liquid water are technically feasible. By installing FBGs at selected locations throughout a fuel cell stack, quasi distributed real time monitoring of these parameters can provide feedback for the control of optimal operating conditions and detect failure modes such as hotspots and flooding. Currently, the cost of FBG sensors (∼$100/FBG) and the associated monitoring system (∼$10k-$20k) is prohibitive for the implementation of distributed FBG sensing systems in all but the most high value applications (i.e., fuel cell buses and research stacks). This high cost of implementation may be prohibitive at the moment, but provides incentive for the efficient usage of FBGs within a PEMFC to obtain the most meaningful measurements.

A schematic representation of an FBG array distributed throughout a PEM fuel cell stack is depicted in Fig. 2.6. Current wavelength division multiplexing interrogation systems have multiple channels, each capable of monitoring up to ∼40 FBGs on a single fibre. As mentioned, however, economic considerations require efficient use of FBGs, and hence careful consideration of the locations of the FBGs throughout the flow field of the bipolar plates and throughout the stack.

For temperature measurements, which are useful for the detection of hotspots forming in the membrane, locating the FBGs nearest the membrane can be achieved by embedding the FBG into the lands, between the flow channels. This technique was demonstrated in the manuscript presented in Appendix A. For the measurement of relative humidity, the FBG RH sensor should be located in the flow channel, but in an area that is not prone to flooding. From the diagrams of the common two-phase flow patterns that occur in PEMFC operation (Figure 1.5), the centre of the flow channel is the least likely to be covered by a film of liquid water. Conversely, for the measurement of liquid water using FBGs, installation on the side wall of the channel, where film flow regimes are most common, would be most useful. A schematic of the various sensor locations is shown in Fig.2.5.

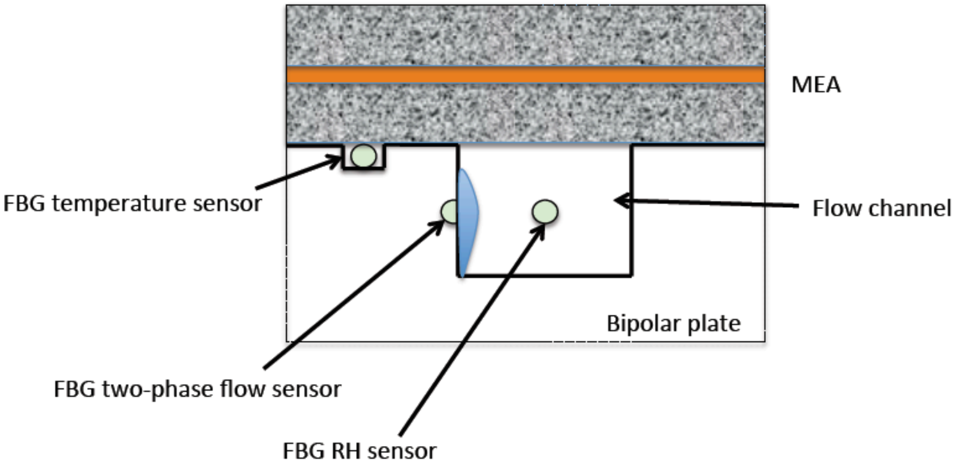

Figure 2.5: Schematic showing the preferred installation locations of FBG sensors within the bipolar plate.

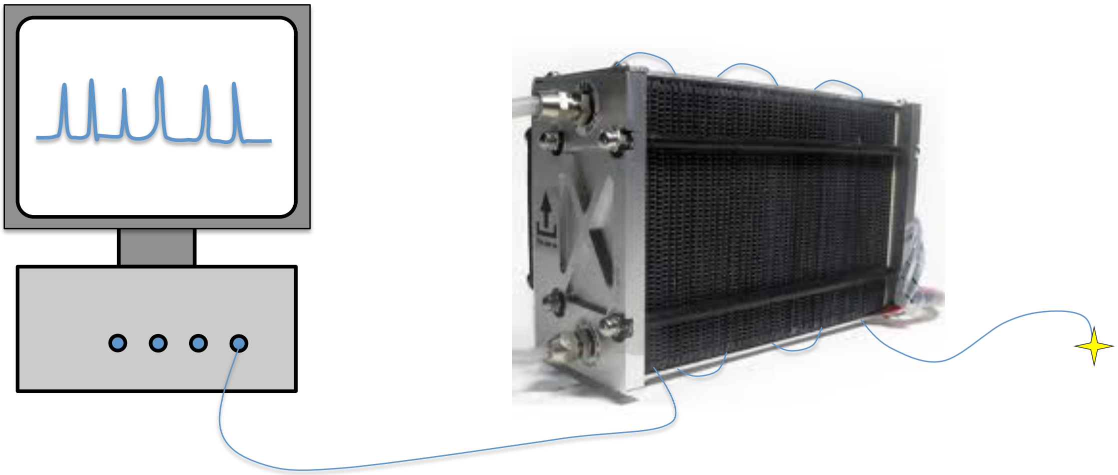

Figure 2.6: Schematic showing a multiplexed FBG sensor implemented into a PEMFC stack.

Chapter 3

Summary of Key Results

Selected studies undertaken during this dissertation resulted in significant contributions that were presented at international conferences and published in science and engineering journals. These studies are described in detail in the manuscripts included in Appendix A through D. This chapter serves to provide an overview of the motivations, methods and key results of these studies in logical progression. The order of the sections in this chapter, and the corresponding appendices, represent a progression from sensor implementation to sensor design improvement to novel sensor development for the parameters of temperature, RH and liquid water, respectively.

3.1 In-fibre Bragg Grating Sensors for Distributed Temperature Measurement in a Polymer Electrolyte Membrane Fuel Cell

Temperature distribution data inside commercial PEM fuel cell stacks could be used to improve the effectiveness of cooling systems and to identify where potentially damaging hotspots may occur across the membrane. Monitoring of the temperature distribution over such a large active area using current state-of-the-art techniques is technically challenging. As discussed, many of these challenges can be overcome by using optical fibre Bragg grating sensors. The primary objective of this study was to demonstrate the feasibility of using FBG sensors to measure temperature near the MEA in an operating fuel cell.

To demonstrate feasibility, four FBG sensors were installed in a single test cell and used to measure steady-state and transient temperature profiles. To measure the temperature near the MEA, the FBGs were installed on the lands between the flow channels in the cathode collector plate. In contrast to electrical sensors that use wire leads, particular attention needed to be given to strain relief and minimizing bending of the optical fibre. Validation of the installation technique was determined with *in situ* calibration against a co-located thermocouple. The calibration of the sensors was linear and repeatable, with sensitivities in good agreement with the expected value.

Resolution of the installed and calibrated FBG sensors was shown to be 0.2° C over the operating range of the fuel cell, offering sufficient resolution to measure small gradients between sensors. During cell operation under co-flow conditions, steady-state temperature profiles showed gradients increasing from inlet to outlet. This result was consistent with measurements presented in the literature that were made using other techniques [1, 2, 33]. The small thermal mass of the FBG, combined with the installation technique enabled fast response *in situ* measurements that were comparable to, if not more insightful than those made with the co-located micro-thermocouple.

This work demonstrated for the first time that FBGs can be embedded inside a PEM fuel cell to reliably measure temperature dynamically with resolution comparable to micro-thermocouples. Based on the results of this study, it was shown that this technique could prove useful as a diagnostic tool to identify hot spots on the membrane and validate thermal management strategies in commercial stacks.

For further information, the reader is directed to Appendix A, or [31].

3.2 Parametric Study of an FBG Relative Humidity Sensor

Another key parameter in the water management of PEM fuel cells is the relative humidity (RH) of the gases inside the cell. The RH inside the cell should be high enough to ensure good membrane hydration. When this is achieved, ohmic losses in the membrane are minimized. Recently reported *in situ* measurements of RH in single cell PEMFCs have shown significant gradients across the flow field as well as interesting dynamic behaviour [37]. None of these techniques, however, can be implemented into commercial bipolar plates due to sensor size [37] or performance limitations [24,33]. As discussed above, FBG sensors possess many qualities that are well suited towards their implementation in PEMFCs. The objective of this study was to design a fibre optic RH sensor that addresses the response time and sensitivity limitations of the previous designs such that it can be implemented as a diagnostic tool in PEM fuel cells.

The proposed sensor design is based on a polyimide recoated FBG. The polymer coating swells in the presence of increased RH, imparting strain on the fibre, which is detected as a Bragg wavelength shift. Such a design, consisting of a standard single mode fibre coated with polyimide was previously reported, but lacked the sensitivity and response time required for measurements inside a PEM fuel cell. The method for improving sensitivity and response time was to thin the optical fibre, which for equal coating thicknesses, provides a more sensitive response than a standard diameter FBG. Less coating thickness yields a faster response since it is a diffusion driven response.

Sensors of varying fibre diameter and coating thickness were fabricated and tested for steady-state and transient response. The experimental investigation was complimented by 1-D and 3-D numerical simulations of the design. A coating device was constructed to apply thin and uniform coatings of the polyimide Pyralin®. Transient simulations and experiments on standard diameter fibres suggested that a coating thickness of less than 4μm is needed to achieve a response time of 5 s, competitive with commercial capacitive RH sensors. Such a thin coating on a standard single mode fibre, however, yields a low sensitivity and thus low sensing resolution.

Both 1-D and 3-D models suggested a increase in sensitivity when the fibre diameter is reduced. Using a 2.5 μm coating on a fibre with a diameter of 20 μm a seven times increase in sensitivity over an unetched fibre was achieved. Tests showed that the etched fibre sensor exhibited a linear, repeatable response to changes in RH over the range of 15-95 %RH. Rapid recovery (20s) from saturation with liquid water was also demonstrated, which is in contrast to commercial RH sensors.

The proof of concept study showed that an FBG RH sensor with sufficient sensitivity and dynamic resolution can be realized. In addition to its application to PEMFCs, this design may equally well be suited to many other applications.

For more information, please refer to Appendix B or [32]

3.3 Simultaneous *In Situ* Measurement of Temperature and Relative Humidity in a PEMFC using Optical fibre Sensors

In the previously discussed study, an FBG RH sensor with good dynamic resolution was demonstrated. The objective of this study was to implement this FBG RH sensor in a single cell PEMFC to demonstrate its feasibility. Two etched FBG RH sensors with FBG temperature compensation were fabricated and installed in the cathode flow-channels, one near the inlet and one near the outlet.

Using a method of installation that was similar to the one demonstrated for the FBG temperature sensors [32], minimal intrusion to the flow-field was achieved. RH and temperature data was acquired with the sensors while operating the cell under dry conditions to obtain a steady-state polarization curve. The steady-state measurements were consistent with related studies from the literature, which have shown higher RH towards the outlet due to self-humidification [2]. RH levels approaching 100 %RH were measured near the outlet for high current densities.

Transient measurements were made during sudden changes in cell current. These results exhibited RH transients inside a PEMFC on a time scale approaching the sensor response time of ~5 s.

In situ implementation of FBG RH sensors was demonstrated for the first time in this work. The performance of the novel etched FBG RH sensor proved that it is indeed well suited to application in PEMFCs. The contribution of feasibility demonstration has set the course for a multiplexed FBG approach using the same basic sensor design. In the interest of improved cell design, particularly with regard to water management strategies, this technique could prove useful as a non-invasive diagnostic tool.

For more information, please refer to Appendix C.

3.4 Fibre Bragg Grating Sensor for Two-Phase Flow in Microchannels

Performance loss due to flooding in the flow channels and GDL of a PEM fuel cell is common, particularly at high current densities [9]. Despite a general understanding of flooding phenomena in a PEMFC and the associated degradation mechanisms, however, there is a lack of in situ diagnostic tools for the detection of flooding.

In the studies summarized thus far, FBG sensors were demonstrated for non invasive *in situ* measurements of temperature and RH in PEMFCs. To extend the use of FBGs to include liquid water detection, the sensing mechanism of evanescent field interaction was exploited in this work.

Previously reported FBG refractive index sensors based on this evanescent field interaction are either extremely thin and prone to breakage [6], not easily reproduced [67], or not embedded into a surface [76]. Furthermore, none have been used to detect two-phase flow on a surface. Surface embedding is essential to enable non-intrusive measurements of two-phase flow in a microchannel, as would be needed in a PEMFC. The objective of this study was to develop an FBG based liquid water sensor for measuring and characterizing two-phase flow in a microchannel that is designed to emulate a gas flow channel in a PEMFC.

Based on a D-shaped optical fibre, a refractive index sensor comprising two adjacent FBGs was made by chemically etching the cladding to expose the evanescent field. The D-fibre was embedded into a polydimethylsiloxane (PDMS) polymer substrate. This substrate with the sensor was then used as a wall of a microchannel in which two-phase flow regimes were created. Two adjacent FBGs with known spacing were used in this sensor design so that the size and speed of a droplet could be measured as it passed along the length of the fibre.

Sensor data was synchronously acquired with high speed digital video for validation and correlation. The validated sensor capabilities include excellent spatially and temporally resolved measurements of slug flow and droplet flow regimes.

The initial strategy for measuring the convection speed of water droplets relied on the use of two FBGs and was successfully demonstrated. The results however also showed that in fact such measurements are also possible with a single FBG provided it is short enough.

For more information on this study please refer to Appendix D.

Chapter 4

Conclusions and Future Work

4.1 Conclusions and Contributions

This dissertation was dedicated to the development and demonstration of FBG sensor techniques for the measurement of temperature, humidity and two-phase flow in PEMFCs. Techniques for the installation of FBG temperature and RH sensors into fuel cell plates were developed to ensure reliable and repeatable measurements. These installation techniques were validated experimentally by calibration and *in situ* measurements in an operating fuel cell. Novel FBG sensors for RH and water detection were developed and demonstrated. This development work spanned the disciplines of heat transfer, diffusion, mechanics, optics, and microfluidics and involved a combination of experimental and numerical modelling studies. The specific contributions resulting from this dissertation are summarized below and organized with respect to the four studies outlined in Chapter 3.

1. In-fibre Bragg Grating Sensors for Distributed Temperature Measurement in a Polymer Electrolyte Membrane Fuel Cell:

   In this work, the use of FBGs in a PEMFC was demonstrated for the first time.

A significant challenge of this component of the work is in sensor installation. Key considerations for FBG temperature sensor installation in a PEMFC were identified and implemented in the techniques. These installation design considerations include the sensor proximity to the catalyst layer, sensor strain relief and minimal bending of the fibre. In an effort to measure the temperature close to the MEA, which is the area of most interest to fuel cell researchers, the FBGs were located in grooves on the land areas between the flow channels of the graphite collector plate. To promote heat transfer between the FBG and the GDL rather than the flow plate, the groove was machined deeper directly underneath the FBG sensor. This feature, combined with the small thermal mass of the fibre contributed to good *in situ* temporal resolution of the FBG temperature sensors. Angled holes were used at the entry point of the fibre into the graphite plate. This feature is necessary to ensure minimal bending of the fibre, as excessive bending of the fibre causes light loss, and the possibility of fibre cracking and breakage.

2. Parametric Study of a Polymer-Coated Fiber-Optic Relative Humidity Sensor: In this study, a polyimide-coated FBG based RH sensor was demonstrated with significantly improved response time and sensitivity over previously reported designs. Sensor response times of $\tau_{63} < 5s$ were demonstrated for thin polymer coatings and a seven times increase in sensitivity was achieved by chemical etching of the fibre cladding around the FBG. In addition, quick recovery from saturation by liquid water was demonstrated for the sensor. These sensor characteristics are particularly important for implementation of the sensor into a PEMFC. Further to the experimental findings of this study, numerical analysis of transient response of the sensor design was presented for the first time.

3. Simultaneous In Situ Measurement of Temperature and Relative Humidity in a PEMFC Using Optical FIbre Senors:

   Following the progression from sensor design to sensor implementation, the aforementioned polymer-coated FBG RH sensor was used for *in situ* measurements in a PEMFC. This was the first reported demonstration of FBG RH sensors for fuel cell application. For the simultaneous temperature measurements and temperature compensation of the RH sensitive FBG, a sensor comprising an adjacent uncoated multiplexed FBG at a different wavelength was described. Two of the sensors were embedded directly into the cathode flow channels of a single test cell and were used to make real-time measurements of RH and temperature during cell operation. Results showed that for an increased current density, much larger increases in RH occur near the outlet than near the inlet, a trend that has been reported in other studies. From the results, it was also determined that RH transients inside a PEMFC exist on a time scale approaching the sensor response time, proving that the sensor could provide information on the dynamics of water transport in the MEA. The contributions of this work serve to validate the contribution made in the previous study on sensor design improvements for PEMFC implementation.

4. Fibre Bragg Grating Sensor for Two-Phase Flow in Microchannels:

   An evanescent field based FBG sensor for surface measurements of two-phase flow was demonstrated for the first time. The contributions of this work are in the techniques of sensor fabrication and in the data analysis that suggests the use of a simplified design for effective measurements. An etched D-shaped fibre with two adjacent FBGs was cast into the surface of a PDMS polymer substrate, which was then used as one of the surfaces in a PDMS microchannel. High speed digital video of two-phase flow created in the channel was captured synchronously with sensor data acquisition. The FBGs exhibited an on-off type response to the passage of droplets, which correlated precisely with liquid water flowing over the FBG locations. This correlation enabled the measurement of droplet average velocity size using only the sensor data. Upon close inspection of the correlated data, it was shown that for droplets larger than the FBG length, a single FBG can be used to estimate the speed and size of a fast moving droplet. This study suggests that an evanescent field FBG sensor could be adapted for use in the flow-channel of a PEMFC to investigate droplet and flooding phenomena. This new sensor concept could be applied, for example, to micro-fluidic devices or to the detection of condensation.

4.2 Future Work

Although one of the key motivations for using FBGs in this work was their ability to be multiplexed, this functionality was only demonstrated in the temperature compensation of the RH sensor. The development of multiplexed FBG sensors that incorporate the sensors for temperature, RH, and phase that were developed during this thesis work is reserved for future engineering work. Ideas for doing this include the use of thinner fibre so that chemical etching is not needed for the RH sensor, and the use of micro-machining techniques on the same fibre to access the evanescent field for phase detection. Each sensor will consist of three adjacent FBGs, on for each parameter, and will require the use of a package or superstructure to isolate the sensor from extraneous mechanical strain.

Other future extensions of this work can be divided into the implementation of fibre optic sensors for fundamental research into PEMFCs and implementation of these diagnostic tools into commercial fuel cell plates for distributed monitoring. Of particular interest is the potential for obtaining real time data under various operating conditions to improve understanding of degradation mechanisms.

Bibliography

[1] M. Wang, H. Guo, C. Ma, Temperature distribution on the MEA surface of a PEMFC with serpentine channel flow bed, Journal of Power Sources 157 (2006) 181–187. doi:10.1016/j.jpowsour.2005.08.012.

[2] G. Hinds, M. Stevens, J. Wilkinson, M. de Posta, S. Bell, Novel in situ measurements of relative humidity in a polymer electrolyte membrane fuel cell, Journal of Power Sources 186 (2009) 52–57.

[3] R. Anderson, L. Zhang, Y. Ding, M. Blanco, H. T. Bi, D. P. Wilkinson, A critical review of gas-liquid two-phase flow in pem fuel cells, Journal of Power Sources 12 (2010) 123.

[4] J. Dillet, O. Lottin, G. Maranzana, S. Didierjean, D. Conteau, C. Bonnet, Direct observation of the two-phase flow in the air channel of a proton exchange membrane fuel cell and of the effects of a clogging/unclogging sequence on the current density distribution, Journal of Power Sources 195 (2010) 2795–2799.

[5] A. Bazylak, Liquid water visualization in PEM fuel cells: A review, International Journal of Hydrogen Energy 34 (2009) 3845–3857. doi:10.1016/j.ijhydene.2009.02.084.

[6] A. Iadicicco, A. Cusano, A. Cutolo, R. Bernini, M. Giordano, Thinned fiber bragg gratings as high sensitivity refractive index sensors, IEEE Photo 16 (2004) 1149–1151.

[7] J. Lariminie, A. Dicks, Fuel Cell Systems Explained, Wiley, New York, 2000.

[8] M. Mench, Fuel Cell Engines, John Wiley & Sons, Inc., 2008.

[9] N. Yousfi-Steiner, P. Mocoteguy, D. Candussco, D. Hissel, A. Hernandez, A. Aslanides, A review on pem voltage dergadation associated with water management: Impacts, influent factors and characterization, Journal of Power Sources 183 (2008) 260–274.

[10] H. Li, Y. Tang, Z. Wang, e. al., A review of water flooding issues in the proton exchange membrane fuel cell, Journal of Power Sources 178 (2008) 103–117.

[11] N. Djilali, P. Sui, Transport phenomena in fuel cells: from microscale to macroscale, International Journal of Computational Fluid Dynamics 22 (2008) 115–133.

[12] I. EG&G Technical Services (Ed.), Fuel Cell Handbook, Seventh Edition, U.S. Department of Energy, Office of Fossil Energy, National Energy Technology Laboratory, Morgantown, West Virginia, 2004.

[13] M. Wilkinson, M. Blanco, E. Gu, J. J. Martin, D. P. Wilkinson, J. J. Zhang, H. Wang, In situ experimental technique for measurement of temperature and current distribution in proton exchange membrane fuel cells, Electrochemical and Solid-State Letters 9 (2006) A507–A511.

[14] M. H. Wang, H. Guo, C. F. Ma, F. Ye, J. Yu, X. Liu, Y. Wang, C. Y. Wang, Temperature measurement technologies and their application in the research

of fuel cells, in: Proceedings of the 1st International Conference on Fuel Cell Science, Engineering and Technology, 2003, pp. 95–100.

[15] J. Lebæk, S. T. Ali, P. Møller, C. Mathiasen, L. P. Nielsen, S. K. Kær, Quantification of *in situ* temperature measurements on a PBI-based high temperature PEMFC unit cell, International Journal of Hydrogen Energy 35 (2010) 9943–9953. doi:10.1016/j.ijhydene.2009.10.002.

[16] M. M. Mench, D. J. Bufford, T. W. Davis, *In situ* temperature distribution measurement in an operating polymer electrolyte fuel cell, in: Proceedings of the IMECE'03 2003 ASME International Mechanical Engineering Congress & Exposition, ASME, Washington DC, (USA), 2003, p. 14 pp.

[17] G. Zhang, L. Guo, L. Ma, H. Liu, Simultaneous measurement of current and temperature distributions in a proton exchange membrane fuel cell, Journal of Power Sources 195 (2010) 3597–3604. doi:10.1016/j.jpowsour.2009.12.016.

[18] S. He, M. M. Mench, S. Tadigadapa, Thin film temperature sensor for real-time measurement of electrolyte temperature in a polymer electrolyte fuel cell, Sensors and Actuators A 125 (2006) 170–177. doi:10.1016/j.sna.2005.05.021.

[19] C.-Y. Lee, S.-J. Lee, C.-L. Hsieh, Application of micro sensor on diagnosis of micro fuel cells, in: Proceedings of the 2nd IEEE international conference on Nano/Micro Engineered Molecular Systems, IEEE, 2007, pp. 434–437.

[20] J.-R. Lee, H. Tsuda, B.-Y. Koo, Single-mode fibre optic Bragg grating sensing on the base of birefringence in surface-mounting and embedding applications, Optics & Lasers Technology 39 (2007) 157–164.

[21] K.-H. Lee, Y.-D. Su, S.-J. Chen, F.-G. Tseng, G.-B. Lee, Microfluidic systems integrated with two-dimensional surface plasmon resonance phase imaging systems for microarray immunoassay, Biosensors and Bioelectronics 23 (2007) 466–472.

[22] Chi-Yuan Lee, Guan-Wei Wu, Chi-Lieh Hsieh, In situ diagnosis of micrometallic proton exchange membrane fuel cells using microsensors, Journal of Power Sources 172 (2007) 363–367. doi:10.1016/j.jpowsour.2007.07.032.

[23] K.-S. Lee, R. H. Kim, D.-Y. Yang, S. H. Park, Advances in 3D nano/microfabrication using two-poton initiated polymerization, Prog. Polym. Sci. 33 (2008) 631–681.

[24] C.-Y. Lee, C.-H. Lin, A novel integration approach for combining the micro thermal sensor and stainless steel foil as gas diffusion layer in micro fuel cell, Renewable Energy 35 (2010) 759–762. doi:10.1016/j.renene.2009.09.011.

[25] C.-Y. Lee, C. Chang, P.-C. Chan, R.-D. Huang, M.-S. Tong, Fabrication of Micro-sensors based on a parylene thin-film substrate for monitoring proton exchange membrane fuel cells, in: Proceedings of the 2010 5th IEEE International Conference on Nano/Micro Engineered and Molecular Systems, IEEE, Xiamen (CN), 2010, pp. 102–105.

[26] C.-Y. Lee, C. Chang, W.-J. Hsieh, W.-Y. Fan, C.-Y. Huang, C.-Y. Chao, Flexible micro-sensors on stainless steel foil for monitoring proton exchange membrane fuel cells, in: Proceedings of the 2010 5th IEEE International Conference on Nano/Micro Engineered and Molecular Systems, 2010, pp. 106–109.

[27] C. Lee, F. Weng, C. Cheng, H. Shiu, Shiqah-Ping Jung, Wen-Chen Chang, Pin-Cheng Chan, Wen-Ting Chen, Chung-Ju Lee, Use of flexible micro-temperature sensor to determine temperature *in situ* and to simulate a pro-

ton exchange membrane fuel cell, Journal of Power Sources 196 (2011) 228–234. doi:10.1016/j.jpowsour.2010.06.051.

[28] T. J. McIntyre, W. P. Partridge, S. W. Allison, L. C. Maxey, M. R. Cates, C. L. Britton, R. Lenarduzzi, T. J. Toops, T. K. Plant, Fiber optic temperature sensors for PEM fuel cells, Presentation Department of Energy Hydrogen, Fuel cells, and Infraestructure program revier meeting (2005).
URL `http://www.hydrogen.energy.gov/pdfs/progress04/ivh4_mcintyre.pdf`

[29] K. Inman, X. Wang, B. Sangeorzan, Design of an optical thermal sensor for proton exchange membrane fuel cell temperature measurement using phosphor thermometry, Journal of Power Sources 195 (2010) 4753–4757. doi:10.1016/j.jpowsour.2010.02.071.

[30] S. Tao, J. C. Fanguy, X. Hu, Q. Yan, Fiber optic sensors for *in situ* real-time monitoring PEM fuel cell operation, in: Proceedings of FUELCELL2005 Third International Conference on Fuel Cell Science, Engineering and Technology, ASME, Ypsilanti, Michigan (US), 2005, pp. 231–234.

[31] N. A. David, P. M. Wild, J. Hu, N. Djilali, In-fibre Bragg grating sensors for distributed temperature measurement in a polymer electrolyte membrane fuel cell, Journal of Power Sources 192 (2009) 376–380. doi:10.1016/j.jpowsour.2009.03.021.

[32] N. A. David, P. M. Wild, J. Jensen, T. Navessin, N. Djilali, Simultaneous in situ measurement of temperature and relative humidity in a PEMFC using optical fiber sensors, Journal of The Electrochemical Society 157 (8) (2010) B1173–B1179. doi:10.1149/1.3436652.

[33] S. Basu, H. Xu, M. W. Renfro, B. M. Cetegen, *In situ* optical diagnostics for measurements of water vapor partial pressure in PEM fuel cell, Journal of Fuel Cell Science and Technology 3 (2006) 1–7. doi:10.1115/1.2133799.

[34] S. Basu, M. W. Renfro, H. Gorgun, B. M. Cetegen, *In situ* simultaneous measurements of temperature and water partial pressure in a PEM fuel cell under steady state and dynamic cycling, Journal of Power Sources 159 (2006) 987–994. doi:10.1016/j.jpowsour.2005.11.091.

[35] S. Basu, M. Renfro, B. Cetegen, Spatially resolved optical measurements of water partial pressure and temperature in a PEM fuel cell under dynamic operating conditions, Journal of Power Sources 162 (2006) 286–293. doi:10.1016/j.jpowsour.2006.06.073.

[36] R. Sur, T. Boucher, M. Renfro, B. Cetegen, In situ measurements of water vapor partial pressure and temperature dynamics in a PEM fuel cell, Journal of The Electrochemical Society 157 (1) (2010) B45–B53. doi:10.1149/1.3247355.

[37] G. Hinds, M. Stevens, J. Wilkinson, M. de Podesta, S. Bell, Novel *in situ* measurements of relative humidity in a polymer electrolyte membrane fuel cell, Journal of Power Sources 186 (2009) 52–57. doi:10.1016/j.jpowsour.2008.09.109.

[38] Z. Chen, C. Lu, Humidity sensors: A review of materials and mechanisms, Sensor Letters 3 (2005) 274–295.

[39] R. H. Perry, D. W. Green (Eds.), Perry's Chemical Engineers' Handbook, 8th Edition, McGraw-Hill, 2007.

[40] Sensirion, Datasheet SHT7x (SHT71, SHT75) Humidity and Temperature Sensor, Online (2010).
URL `http://www.sensirion.com/en/pdf/product_information/Datasheet-humidity-sen`

[41] O. Herrera, W. Mérida, D. P. Wilkinson, Sensing electrodes for failures diagnostics in fuel cells, Journal of Power Sources 190 (2009) 103–109. doi:10.1016/j.jpowsour.2008.08.034.

[42] M. Mench, Q. Dong, C. Wang, In situ water measurements in a polymer electrolyte fuel cell, Journal of Power Sources 124 (2003) 90–98.

[43] W. P. Partridge, T. J. Toops, J. Green, T. R. Armstrong, Intra-fuel cell stack measurements of transient concentration distributions, Journal of Power Sources 160 (2006) 454–461.

[44] J. Wu, X. Z. Yuan, H. Wang, M. Blanco, J. J. Martin, J. Zhang, Diagnostic tools in PEM fuel cell research: Part II Physical/chemical methods, International Journal of Hydrogen Energy 33 (2008) 1747–1757. doi:10.1016/j.ijhydene.2008.01.020.

[45] Z. Zhang, J. Martin, J. Wu, H. Wang, K. Promislow, B. Balcom, Magnetic resonance imaging of water content across the nafion membrane in an operational fuel cell, Journnal of magnetic resonance 193 (2008) 259–266.

[46] D. Hussey, D. Jacobson, M. Arif, J. Owejan, J. Gagliardo, T. Trabold, Neutron images of the through-plane water distribution of an operating fuel cell, Journal of Power Sources 172 (2007) 225–228.

[47] I. Manke, C. Hartnig, N. Kardjilov, H. Riesemeier, J. Goebbles, R. Kuhn, P. Kruger, J. Banhart, In situ synchrotron x-ray radiography investigations of water transport in pem fuel cells, Fuel Cells 10 (2010) 26–34.

[48] D. Conteau, C. Bonnet, D. Funfschilling, M. Weber, S. Didierjean, F. Lapicque, Detection of liquid water in pem fuel cells' channels: design and validation of a microsensor, Fuel Cells 4 (2010) 520–529.

[49] Q. Wang, L. Zhang, C. Sun, Q. Yu, Multiplexed fiber-optic pressure and temperature sensor system for down-hole measurements, IEEE Sensors 8 (2008) 1879–1883.

[50] Y.-J. Rao, D. J. Webb, D. A. Jackson, L. Zhang, I. Bennion, In-fiber Bragg-grating temperature sensor system for medical applications, J. Lightwave Technol. 15 (5) (1997) 779–785.

[51] T. L. Yeo, T. Sun, K. T. V. Grattan, Fibre-optic sensor technologies for humidity and moisture measurement, Sensors and Actuators A 144 (2008) 280–295.

[52] P. Kronenberg, P. K. Rastogi, P. Giaccari, H. G. Limberger, Relative humidity sensor with optical fiber bragg gratings, Optics Letters 27 (16) (2002) 1385–1387.

[53] H. Lim, K. Chang, C. Su, e. al., Bubble velocity, diameter, and void fraction measurements in a multiphase flow using fiber optic reflectometer, Review of Scientific Instruments 79 (12) (2008) 125105.

[54] M. Pettigrew, C. Zhang, N. Mureithi, D. Pamfil, Detailed flow and force measurements in a rotated triangular tube bundle subjected to two-phase cross-flow, Journal of Fluids and Structures 20 (2005) 567–575.

[55] S. G. Lipson, H. Lipson, D. S. Tannhauser, Optical Physics, Cambridge University Press, 2001.

[56] E. Udd (Ed.), Fiber Optics Sensors: An Introduction for Engineers and Scientists, Wiley, New York, 1991.

[57] B. Lee, Review of the present status of optical fiber sensors, Optical Fiber Technology 9 (2003) 57–79.

[58] R. Measures, Structural Monitoring With Fiber Optic Technology, Academic Press, San Diego, 2001.

[59] M. Majunder, T. K. Gangopadhyay, A. K. Chakroborty, K. Dasgupta, D. K. Bhattacharya, Fibre Bragg gratings in structural health monitoring - Present status and applications, Sensors and Actuators A 147 (2008) 150–164.

[60] Yun-Jiang Rao, In-fibre Bragg grating sensors, Meas. Sci. Technol. 8 (4) (1997) 355–375. doi:10.1088/0957-0233/8/4/002.

[61] T. L. Yeo, T. Sun, K. T. V. Grattan, D. Parry, R. Lade, B. D. Powell, Polymer-coated fiber bragg grating for relative humidity sensing, IEEE Sensors 5 (5) (2005) 1082–1089.

[62] K. O. Hill, G. Meltz, Fiber bragg grating technology fundamentals and overview, Journal of Lightwave Technology 15 (1997) 1263–1276.

[63] T. Edrogan, V. Mizrahi, P. J. Lemaire, D. Monroe, Decay of ultraviolet-induced fiber bragg gratings, Journal of Applied Physics 76 (1994) 73.

[64] Y.-J. Rao, In-fibre bragg grating sensors, Measurement Science and Technology 8 (1997) 355–375.

[65] L. Wang, Y. Liu, M. Zhang, D. Tu, X. Mao, Y. Liao, A relative humidity sensor using a hydrogel-coated long period grating, Measurement Science and Technology 18 (2007) 3131–3134.

[66] Micron Optics, Optical fiber sensors guide Fundamental & Applications (2005 2005).

[67] K. Schroeder, W. Ecke, R. Willsch, Optical fiber bragg grating hydrogen sensor based on evanescent-field interaction with palladium thin-film transducer, Optics and Lasers in Engineering 47 (2009) 1018–1022.

[68] P. Giaccari, H. G. Limberger, P. Kronenberg, in: Influence of humidity and temperature on polyimide-coated fiber Bragg gratings, in: Proceedings OSA Trends in Optics and Photonics Series: Bragg gratings, Photosensitivity, Poling in Glass Waveguides, vol. 61, Washington, DC, USA, p. BFB2.

[69] W. Cao, Y. Duan, Optical fiber-based evanescent ammonia sensor, Sensors and Actuators B 110 (2005) 252–259.

[70] A. Leung, M. Shankar, R. Mutharasan, A review of fiber-optic biosensors, Sensors and Actuators B 125 (2007) 688–703.

[71] J. Chen, W. Bock, P. Mikulic, Simple fiber-optic refractive index sensor based on evanescent higher order modes, in: Proceedings of the SPIE, Vol. 7386, 2009, pp. 73861K–1–73861K–6.

[72] W. Liang, Y. Huang, Y. Xu, R. K. Lee, A. Yariv, Highly sensitive fiber Bragg grating refractive index sensors, Appl. Phys. Lett. 86 (2005) 151122 (3pp).

[73] J. Dakin, B. Culshaw, Optical FIber Sensors: Principles and Components, Artech House, Inc., 1988.

[74] K. Zhou, Y. Lai, X. Cheng, K. Sugden, L. Zhang, I. Bennion, A refractometer based on a micro-slot in a fiber Bragg grating formed by chemically assisted femtosecond laser processing, Opt. Express 15 (24) (2007) 15848–15853.

[75] H. Alemohammad, E. Toyserkani, J. Pinkerton, Femtosecond laser micromachining of fibre Bragg grating for simultaneous measurement of temperature and concentration of liquids, J. Phys. D: Appl. Phys. 41 (2008) 185101.

[76] G. Meltz, S. J. Hewlett, J. D. Love, Fiber grating evanescent-wave sensors, in: Proceedings of the SPIE, Vol. 2836, 1996, pp. 342–350.

Appendix A

In-fibre Bragg grating sensors for distributed temperature measurement in a polymer electrolyte membrane fuel cell

Journal of Power Sources 192 (2009) 376–380

Contents lists available at ScienceDirect

Journal of Power Sources

journal homepage: www.elsevier.com/locate/jpowsour

Short communication

In-fibre Bragg grating sensors for distributed temperature measurement in a polymer electrolyte membrane fuel cell

Nigel A. David*, Peter M. Wild, Jingwei Hu, Nedjib Djilali

Department of Mechanical Engineering, University of Victoria, Canada

ARTICLE INFO

Article history:
Received 25 January 2009
Received in revised form 5 March 2009
Accepted 6 March 2009
Available online 19 March 2009

Keywords:
Fibre Bragg grating
Polymer electrolyte membrane fuel cell
Temperature

ABSTRACT

A new application of in-fibre Bragg grating (FBG) sensors for the distributed measurement of temperature inside a polymer electrolyte membrane fuel cell is demonstrated. Four FBGs were installed on the lands between the flow channels in the cathode collector plate of a single test cell, evenly spaced from inlet to outlet. *In situ* calibration of the FBG sensors against a co-located micro-thermocouple shows a linear, non-hysteretic response, with sensitivities in good agreement with the expected value. A relative error of less than 0.2 °C over the operating range of the test cell (∼ 20–80 °C) was achieved, offering sufficient resolution to measure small gradients between sensors. While operating the fuel cell at higher current densities under co-flow conditions, gradients of more than 1 °C were measured between the inlet and outlet sensors. Due to their small thermal mass, the sensors also exhibit good temporal response to dynamic loading when compared with the thermocouple. Design and instrumentation of the graphite collector plate features minimal intrusion by the sensors and easy adaptation of the techniques to bipolar plates for stack implementation.

1. Introduction

Heat and water management are two of the most critical determinants of PEM fuel cell performance and have consequently been the subject of numerous experimental and theoretical studies [1–5]. Progress in fully controlling heat and water transport has been limited by the coupling of the processes, lack of understanding of some of the underlying mechanisms, and limitations of experimental techniques. Recent multi-physics computational models have provided significant insight, but their predictive capabilities are not entirely established due to the limited availability of *in situ* experimental measurements [5].

Measurement of the temperature distribution inside an operating fuel cell has been reported by a handful of groups using methods involving electrical based microsensors and optical techniques. Wilkinson and coworkers used a series of micro-thermocouples embedded in the graphite collector plate of a single test fuel cell to measure the temperature at the interface of the gas diffusion layer (GDL) and the graphite plate [6]. They demonstrated this as a useful technique for indirectly mapping the current density across the active area of cell, but only half of their sensors were operational during the experiments due to the fragility of the fine leads.

Micro-fabricated thin film thermistor based temperature sensors were demonstrated by He et al. for measuring the temperature inside a PEM bilayer [7]. The 16 μm thick and 0.25 mm^2 sensors were positioned at the reactant inlet and outlet, and showed a linear response *in situ*, even as the membrane swelled from hydration. Microsensors for the *in situ* measurement of temperature and humidity in micrometallic fuel cells were demonstrated by Lee et al. [8]. These sensing techniques could be useful for studying fundamental heat transfer in PEM fuel cells, but due to the custom nature of the MEAs and elaborate fabrication processes, their scope of application is limited.

An optical technique that does not require the preparation of a custom MEA is described by Wang et al. An infrared camera was used to view the anode side of a fuel cell under different operating temperatures and current densities [9]. They report a temperature resolution of less than 0.3 °C with their technique, and were able to clearly observe gradients of up to 5 °C from inlet to outlet at higher current densities. The gradients were attributed to increased current density along the flow path resulting from increased water production at the cathode, hydrating the membrane more towards the outlet.

Wang et al. see this method as a means of locating hot spots (local higher temperature regions); aiding in proper thermal management and, ultimately, to suggest better cell design. This technique is limited in its application, however, as the anode polar plate needs to

---

* Correspondingauthor at: Department of Mechanical Engineering, University of Victoria, PO Box 3055 STN CSC, Victoria, BC, Canada V8W 3P6. Tel.: +1 250 853 3198; fax: +1 250 721 6323.

E-mail address: nadavid@uvic.ca (N.A. David).

0378-7753/$ – see front matter © 2009 Elsevier B.V. All rights reserved.
doi:10.1016/j.jpowsour.2009.03.021

be modified with a barium fluoride window, allowing it to be transparent to infrared light for camera viewing. It can, therefore, only be applied to a single cell, or an end cell of a stack. Optical access into a PEM fuel cell is also required in the technique recently developed by Basu et al. [10]. They use tunable diode laser absorption spectroscopy to measure water partial pressure and temperature along individual flow channels of a prototype cell. The temperature measurements however, are not sufficiently accurate nor spatially well resolved for the detailed study of temperature distribution inside a fuel cell.

In this paper, fibre-optic based measurements are presented based on a novel application of in-fibre Bragg grating (FBG) sensors. The use of FBGs is particularly well suited for *in situ* measurements. Optical fibres are not only sufficiently small for minimal impact on cell performance, but when coated with polyimide FBGs are immune to moisture and the electrochemically active environment found inside the cell. In addition, being optical devices, they are inherently insensitive to electromagnetic interference.

2. In-fibre Bragg grating sensing principle

A FBG typically consists of a short segment of single mode optical fibre with a photoinduced periodically modulated index of refraction. See Fig. 1(a). When the grating is illuminated with broadband light, the reflected power spectrum has structure caused by interference of the light with the planes of the grating, much like Bragg diffraction. See Fig. 1(b). The peak of the spectrum in this case occurs at a wavelength corresponding to twice the optical path length between adjacent planes, and is called the Bragg wavelength, $\lambda_B = 2\Lambda n$, where n is the index of refraction of the silica fibre and Λ is the grating pitch. When the grating is subjected to mechanical or thermal strain its pitch changes, causing a shift in the Bragg wavelength.

This shift is given by

$$\frac{\Delta\lambda_B}{\lambda_B} = (1 - Pe)\varepsilon + [(1 - Pe)\alpha + \xi]\Delta T, \qquad (1)$$

where Pe is the photo-elastic constant of the fibre, ε is the mechanical strain induced in the fibre, α is the coefficient of thermal expansion of the optical fibre, and ξ is the thermo-optic coefficient.

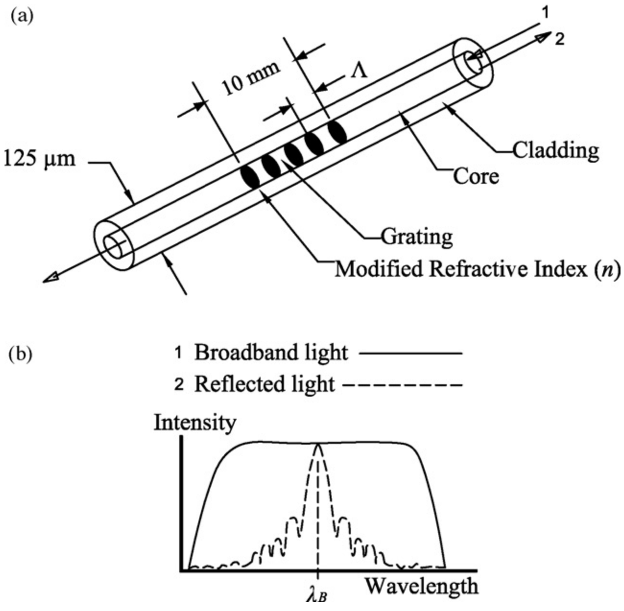

Fig. 1. Schematic of an in-fibre Bragg grating sensor.

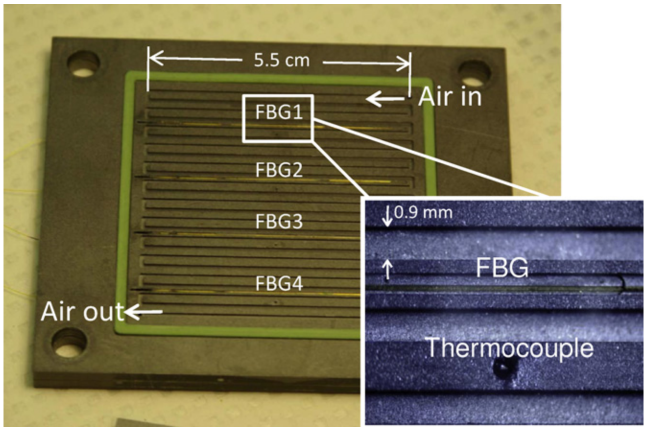

Fig. 2. Graphite bipolar plate with four FBG sensors.

A comprehensive review of FBGs, along with a description of many of their important applications can be found in Rao [11].

3. Experimental setup

3.1. Instrumentation

The FBGs used in this work are 10 mm long, with a nominal room temperature Bragg wavelength of 1550 nm. These are available for purchase from Micron Optics, Inc., Atlanta, GA (model os1100). The standard single mode fibre on to which they are written is 125 μm in diameter and is coated with a thin polyimide layer for durability. The FBG data for calibration and *in situ* measurements is collected with a Micron Optics, Inc. sm130 interrogation unit, with a specified wavelength resolution of 0.1 pm at 10 Hz sampling rate.

Four FBGs have been embedded in the lands separating the serpentine flow channels of a custom two-piece graphite cathode plate machined in house. A top view of this plate is shown in Fig. 2. The fibres lie in milled grooves, 150 μm deep, such that they are not compressed when the cell is assembled and clamped. Deeper sections were milled directly underneath the FBGs to eliminate conductive heat transfer with the graphite plate and ensure the temperature measured by the FBGs is more representative of the MEA. A schematic of the instrumentation is shown in Fig. 3(b).

The two major design challenges of instrumenting the FBGs were limiting bending of the fiber as it entered the cell, and isolating it from strain, which could cause unpredictable measurements. To limit bending, an angled hole was drilled at one end of the groove next to the gasket, connecting to a relief channel milled in the graphite backing plate. This is shown in the schematic of Fig. 3(b). In addition to having a sufficiently deep groove for the FBG to lie in without being compressed by the MEA, cyanoacrylate adhesive was used to fix the fibre in place, isolating it from any strain transferred from outside the cell.

A miniature T-type thermocouple with a wire diameter of 0.13 mm from Omega Engineering, Inc. (Stamford, CT) was installed adjacent to the FBGs for their calibration. The thermocouple was inserted into a 300 μm hole drilled perpendicular to the graphite plate and potted in silicone for insulation. As shown in the schematic of Fig. 3, the thermocouple junction lies in the same plane as the FBGs and, therefore, is well situated for calibration purposes and also provides a comparative measurement during *in situ* testing of the fuel cell.

3.2. Test cell

The instrumented graphite plate described above was sized to fit into a pre-existing test fuel cell assembly in our laboratory. The

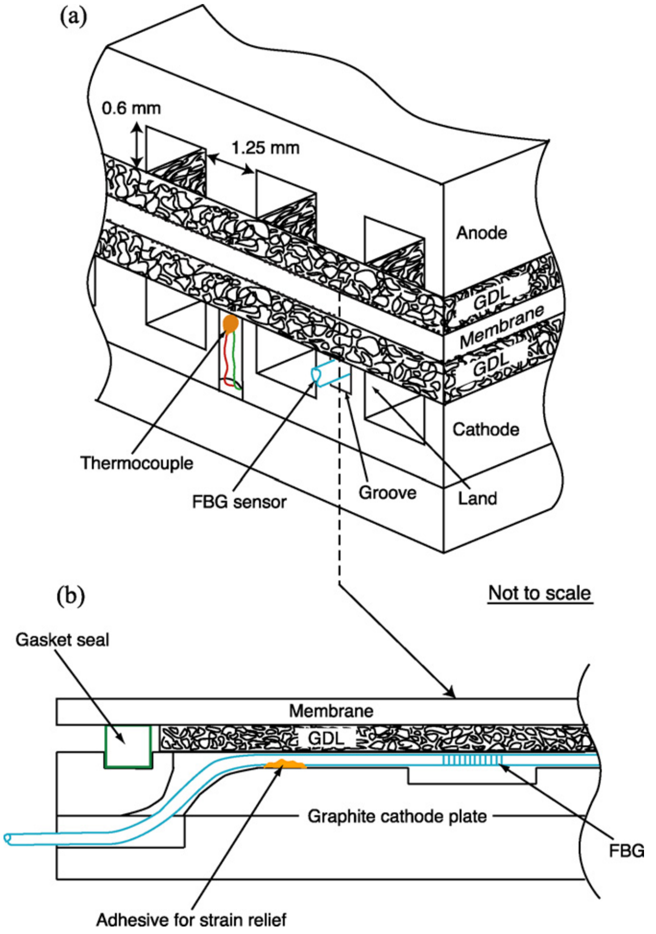

Fig. 3. Schematic of the *in situ* FBG sensor with adjacent thermocouple for calibration (a). The side view schematic in (b) shows how the FBGs were installed into the two-piece graphite cathode plate.

assembly consists of gold plated current collector plates, and stainless steel manifolds for gas distribution and water circulation for the cell heating system. This assembly can be seen in Fig. 4, where the fibre optics are also shown entering the cathode plate.

MEAs for the test cell were fabricated at the National Research Council Institute for Fuel Cell Innovation, Vancouver, Canada. An active area of 30.25 cm^2, with platinum loading of 0.4 mg/cm^2 was achieved by masking and spray deposition of a carbon catalyst ink onto Nafion © 115 membrane. The GDL used for the MEAs is Toray paper with 10% PTFE content and was hot pressed onto the carbon catalyst.

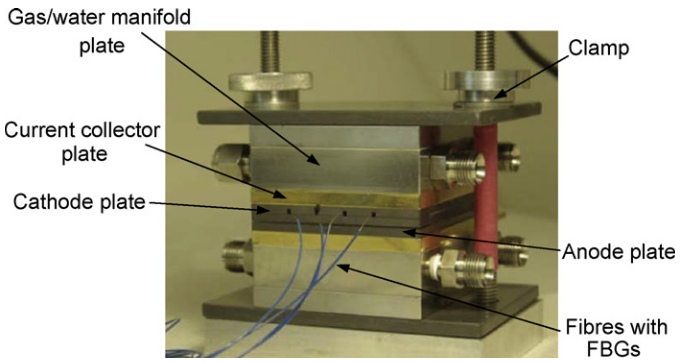

Fig. 4. Photograph of the the single test cell assembly. The cell temperature is set by circulating deionized water from a temperature controlled bath in the test station through the stainless steel plates on either side of the cell.

Table 1
Sensitivities of the four FBG sensors calibrated before and afer experimental testing, 11 days apart.

FBG	Sensitivity (pm °C^{-1})	Sensitivity after 11 days
1	10.84	10.76
2	10.73	10.69
3	10.85	10.81
4	10.84	10.79

The test cell is operated using a Ballard 3kW fuel cell test station, which enables the control of the fuel and oxidant flow rate, and the cell temperature with a water heating system. The current density of the fuel cell is varied using an electronic load bank (Dynaload Inc., MCL488, Hackettstown, NJ) that is connected via copper leads to the gold plated collector plates on either side of the single cell. The cell voltage and the thermocouple voltage were measured using analog inputs on a 16 bit data acquisition device (National Instruments Inc.).

4. Experimental methods

4.1. Calibration

Calibration of the four FBGs was routinely carried out before and after acquisition of each data set. The FBGs were calibrated against the thermocouple situated in the same plane as the fibres. See Fig. 3. To reproduce the *in situ* environment, the sensors were covered with a piece of GDL and then clamped between half inch aluminum plates. The high thermal conductivity of aluminum minimizes the potential for thermal gradients within the assembly and allows for thermal cycling in a reasonable amount of time. The assembly was placed in a programmable laboratory convection oven (Cascade Tek Inc., Hillsboro, OR), and cycled between ~ (30–70 °C) at a rate of ~ 0.2 °C/min. Each data point from the thermocouple was taken as the mean value of 100 samples acquired at a rate 1 kHz, resulting in a resolution of approximately ~ 0.05 ° C for these measurements.

4.2. In situ testing

As a baseline case for the *in situ* measurements, the current was set to zero, and only the cell temperature was varied using the water heating system. This was to provide a reference for the temperatures measured by the FBGs while drawing current from the cell with the load bank.

For the case of cell operation, the hydrogen and air were fed into the cell in co-flow mode at a flow rate of 1.0 standard liters per minute and a pressure of 15 psi. The cell was first conditioned at

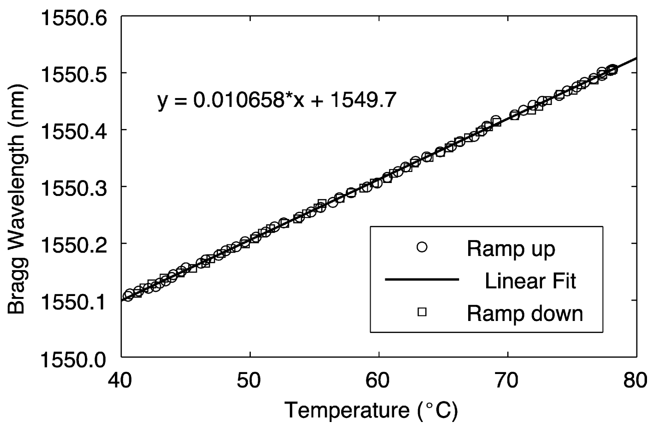

Fig. 5. Calibration data for one of the FBG sensors.

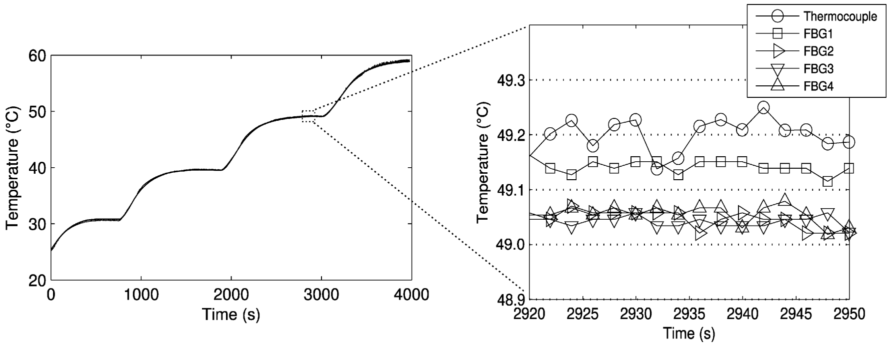

Fig. 6. FBG and thermocouple measurements under varying temperature and zero current conditions.

room temperature with a current density of 0.3 A cm^{-2} for approximately 30 min to humidify the membrane. The current was then increased incrementally like for obtaining polarization curve. During testing, temperature data were taken from the FBGs sensors and the co-located thermocouple every 2 s to gain dynamic information of the temperature profile at the MEA/graphite plate interface inside the cell.

5. Results and discussion

5.1. Calibration

A representative calibration curve for one of the FBGs is presented in Fig. 5 and shows that there is essentially no hysteresis. The sensitivity of this particular FBG was determined to be 10.7 pm $^{\circ}C^{-1}$, from a linear fit to the data, which is in good agreement with the literature [11]. There was good agreement between the four sensors, as well as good repeatability; Table 1 shows the sensitivities of all four FBGs measured 11 days apart. By interrogation of the FBGs using the Micron Optics unit, a temperature resolution of 0.01 ° C for the individual FBG sensors was possible.

5.2. In situ tests

Shown in Fig. 6 are the results from the base case in which temperature was varied under zero current conditions. As seen in the close up, a maximum spread of 0.2 ° C was measured between the sensors. This very small offset could be due to the position of the sensors relative to the inlet of the heating water, with FBG1 and the thermocouple being nearest the water inlet.

If the temperature across the cell were indeed uniform, with no gradient induced by the heating system, the data from this baseline would indicate a relative uncertainty between the sensors over the measurement range shown. With this established, any temperature gradients higher than 0.2 ° C during cell operation could be attributed to factors other than the heating system, namely local current flow and associated irreversibilities.

Departure from the baseline case temperature profile was clearly seen while drawing current through the cell at the different cell temperatures. Fig. 7 shows the results of a case where the cell temperature was set to 50 °C. The current was increased from 6 to 12 A allowing the cell voltage to reach steady state in between steps. The most prominent features are the jumps in temperature measured by all the sensors, including the thermocouple; these jumps correlate with each step change in current. The data shows that there is no apparent lag in the response time of the FBGs compared to the thermocouple, which is indicative of their comparable sizes, and location relative to the MEA. In addition, the thermocouple data lies just above FBG1, which is consistent with its physical location and the apparent gradient in temperature across the cell.

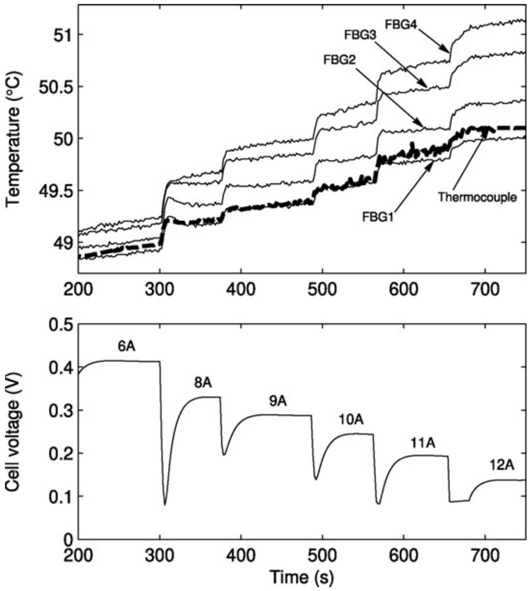

Fig. 7. Time response of FBG and thermocouple (top) with increasing cell current (below). Water temperature for the cell heating system was maintained constant at 50 °C.

An increased in temperature with current draw was expected to be measured by all sensors due primarily to ohmic losses, but gradients across the cell of more than 1 ° C were also observed. Shown in Fig. 8 are the temperatures measured by the FBGs plotted against their location for the same time series of Fig. 7. A positive gradient from inlet to outlet is clearly shown and becomes larger at higher currents indicating a non-uniform current density across the cell. This is consistent with the experimental observations of Wang

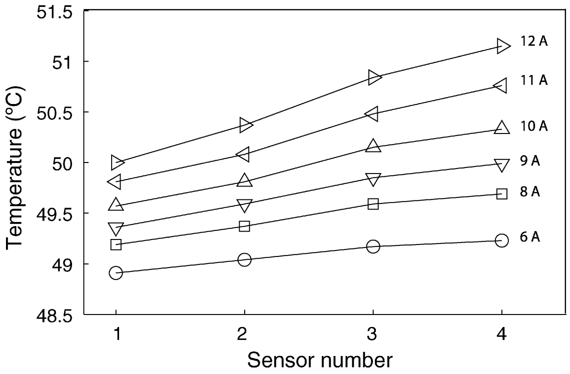

Fig. 8. Temperature profiles for different current densities with cell temperature set near 50 ° C with water heating system.

et al. who attributed this to the improved humidification of the membrane towards the outlet resulting in higher current densities [9].

6. Conclusions

The research presented here demonstrates that FBGs can be embedded inside a PEM fuel cell to reliably measure temperature dynamically with a relative resolution of less than 0.2°. In the interest of improved cell design, this relatively inexpensive technique could prove useful as a diagnostic tool to identify hot spots on the membrane, or as an indirect means of determining current distribution across the cell as done by Wilkinson et al. [6].

Further improvement of the technique will involve the multiplexing of several FBGs on a single fiber. This will increase the number of measurement points from four to upwards of ten resulting in the possibility for truly distributed temperature data within a an operating fuel cell, and the eventual extension of the technique to multi-point monitoring in complete stacks.

Acknowledgements

This work was funded by the Natural Sciences and Engineering Research Council (NSERC) of Canada. Access to the NRC Institute for Fuel Cell Innovation, Vancouver, Canada, and the assistance of Dr. Titichai Navessin in fabricating MEAs is gratefully acknowledged.

References

[1] A. Rowe, X. Li, Journal of Power Sources 102 (2001) 82–96.
[2] N. Djilali, D. Lu, International Journal of Thermal Sciences 41 (2002) 29–40.
[3] A.Z. Weber, J. Newman, Journal of the Electrochemical Society 153 (2006) A2205–A2214.
[4] A. Faghri, Z. Guo, International Journal of Heat and Mass Transfer 48 (2005) 3891–3920.
[5] N. Djilali, Energy 32 (2007) 269–280.
[6] M. Wilkinson, M. Blanco, E. Gu, J.J. Martin, D. Wilkinson, J.J. Zhang, H. Wang, Electrochemical and Solid-State Letters 9 (11) (2006) A507.
[7] S. He, M.M. Mench, S. Tadigadapa, Sensors and Actuators A 125 (2006) 170.
[8] C.-Y. Lee, G.-W. Wu, C.-L. Hsieh, Journal of Power Sources 172 (2007) 363–367.
[9] M. Wang, H. Guo, C. Ma, Journal of Power Sources 157 (2006) 181.
[10] S. Basu, M.W. Renfro, B.M. Cetegen, Journal of Power Sources 162 (2006) 286.
[11] Y.-J. Rao, Measurement Science and Technology 8 (1997) 355–375.

Appendix B

Parametric Study of a Polymer-Coated Fibre-Optic Humidity Sensor

Parametric Study of a Polymer-Coated Fibre-Optic Humidity Sensor

Nigel A. David, Peter M. Wild, Ned Djilali

Department of Mechanical Engineering and Institute for Integrated Energy Systems,
University of Victoria

Abstract. A relative humidity sensor based on polymer coated optical fibre Bragg gratings is presented. This fully functional sensor has response time and resolution comparable to the current capacitive RH sensors but with greater applicability. In this paper, numerical and experimental methods are used to determine the affects of coating thickness and fibre diameter on the response time and sensitivity of Bragg gratings coated with Pyralin. Transient results indicate that coating thicknesses of less than 4μm are needed to achieve a response time of 5 s, competitive with commercial capacitive RH sensors. Using thin coatings of $\sim$2 μm, for a short response time, sensors with reduced fibre diameter were fabricated and tested under steady state, transient and saturated conditions. By chemical etching from 125 μm to 20 μm, the sensitivity increased by a factor of seven. Such an increase in sensitivity allows for the resolution and response time of the Pyralin-coated sensor to be comparable to commercial capacitive RH sensors. These characteristics, in addition to the sensors rapid recovery from saturation in liquid water, indicates good potential for use of this sensor design in applications where electronic RH sensors are not suitable.

Submitted to: *Meas. Sci. Technol.*

Table 1. Table of nomenclature

λ_B	Bragg wavelength
ε_i	principal strains
n_0	effective index of refraction
ξ	thermo-optic coefficient
P_e	effective strain-optic coefficient
α	coefficient of thermal expansion
S_T	sensitivity to temperature
S_{RH}	sensitivity to RH
k	stiffness weighting factor
β	coefficient of hygroscopic expansion
E	Young's modulus
A	cross sectional area
η	moisture concentration
D	diffusion coefficient
τ_{63}	1/e response time

1. Introduction

Relative humidity (RH) is a parameter that must be measured and controlled in many environments and industrial processes. Many of the miniature RH sensors on the market today are capacitive, and based on MEMS technology [1]. These types of sensors offer low-cost, accurate, fast response measurements over a large humidity range, satisfying the demands of most applications. In some instances, however, the sensor size, and inability to recover quickly from saturation are limiting factors in their usage. Further limitations are typical of electronic sensors, such as the need to isolate the leads from electromagnetic interference and the restricted ability of multi-channel multiplexing.

An application where the limitations of miniature capacitive RH sensors have become evident is in polymer electrolyte membrane fuel cells (PEMFCs). Humidity levels in the gas streams of commercial PEMFCs often need to be controlled to achieve optimal performance [2, 3]. Recent *in situ* measurements across the active area of a single cell have indicated significant gradients in RH arising during cell operation [4, 5]. These gradients, if extending over the relatively large active area of commercial fuel cell stacks, could be a source of performance loss and degradation. Further understanding of this phenomenon requires non-invasive distributed measurements of RH in commercial PEMFC stacks.

The current commercially available miniature RH sensors are not particularly well suited for use in fuel cells. The sensor size is too large for the confined flow channels; the sensors are slow to recover from condensation, which is common in a PEMFC; the sensor leads need to be carefully isolated since a fuel cell is electrically active; and there is limited space inside the PEMFC for multiple leads that would be required for distributed measurements.

Fibre optic sensors, unlike the current capacitive RH sensors, have the advantages of being intrinsically small and immune to electromagnetic interference. Among the fibre optic sensor technologies for humidity measurement discussed in a recent review by Yeo *et al.* [6], the polymer-coated fibre Bragg grating (FBG) RH sensor stands out for having a wide measurement range combined with the capability of multiplexing several sensors on a single fibre. Multiple studies have shown these sensors to have a linear, reversible, and accurate response over the range of 10-100% RH [7, 8, 9].

FBGs have found myriad sensing applications [10], particularly for the measurement of strain and temperature, to which an FBG is inherently sensitive. The sensing principle of the polymer-coated FBG is based on the hygroscopic expansion of the polymer coating, which induces strain in the fibre core. The strain is detected as a wavelength shift in the FBG signal. The FBG-based RH sensor was first reported by Giaccari *et al.* after researchers found that commercially available FGBs that had been recoated with polyimide were sensitive to changes in humidity [11]. Polyimide is often used for coating optical fibre and FBGs to provide increased tensile strength and durability. In addition to its favourable thermomechanical properties, polyimide exhibits fast and reversible moisture absorption, making it ideal as the sensing layer in capacitive RH sensors [1], and since the work of Giacarri, in fibre-optic RH sensors.

Sensitivity and response time of polyimide-coated FBG RH sensors have been shown to increase with increasing coating thickness. In studies by Kronenberg *et al.* [8] and Yeo *et al.* [7] FBGs were coated with the polyimide Pyralin®(HD Microsystems) and tested for steady-state sensitivity and response time, respectively. The shortest response time reported by Yeo *et al.* [7] was approximately $\tau_{63} = 5$ minutes for a coating thickness of 10μm. Thinner coatings, down to 3.6 μm, were tested by Kronenberg *et al.*, but only for steady-state sensitivity. The sensitivity of their thinnest coating sensor, which would have the shortest response time, was 0.3 pm%RH^{-1}. Optical interrogators for FBGs typical have wavelength resolution of ∼1 pm. This implies a minimum detectable change in RH of no less than 3% RH for the fast FBG RH sensor. Operating characteristics of commercial miniature capacitive RH sensors, such as the HIH-4000 from Honeywell, Inc. [12], with $\tau_{63} = 5$ s and resolution of 0.5% RH indicate a need for design improvements on the polyimide-coated FBGs sensors for them to be competitive.

Following our recent work in which the use of FBG RH sensors was demonstrated in situ in an operating fuel cell, the focus of this paper is the realization of fully functional FBG sensors with response time and resolution comparable to the current capacitive RH sensors, but with greater applicability. A numerical analysis is presented allowing systematic investigation of the effect of coating thickness and fibre diameter on the steady-state and transient response of the coated FBG sensor. The fabrication process to realize sensors with varying coating thickness and fibre diameters is described, and experimental results obtained under a range of environmental conditions are presented.

2. Methodology

2.1. Theoretical background

An FBG typically consists of a short segment of single mode optical fibre with a photo-induced periodically modulated index of refraction in the core of the fibre. When the grating is illuminated with broadband light, the reflected spectrum has a peak at the Bragg wavelength, $\lambda_B = 2\Lambda n_0$, where n_0 is the effective index of refraction of the silica fibre core and Λ is the grating pitch. The dependence of both n_0 and Λ on strain and temperature allows the use of FBGs for sensing these and other parameters. Many of the growing number of sensing applications for FBGs have been reviewed by Rao [10].

The influence of strain and temperature changes on the Bragg wavelength of an FBG sensor can be obtained by Taylor series expansion of the expression for the Bragg wavelength about a reference state of strain and temperature. Assuming zero reference strain and keeping only first order terms in the expansion, a general expression for the relative Bragg wavelength shift for unpolarized light is given by [13]

$$\frac{\Delta\lambda_B}{\lambda_B} = \varepsilon_z - \frac{n_0^2}{2}(\varepsilon_z p_{12} + \varepsilon_r(p_{11} + p_{12})) + \xi\Delta T \tag{1}$$

The first term, ε_z, is the thermally and mechanically induced axial strain in the grating, which changes the grating pitch. The second term represents the strain-optic effect, where p_{11} and p_{12} are the principal components of the strain-optic tensor and ε_z and ε_r are the corresponding axial and radial strains. The third term represents the thermo-optic effect, where ξ is thermo-optic coefficient.

For a Bragg grating written in single mode optical fibre subjected only to axial strain the following simplified version is often used [7],

$$\frac{\Delta\lambda_B}{\lambda_B} = (1 - P_e)\varepsilon_z + ((1 - P_e)\alpha + \xi)\Delta\mathrm{T}, \tag{2}$$

where

$$P_e = p_{12} - \nu(p_{11} + p_{12}) \tag{3}$$

represents the effective strain optic coefficient in which the radial strain is accounted for by the Poisson effect. Equation 2 is a superposition of the mechanical and thermal response of the FBG; α is the coefficient of thermal expansion (CTE) of the fibre; and ξ is the thermo-optic coefficient.

For a polymer-coated FBG humidity sensor, shown in Fig. 1, the RH and temperature induced axial strain in the fibre can be separated as follows:

$$\frac{\Delta\lambda_B}{\lambda_B} = (1 - P_e)\varepsilon_{RH} + (1 - P_e)\varepsilon_T + \xi\Delta T \tag{4}$$

$$\frac{\Delta\lambda_B}{\lambda_B} = S_T\Delta\mathrm{T} + S_{RH}\Delta\mathrm{RH}. \tag{5}$$

S_T and S_{RH} are the temperature and RH sensitivity coefficients, respectively. To relate the RH sensitivity to material properties, one may express S_{RH} as the sum of a mechanical and a strain-optic contribution:

$$S_{RH} = (1 - P_e)k\beta_c \; [\%RH^{-1}]. \tag{6}$$

k is a stiffness-weighting factor for the coefficient of hygroscopic expansion, β_c, of the polymer coating.

The one-dimensional (1-D) model of the sensor used by Kronenberg *et al.* [8], in which radial strain is neglected, consists of an infinitely long bi-material rod in which the two materials adhere perfectly. See Fig. 1. Plain strain and plain stress are assumed in this model. The axial stresses in the materials must balance at equilibrium according to,

$$\sigma_f A_f + \sigma_c A_c \;=\; 0, \tag{7}$$

where the subscripts c and f represent the coating and the fibre. σ is the normal stress and A is the cross-sectional area. Since the two materials are fused at the interface, their axial deformation must be equal, satisfying the following condition:

$$\Delta L_f = \Delta L_c \;=\; k\beta_c \Delta \mathrm{RH} L, \tag{8}$$

Assuming linear, elastic, and isotropic behavior for the silica and Pyralin®, the stress and strain are related by

$$\varepsilon_z \;=\; \sigma_c / E_c \tag{9}$$

and

$$\varepsilon_z \;=\; \sigma_f / E_f \tag{10}$$

where E is the Young's modulus. From these relations, k is determined to be

$$k = \frac{E_c A_c}{E_c A_c + E_f A_f}. \tag{11}$$

Substituting k into Equations 6 and 5 yields the following expression for the sensor's response to changes in RH:

$$\frac{\Delta\lambda_B}{\lambda_B} = (1 - P_e)\frac{E_c A_c}{E_c A_c + E_f A_f}\beta_c \Delta \mathrm{RH}. \tag{12}$$

In Kronenberg *et al.* and Yeo *et al.* [8, 7], known values of E and P_e were used in Eq. 12. By varying β_c, Eq. 12 was fitted to experimental sensitivity results for sensors of increasing coating thickness. Values for the 1-D coefficient of hygroscopic expansion, β_c^{1-D}, determined in both studies were in good agreement with each other. Kronenberg *et al.* also used a three-dimensional (3-D) finite element model to determine β_c; however there was a discrepancy between β_c^{1-D} and β_c^{3-D}, indicating a dependence on the radial strain.

2.2. Transient model

In the current study, for a more complete representation of the coated fibre that includes radial strain and diffusion, the sensor is modeled in 3-D using the commercial finite element software Comsol®. In this model, the diffusion of moisture into the Pyralin® is assumed to be Fickian and, therefore, governed by Eq. 13, where η is the moisture concentration and D is the diffusion coefficient. The diffusion driven moisture concentration in the polymer is coupled to the mechanical behaviour of the sensor by prescribing an isotropic 3-D coefficient of hygroscopic expansion β_c^{3-D}, a Poisson ratio, ν and a Young's modulus E_c to the polymer coating silica fibre and the silica fibre. Where, of course, the hygroscopic coefficient of the glass fiber is set to zero.

$$\frac{\partial \eta}{\partial t} = D\nabla^2\eta, \tag{13}$$

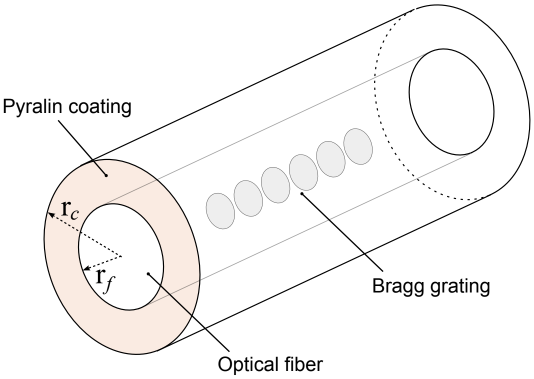

Figure 1. Schematic of the Pyralin® coated FBG sensor.

Given the axial symmetry of the sensor and negligible azimuthal changes in the surface conditions, only radial (r) and axial (z) dependence was considered in the simulation and the computational domain was restricted to the half plane. The length of the coated fibre domain was set to 800 μm, which ensured that edge effects were avoided. A mesh of about 30,000 triangular elements was used, with a higher density of points near the interface of the two materials.

Transient simulations of the sensor response to a step change in humidity were run by prescribing initial and boundary conditions on the moisture concentration. Time dependent radial and axial strains along the fibre axis were obtained and then converted to a Bragg wavelength shift using Eq. 1. By comparing simulation results to those obtained from transient experiments for different coating thicknesses, an estimate of the diffusion coefficient for the Pyralin coating was made and the Fickian diffusion model validated.

Steady-state strains induced by RH changes were converted to Bragg wavelength shifts using Eq. 1. Sensitivity to RH for different coating thicknesses and reduced fibre diameters were obtained and compared to experiment. The coefficient of hygroscopic expansion, β_c^{3-D} was varied in the 3-D model to fit the model results to the data.

2.3. Experimental

Several Pyralin® coated FBG sensors with varying coating thickness and fibre diameter were fabricated in-house and tested for static sensitivity and transient response. Methods for fabrication and testing are described in the following sections.

2.3.1. Sensor fabrication 10 mm long Bragg gratings from Micron Optics, Inc. (Atlanta, GA.) were used for the full diameter fibre sensors. For the reduced fibre diameter sensors, 2 mm long gratings from Technica SA (Zug, Switzerland) were used in the interest of miniature sensor development. The gratings were written in standard SMF 28 optical fibre with nominal Bragg wavelengths of 1550 nm. The moisture sensitive Pyralin coating was applied to the FBG using the procedure outlined in Yeo *et al.* [7]. The stock polyimide recoat was first removed by immersion in 98% sulfuric acid for approximately 10 minutes. The fibre was then rinsed in de-ionized water and wiped with isopropyl alcohol. The FBG was then dipped in Pyralin and withdrawn at a speed slow enough to produce a uniform coating without bead formation. Speeds of 10-20 mm/min were used, depending on the fibre diameter. Each coat was pre-cured in an oven for 5 minutes at 150° C. Subsequent coats were applied to obtain the desired thickness. The final baking of the fibre was done at 180° C for one hour.

To reduce the fibre diameter for increased sensor sensitivity, the fibre was etched with hydrofluoric acid (HF) prior to coating with the Pyralin. The section of bare fibre with a 2 mm Bragg grating was immersed in 48% HF for sufficient time, using a pretedermined etching rate, to produce the desired diameter. The etched fibre was then neutralized in a saturated CaOH solution to stop the etching. The same procedure as described above was then used to coat the etched fibre with Pyralin.

The fibre diameters and coating thicknesses of the sensors were measured with an optical microscope and are shown in Table 2. Uncertainty for the coating thickness due to slight non-uniformities over the length of the grating and was estimated to be 1.0 μm.

2.3.2. Sensor testing The sensors' steady-state response to RH was measured at constant temperature in a programmable environmental chamber. The individual FBG sensors were protected with perforated hypodermic tubing. During calibration the sensors were placed next to a reference humidity probe, the HX80 from Omega with specified accuracy of ±1 % over a range 0f 10-95 %RH. The Bragg wavelength shift of the FBG was detected using an optical interrogation unit (SM130, Micron Optics, Inc., Atlanta, GA), with a specified wavelength resolution of 0.1 pm at 10 Hz sampling rate. The temperature was held constant at 24.0 $\pm$ 0.2 °C while the RH in the chamber was cycled from 30% to 90% in increments of ~10%, allowing the chamber and sensors to reach eqiulibrium at each step.

Table 2. Unetched and etched FBG sensors fabricated and tested in this work.

Sensor	diameter ($\pm 0.5\mu$m)	coating thickness ($\pm 1.0\mu$m)	S_{RH} ($\pm 0.01[10^{-6}\%\text{RH}^{-1}]$)
FBG 1	125.0	2.7	0.16
FBG 2	125.0	9.5	0.74
FBG 3	125.0	17.0	1.54
FBG 4	125.0	18.1	2.22
FBG A	75.0	2.0	0.23
FBG B	50.0	2.5	0.41
FBG C	40.0	2.5	0.55
FBG D	31.5	2.3	0.83
FBG E	20.0	2.0	1.42

For the transient testing that was performed on both etched and unetched sensors, a two-compartment chamber was constructed, with which a step change in RH could be applied to the sensor. See Fig. 2. The upper compartment is exposed to ambient RH while the lower compartment is sealed with a pierceable Teflon diaphragm and held at 85 %RH achieved using a saturated KCl salt solution. During testing the chamber was placed in the environmental chamber set to 45 %RH and 24° C. Beginning in the upper compartment, the FBG sensor gets pushed through the diaphragm such that it is immediately exposed to the high humidity level. From the Bragg wavelength data acquired during this procedure it is possible to characterize the response time of the sensor. The sensor response to saturation with liquid water was tested by using water in the lower chamber.

3. Results and discussion

3.1. Unetched sensors

3.1.1. Steady-state Calibration data for FBG 2 is plotted in Fig. 3 and shows linearity that is representative of the other sensors. A linear fit to the data yields a slope of $m = 1.00 \pm 0.02$ pm%RH^{-1}, which, for a nominal Bragg wavelength of 1550 nm, gives RH sensitivity, $S_{RH} = (0.64 \pm 0.01) \times 10^{-6}$ %RH^{-1}. See Eq.5. Upon cyling the chamber three times there was no apparent hysterisis nor was there a change in sensitivity. Sensitivities for all of the unetched sensors are given in Table 2. The calibration results for the unetched Pyralin-coated sensors confirmed the linear and reversible behavior of this sensor design reported in previous studies.

Shown in Fig. 4 is a plot of S_{RH} of the four unetched sensors versus the coating cross sectional area. Also plotted are curves obtained using the 1-D and 3-D models as well as data points from the work of Kronenberg *et al.*, which are shown for comparison. In the models, the mechanical properties of $E_f = 72$ GPa [8], and $E_c = 2.45$ GPa[14] were used along with a bare fibre diameter of 125 μm.

In the case of the 1-D model, a value of $\beta_c^{1-D} = 7.7 \times 10^{-5}$ %RH^{-1} gives the best

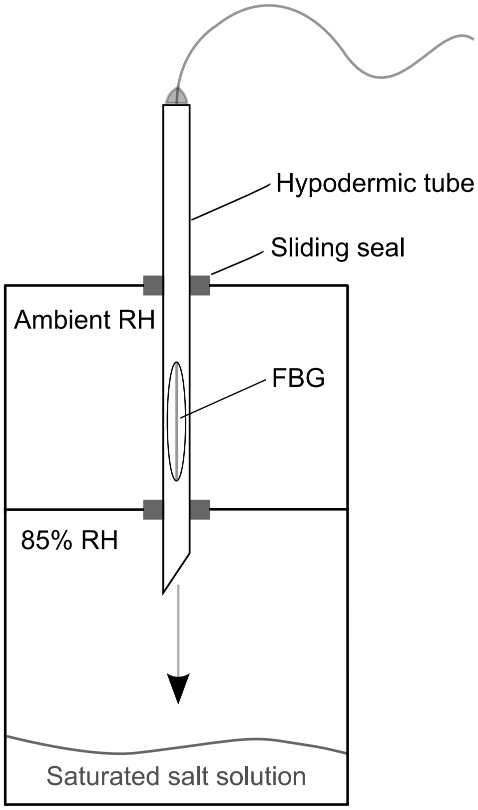

Figure 2. Schematic of the two-part chamber used for transient testing of the sensors.

fit Eq.12 to our data. This value is 7% lower than that of Kronenberg *et al.* who used the same model. This difference is attributed to our use of strain optic coefficients, p_{1i}, that are specific to SMF 28 fibre core [15], and are 7% lower than the bulk silica values used by Kronenberg *et al.*.

With the use of $\beta_c^{3-D} = 7.3 \times 10^{-5}$ %RH^{-1} in the 3-D model, the steady-state sensitivities obtained were in good agreement with the data from both groups. This value of β_c^{3-D} is only 1 % lower than that of Kronenberg *et al.*.

3.1.2. Transient Results from the transient tests for three sensors of increasing coating thickness are shown in Fig. 5. It is clear from these results that the response time of the sensor increases significantly with coating thickness and that a thin coating is desirable for applications where transient RH conditions are to be investigated.

Transient simulation results for FBG 2 (9.5 μm coating) using three different diffusion coefficients are shown in comparison to an experimental response curve in Fig. 6. The strains in the fibre core for each time step in the simulation were used to compute the wavelength shift as a function of time. The agreement between the shape of the simulation curve and the actual response curve validates the assumption that Fickian diffusion governs the transient behaviour of the sensor.

Figure 7 shows radial concentration profiles for FBG 2 obtained with the 3-D

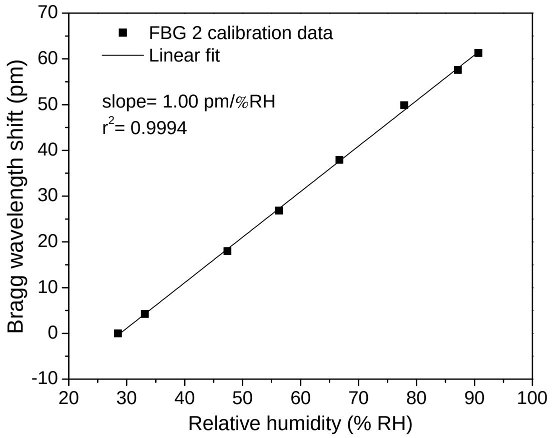

Figure 3. Bragg wavelength shift as a function of RH for FBG 2 with a 9.5 μm thick Pyralin coating. The measurement errors are indicated by the symbol size on the plot.

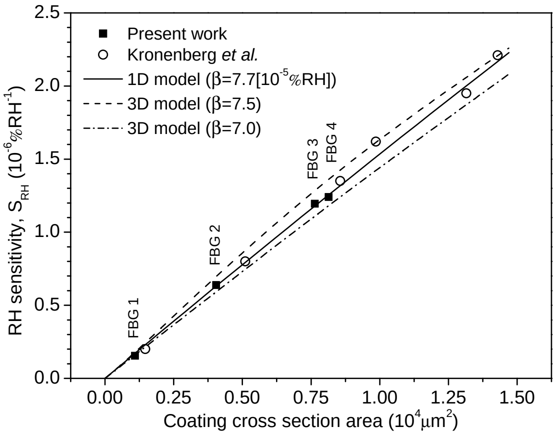

Figure 4. RH sensitivity for sensors of different coating thickness including results from the 1-D and 3-D models and results from Kronenberg *et al.*.

transient model. It is more appropriate to refer the moisture concentration rather than relative humidity, since water diffuses in the material as liquid rather than gas. To simulate the experiment, the moisture concentration, η, throughout the polymer was initially set to 9.79 gm^{-3}, which is equivalent to the water vapor concentration in air at 45 %RH and 24 °C. The boundary conditions for $t > 0$ of the simulation, were $\eta = 18.5$ gm^{-3} at the outer surface of the coating and zero flux, or $\partial\eta/\partial r = 0$, at the glass-polymer interface.

Transient simulations were carried out for coating thicknesses from 1 μm to 20 μm. It was found that by using $D = 8.5 \pm 1.0 \times 10^{-13}$ m^{2}s^{-1}, τ_{63} of the tested FBGs could be predicted within experimental uncertainty. See Fig. 8. This value for the diffusion coefficient is within 10% of literature values for polyimide that have been measured using two different techniques [16].

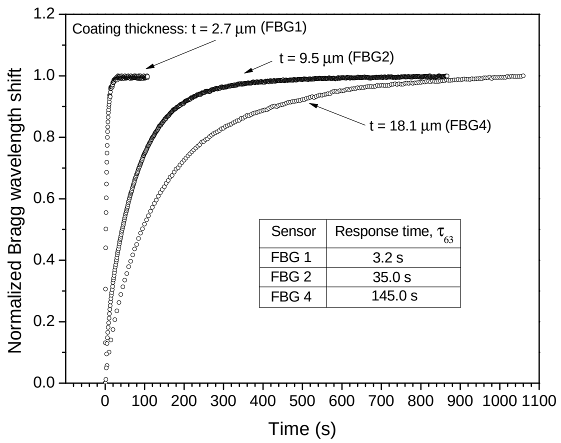

Figure 5. Transient response of 3 unetched fibre sensors of increasing coating thickness to a step change in RH from 45 % to 85 %. The wavelength shift was normalized relative to the sensor value reached at equilibrium at 85 % RH.

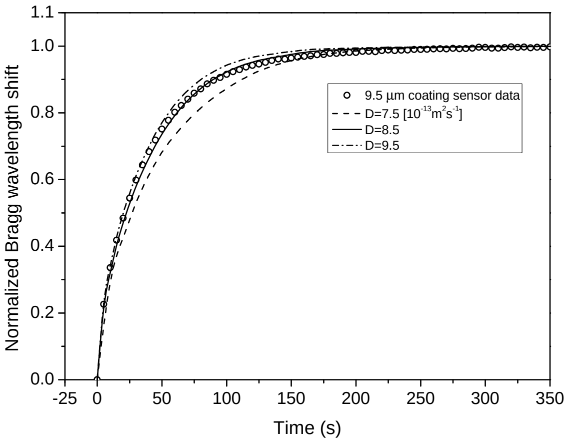

Figure 6. Transient response of FBG 2 (9.5 μm coating) after a step change from 45-85% RH. Data is shown in comparison with simulation results obtained using Comsol.

For the response time of Pyralin-coated FBG sensor design to be competitive with the Honeywell HIH-4000 mini capacitive sensor ($\tau_{63} = 5$s), the coating thickness must be less than ~ 4 μm. The FBG sensor should also be competitive in terms of RH resolution, which is 0.5% RH for the HIH-4000 mini. FBG 1, for example, with $\tau_{63} = 3$s, and $S_{RH} = (0.16 \pm\ 0.01) \times\ 10^{-6}\%\text{RH}^{-1}$, would carry a minimum detectable change in RH, or resolution, of ~ 4 %RH using a common FBG interrogator. Improved sensitivity is, therefore, necessary for the FBG sensor resolution to rival capacitive sensors. The 1-D model for the FBG sensor (see Eq. 12), however, suggests that a reduced fibre diameter can lead to increased sensitivity, and therefore improved resolution.

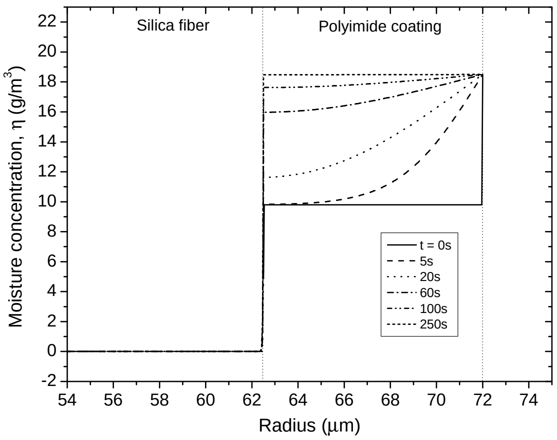

Figure 7. Radial moisture concentration profiles for FBG 2 acquired with Comsol transient simulation.

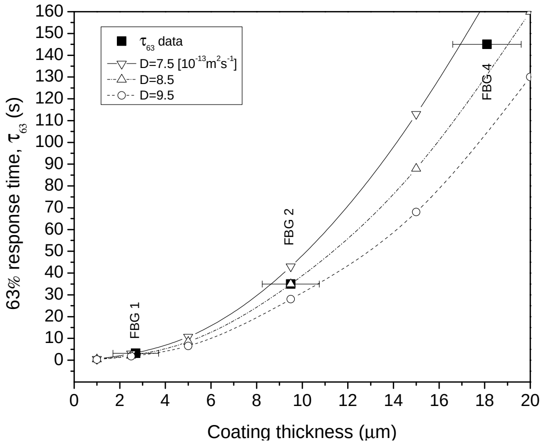

Figure 8. Experimental and model results for τ_{63} as a function of coating thickness.

3.2. Etched sensors

3.2.1. Steady-state Five 2 mm long FBGs were etched with HF to reduce the diameter for increased sensitivity. See Table 2. A coating thickness of $\sim$ 2.5 μm was chosen because, as shown in the preceding section, it yielded a short response time of $\tau_{63} \sim 3$ s for the unetched sensor. The sensors were calibrated in the environmental chamber using the same procedure as for the unetched FBGs. Shown in Fig.9 is the calibration data for the 31.5 μm sensor over the range of $\sim 15 - 95$ %RH. It was seen that in addition to an increase in sensitivity, the linearity and repeatable behavior was preserved with the reduction in diameter.

Sensitivities of the five etched sensors versus fibre diameter are shown in Fig. 10. Also shown are 1-D and 3-D model results, obtained by using β_c^{1-D} and β_c^{3-D} from the unetched fibre analysis. These results show that the 1-D model predict a significantly

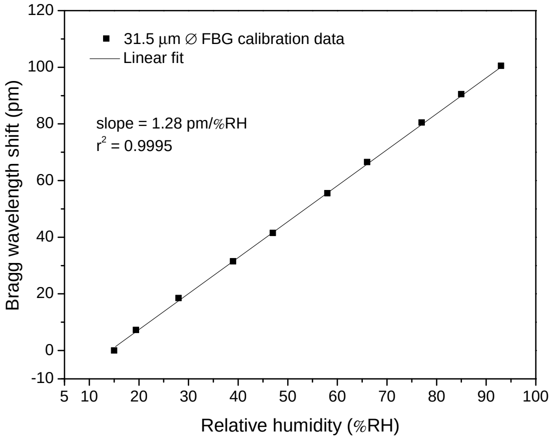

Figure 9. Calibration data for a 31.5 μm etched fibre sensor with 2.3 μm Pyralin coating.

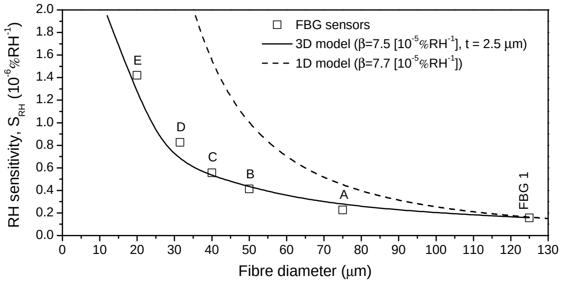

Figure 10. Sensitivity (S_{RH}) versus fibre diameter for etched FBG sensors from Table 1. Solid and dashed lines indicate 3-D and 1-D model results, respectively, using a coating thickness of 2.5 and β_c^{3-D} and β_c^{1-D} from the unetched analysis.

higher RH sensitivities for the etched fibre sensors.

Results from the 3-D model, shown in Fig. 10 can be used to establish a limit on the possible increase in sensitivity that can be achieved by etching the FBG. The sensitivity of a short response time sensor, i.e. FBG 1, can be increased by an order of magnitude if the fibre diameter is etched to 10μm, the diameter of the fibre core. In practice, however, etching to the core is not feasible with this sensor design, as evanescent field interaction would likely comprise the measurements. A factor of 7 increase in sensitivity over FBG 1 was achieved with FBG E, having a diameter of 20 μm. Such an increase in sensitivity brings the resolution of the polyimide-coated RH sensor to less than 1% RH, and into the range of commercial capacitive RH sensors.

3.2.2. Transient The response curves shown in Fig. 11 indicate consistent response times of $\tau_{63} \sim 3$s despite the reduction in fibre diameter, which is to be expected since the coating thickness are all similar.

Tests for effects of liquid water by sensor immersion were performed on FBG D,

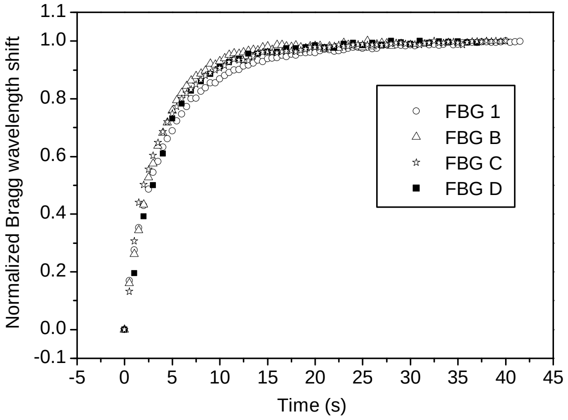

Figure 11. Transient response of Pyralin-coated FBG sensors of varying fibre diameter with similar coating thicknesses ($\sim 2.5\mu$m).

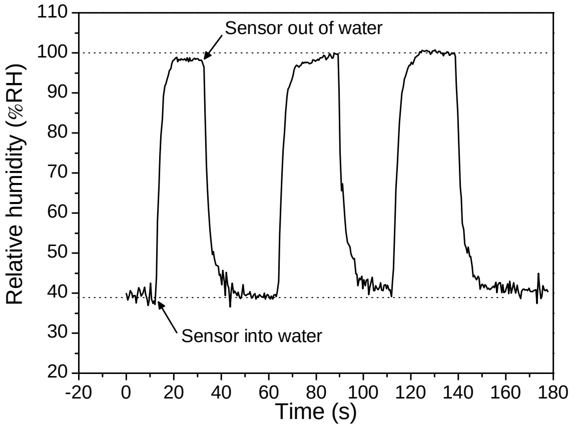

Figure 12. Response to liquid water of a 31.5 μm etched fibre sensor with 2.3 μm Pyralin coating.

with a diameter of 31.5 μm and coating thickness 2.3 μm. Results from this test are shown in Fig. 12. It is seen that upon immersion in water the sensor measures near 100% RH with a response time comparable to the RH transient tests. Full recovery from saturation takes place in 20 s, at which point the sensor again measures the 39% RH of the room.

4. Conclusions

Etched fibre Pyralin-coated FBG humidity sensors were fabricated with varying coating thicknesses and fibre diameters to test the affect these parameters have on response time and sensitivity. Transient results indicated that coating thicknesses of less than 4μm are needed to achieve a response time of 5 s, competitive with commercial capacitive RH sensors. For thin-coating ($\sim$2.5 μm), and hence fast response sensors, it was found that by etching the fibre diameter from 125 μm to 20 μm, the sensitivity increased by a factor of seven. Such an increase in sensitivity allows for the resolution and response time of the Pyralin-coated sensor to be comparable to commercial capacitive RH sensors. These characteristics, in addition to the sensors rapid recovery from saturation in liquid water, indicates good potential for use of this sensor design in applications where electronic RH sensors are not suitable.

5. Acknowledgments

This work was funded through a Strategic Research grant from the Natural Sciences and Engineering Council of Canada.

[1] Z. Chen and C. Lu. Humidity sensors: A review of materials and mechanisms. *Sensor Letters*, 3:274–295, 2005.

[2] S. Lister and N. Djilali. Mathematical modelling of ambient air breathing fuel cells for portable devices. *Electrochemica ACTA*, 52:3849–3862, 2007.

[3] Ch. Hartnig, I. Manke, N. Kardjilo, A. Hilger, M. Gruenerbel, J. Kaczerowski, J. Banhart, and W. Lehnert. Combined neutron radiography and locally resolved current density measurements of operating pem fuel cells. *Journal of Power Sources*, 176:452–459, 2008.

[4] G. Hinds, M. Stevens, J. Wilkinson, M. de Posta, and S. Bell. Novel in situ measurements of relative humidity in a polymer electrolyte membrane fuel cell. *Journal of Power Sources*, 186:52–57, 2009.

[5] N. David, P.M. Wild, J. Jensen, and N. Djilali. Simultaneous in situ measurement of temperature and relative humidity in a pemfc using optical fiber sensors. *Journal of the Electrochemical Society*, 157:B1173–B1179, 2010.

[6] T. L. Yeo, T. Sun, and K. T. V. Grattan. Fibre-optic sensor technologies for humidity and moisture measurement. *Sensors and Actuators A*, 144:280–295, 2008.

[7] T. L. Yeo, T. Sun, K. T. V. Grattan, D. Parry, R. Lade, and B. D. Powell. Polymer-coated fiber bragg grating for relative humidity sensing. *IEEE Sensors*, 5(5):1082–1089, 2005.

[8] P. Kronenberg, P. K. Rastogi, P. Giaccari, and H. G. Limberger. Relative humidity sensor with optical fiber bragg gratings. *Optics Letters*, 27(16):1385–1387, 2002.

[9] L. Wang, Y. Liu, M. Zhang, D. Tu, X. Mao, and Y. Liao. A relative humidity sensor using a hydrogel-coated long period grating. *Measurement Science and Technology*, 18:3131–3134, 2007.

[10] Y.-J. Rao. In-fibre bragg grating sensors. *Measurement Science and Technology*, 8:355–375, 1997.

[11] P. Giaccari, H. G. Limberger, and P. Kronenberg. In *Influence of humidity and temperature on polyimide-coated fiber Bragg gratings, in: Proceedings OSA Trends in Optics and Photonics Series: Bragg gratings, Photosensitivity, Poling in Glass Waveguides, vol. 61, Washington, DC, USA*, page BFB2.

[12] *HIH-4000 Datasheet*. Honeywell Sensing and Control, Golden Valley, MN, USA.

[13] Raymond Measures. *Structural Monitoring With Fiber Optic Technology.* Academic Press, San Diego, 2001.

[14] *Pyralin Technical Information.* HD Microsytems.

[15] A. Bertholds and R. Dandliker. Determination of the individual strain-optic coefficients in single-mode optical fibers. *Journal of Lightwave Technology*, 6:17–20, 1988.

[16] J. L. Mrotek, J. M. Matthewson, and C. R. Kurkjian. Diffusion of moisture through optical fiber coatings. *Journal of Lightwave Technology*, 19:988–993, 2001.

Appendix C

Simultaneous In Situ Measurement of Temperature and Relative Humidity in a PEMFC Using Optical Fiber Sensors

Journal of The Electrochemical Society, **157** (8) B1173-B1179 (2010)
0013-4651/2010/157(8)/B1173/7/$28.00 © The Electrochemical Society

Simultaneous In Situ Measurement of Temperature and Relative Humidity in a PEMFC Using Optical Fiber Sensors

N. A. David,[a,z] P. M. Wild,[a,*] J. Jensen,[a] T. Navessin,[b] and N. Djilali[a,*]

[a]*Department of Mechanical Engineering and Institute for Integrated Energy Systems, University of Victoria, British Columbia, Canada V8W 3P6*
[b]*National Research Council Institute for Fuel Cell Innovation, Vancouver, British Columbia, Canada V6T 1W5*

The development, implementation, and demonstration of in-fiber Bragg grating (FBG) sensors for a simultaneous measurement of temperature and relative humidity (RH) in an operating polymer electrolyte membrane fuel cell (PEMFC) are presented. Etched fiber, polymer-coated FBG sensors with fast response and high sensitivity are installed in situ in a minimally invasive manner in the cathode unipolar plate of a single PEMFC with serpentine flow fields. The performance of the fuel cell under transient operating conditions is monitored. Step increases in current induce significantly larger increases in RH near the outlet than near the inlet of the cell, and associated transients within the fuel cell are found on a time scale approaching the sensor response time (~1 Hz). The improved response of the technique, together with the significantly improved temperature and RH resolution, provides useful information on the dynamics of heat and water management. The technique is well suited for distributed measurements, and its relatively low cost and nonintrusive character make it a good candidate for practical multipoint monitoring of complete stacks.

[DOI: 10.1149/1.3436652]

Manuscript submitted February 22, 2010; revised manuscript received May 5, 2010. Published June 10, 2010.

The temperature and relative humidity (RH) inside a polymer electrolyte membrane fuel cell (PEMFC) have a significant impact on performance, particularly due to the effect these coupled parameters have on the water balance within the cell.[1-5] Optimal water balance is achieved when the membrane is well hydrated, ensuring good proton conductivity, and the electrodes are relatively free of liquid water to maintain effective gas transport to the reaction sites.

Water produced at the cathode during cell operation is effective in hydrating the membrane at lower cell temperatures. But at higher operating temperatures, which are preferred for reduced activation polarization, the cathode RH is insufficient and the membrane dries out. Membrane dry-out not only causes an increase in ohmic overpotential but can also accelerate membrane degradation.[6] To avoid this dry operation, gas streams are typically humidified before entering the cell. Excessive humidification, however, can cause flooding and can severely decrease the cell performance due to mass transport losses. Nonuniformities in the temperature and water distribution are often present[7-9] and add to the challenges of thermal and water management.

Further adding to the difficulty of achieving controlled water balance in a PEMFC are dynamic operating conditions, which are common in transportation applications. Recent experimental and modeling studies further elucidate the roles of temperature and humidity on cell performance under these conditions.[10,11] As predictive models are extended to two and three dimensions, the ability to measure distributed temperature and RH in situ becomes increasingly useful for validation. Techniques developed for these purposes also supplement conventional bulk diagnostic techniques.

Distributed measurements of RH and temperature inside a PEMFC have been performed using electrical and optical techniques with varying degrees of invasiveness and practicality. Microtemperature and humidity sensors were fabricated on a metallic bipolar plate of a PEMFC by Lee et al. for in situ diagnostics.[12] The sensors were calibrated, and polarization curves were reported for an operating fuel cell with and without sensors, indicating a significant drop in performance when sensors were embedded, but no temperature or RH data were presented.

Using tunable laser diode spectroscopy, Basu et al.[13] claimed the first simultaneous nonintrusive measurements of water vapor partial pressure and temperature inside a PEMFC under steady and transient operations. Two channels in the serpentine flow path of a bipolar plate were extended to the edges to allow optical access into a test cell. One sensing channel was located near the inlet, and one was located near the outlet. This technique was limited, however, in its temperature resolution, and temperature differences between the two flow channels were not resolved. The partial pressure of water vapor, which is proportional to RH for a given temperature, was measured to increase linearly with cell current and was higher toward the outlet. These measurements agreed with the calculated production of water at the cathode and were not significantly affected by electro-osmotic drag. A similar approach was proposed by Partridge et al.,[14] who reported on the use of spatially resolved capillary inlet mass spectrometry to measure water concentration at multiple locations in the serpentine flow field of an operating PEMFC. The authors suggest that in combination with spatially resolved temperature measurements, the transient RH distributions could also be measured. Data for such measurements, however, were not presented.

The trends in the partial pressure of water vapor across the cell reported in Basu et al. were confirmed more recently by the distributed RH measurements of Hinds et al.[15] In their work, they used miniature single-chip capacitive sensors from Sensirion Inc. (SHT75) to accurately measure temperature and RH at points around the flow field of a single test cell. The sensors, although relatively small, were still too large to be installed directly into the flow channels in the active area and were therefore recessed into auxiliary channels around the active area. The main constraint of this technique was the sensor size (3×7 mm), which limits the ability to make measurements in the active area and limits the transfer of the technique to commercial plate designs.

The focus of the present work is the development of an in situ fiber-optic-based measurement technique that addresses temperature resolution and sensor size limitations of existing methods.[13,15] Optical fibers have properties that are suitable for the PEMFC environment: In particular, they are nonconductive, chemically inert, and inherently small. They were recently used by Inman et al.[16] for an in situ distributed point measurement of temperature across the surface of the gas diffusion layer. The point sensor they developed, located at the fiber tip, is based on the principle of phosphor thermometry.

In a previous work, we introduced the use of in-fiber Bragg grating (FBG) sensors for distributed temperature measurements in a PEMFC.[17] In contrast to the sensors used by Inman et al., FBGs are installed parallel to the fuel cell plates and can be multiplexed with several sensors on a single fiber. Building on this, in this paper, we

---

[*] Electrochemical Society Active Member.
[z] E-mail: nadavid@uvic.ca

present an extension of the FBG technique to the simultaneous measurement of RH and temperature. Sensors are fabricated and installed in flow channels of the graphite cathode flow plate of a single PEMFC and used to take minimally invasive measurements during cell operation. With the addition of FBG multiplexing, the technique presented here offers the prospect of real-time multipoint monitoring of complete stacks.

Fiber Bragg Gratings: Background

An FBG typically consists of a short segment of a single-mode optical fiber with a photoinduced periodically modulated index of refraction in the core of the fiber. This effectively creates a grating of planes perpendicular to the fiber axis. When the grating is illuminated with broad-band light, the reflected power spectrum has a structure caused by interference of the light with the planes of the grating. The peak of the spectrum occurs at the Bragg wavelength, $\lambda_B = 2\Lambda n$, where n is the index of refraction of the silica fiber and Λ is the grating pitch. When grating is subjected to mechanical or thermal strain, its pitch changes, causing a shift in Bragg wavelength.

This shift is given by

$$\frac{\Delta\lambda_B}{\lambda_B} = (1 - \text{Pe})\varepsilon + [(1 - \text{Pe})\alpha + \xi]\Delta T \qquad [1]$$

where Pe is the photoelastic constant of the fiber, ε is the mechanical strain induced in the fiber, α is the coefficient of thermal expansion of the optical fiber, and ξ is the thermo-optic coefficient. A comprehensive review of FBGs, along with a description of many of their important applications, can be found in Rao.[18]

One such application is RH sensing.[19-21] FBG is coated with a moisture-sensitive polymer that swells as water vapor absorbs into micropores of the material. Swelling of the polymer causes axial strain in the FBG, which is proportional to RH.

In the absence of external mechanical strain, the Bragg wavelength shift can be represented as a linear superposition of response to changes in RH (ΔRH) and temperature (ΔT)

$$\frac{\Delta\lambda_B}{\lambda_B} = S_T\Delta T + S_{\text{RH}}\Delta\text{RH} \qquad [2]$$

where the temperature and RH sensitivity coefficients, S_T and S_{RH}, are given by

$$S_T = (1 - \text{Pe})\frac{E_p(r_f + t)^2}{E_p(r_f + t)^2 + E_f r_f^2}(\alpha_p - \alpha_f) + \xi_f \qquad [3]$$

$$S_{\text{RH}} = (1 - \text{Pe})\left[1 - \frac{E_f r_f^2}{E_f r_f^2 + E_p(t^2 + 2tr_f)}\right]\beta_p \qquad [4]$$

These coefficients were calculated based on a uniform axial strain model, neglecting edge effects.[19,21] The variables α_p, β_p, E_p, and t represent the coefficients of thermal and hygroscopic expansion, the Young's modulus, and the thickness of the polymer material. The Young's modulus and the radius of the fiber are represented by E_f and r_f, and ξ_f is the thermo-optic coefficient of the fiber.

This type of sensor with the moisture-sensitive polyimide Pyralin (PI-2525 from HD Microsystems) was first presented by Kronenberg et al.[19] The authors showed that an FBG coated with polyimide has a linear and reversible response for temperature and RH ranges of 13–60°C and 10–90%, respectively. The highest temperature in their study was limited to the maximum operating range of the electrical gauge used, and they report additional tests showing that the sensor was not damaged when exposed to temperatures ranging from −20 to 160°C. In a similar study by Yeo et al.,[20] Pyralin-coated sensors were characterized with linear response up to an RH level of 97%. The ranges reported by both groups suggest good compatibility of the sensors in a PEMFC.

In both the work of Kronenberg et al. and Yeo et al., several sensors were fabricated from standard single-mode fiber (SMF 28) FBGs, each with a different coating thickness, and were tested in a climatic chamber for sensitivity to temperature and RH. Using these results and published values for other parameters in Eq. 3 and 4, the coefficients of thermal and hygroscopic expansion were identified.

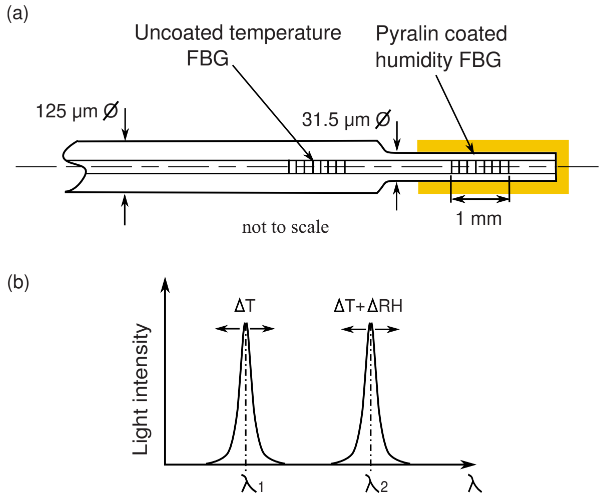

Figure 1. (Color online) (a) Schematic of the RH sensor consisting of two 1 mm FBGs spaced apart by 3 mm. The distal FBG has a reduced diameter coated with the humidity-sensitive polymer, Pyralin, while the other FBG is left unetched and used for temperature compensation. (b) Schematic of the reflected spectrum from the sensor. The uncoated FBG used for temperature compensation has the Bragg wavelength denoted by λ_1, which only shifts with temperature. The etched and coated FBG has Bragg wavelength λ_2 and shifts with both RH and temperature.

The coating thicknesses tested by Kronenberg and co-workers ranged from ~4 to 30 μm with measured RH sensitivities ranging over an order of magnitude, from 0.3 to 3.0 pm $\%^{-1}$. Temperature sensitivity ranged from 10.0 pm $°\text{C}^{-1}$ for a bare fiber to 12.3 pm $°\text{C}^{-1}$ for the thickest coating.

Based on the sensitivities measured by Kronenberg et al. for the Pyralin-coated sensor, the maximum Bragg wavelength shift for a 100% change in RH would be 300 pm. The same order of magnitude Bragg wavelength shift would result from temperature changes of around 30°C. Controlled temperature increases on this scale are common in PEMFCs when bringing the cell up to operating temperatures, after which point smaller variations can occur during normal operation. To decouple the Bragg wavelength shift due to these temperature variations and to make accurate measurement of RH within the PEMFC environment, temperature compensation is required.

The work of Kronenberg suggests using thicker coatings to enhance sensitivity but does not discuss the impact this might have on the sensor time response, which is also an important consideration for use in a PEMFC. Yeo et al. built upon this work, characterizing the time response of the Pyralin-coated FBG RH sensor to step changes in humidity.[20] The response times were 18–45 min for 10–45 μm thick Pyralin coatings, much too long for the investigation of transients in a PEMFC, which are typically on the order of seconds.[22] To reduce the response time of the sensor, thinner coatings must be used, but at the cost of lower sensitivity.

According to Eq. 4, however, sensitivity can be re-established by reducing the fiber diameter. In the present work, an FBG-based sensor is fabricated with reduced fiber diameter and temperature compensation, both important features for implementation inside a PEMFC.

Sensor Fabrication and Characterization

A schematic of one of the RH sensors fabricated for this work is shown in Fig. 1a. It is made up of two 1 mm FBGs spaced apart by 3 mm. The distal FBG was etched and coated with Pyralin for hu-

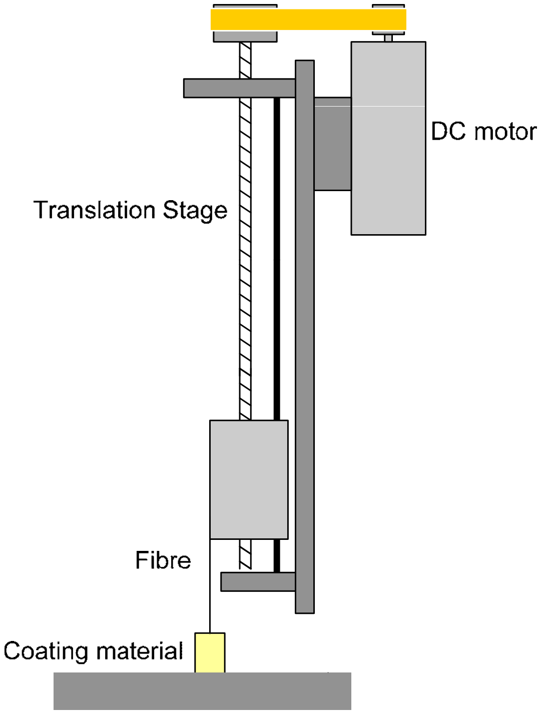

Figure 2. (Color online) Schematic of the dipping procedure used for coating the FBGs with polymer.

midity sensing. The proximal FBG was left unetched and used for temperature compensation, which was necessary due to the dual sensitivity of the coated FBG. The FBGs used for these sensors were written on SMF 28 fiber with Bragg wavelengths of 1540 and 1550 nm and recoated with polyimide for durability (Technica SA Inc., Beijing, China). Depicted schematically in Fig. 1b is a reflected spectrum with two peaks centered on the Bragg wavelengths of each FBG.

A length of fiber with the two FBGs was cut so that one FBG is 2 mm from the distal end. The stock polyimide recoat was removed by immersion in 98% sulfuric acid for approximately 10 min. The fiber was then rinsed in deionized water. To prepare the fiber for HF etching, it was placed in a Teflon tube such that the distal FBG was protruding. Hot wax was used to seal the tube at the midpoint between the two FBGs. The exposed FBG was submerged in 48% HF for 30 min and then immediately neutralized in a saturated CaOH solution to stop the etching. This results in a fiber diameter of 31.5 ± 0.5 μm, measured using an optical microscope with a graticule.

For applying the Pyralin coating on the etched FBG, the procedure outlined in Yeo et al. was followed.[20] The etched FBG was first wiped with isopropyl alcohol and then dipped in Pyralin and withdrawn at a predetermined constant speed. A speed of 20 mm/min was used to produce uniform coatings without bead formation. A schematic of the setup for coating the FBGs is shown in Fig. 2. Each coat was precured in an oven for 5 min at 150°C. For the sensors in this work, three coats of polymer were applied to obtain a thickness of 2.5 ± 0.5 μm. The final baking of the fiber was at 200°C for 1 h.

Calibration of the sensors to RH was carried out using a series of small chambers containing saturated salt solutions to produce humidity fixed points that are in accordance with ASTM 104-02.[23] In this way, the individual sensors, before installation in the fuel cell, are characterized in terms of sensitivity and temporal response to humidity. The temperature calibration of the sensors was conveniently performed in situ where dry gas can be easily flowed through the channels to create a low constant humidity environment.

Table I. RH fixed points for the saturated salt solutions used for sensor calibration.[24]

Salt	RH at 25°C
K_2Co_3	43.16 ± 0.39
NaBr	57.57 ± 0.4
KI	68.86 ± 0.24
KCl	84.34 ± 0.26

Nalgene bottles with a volume of 125 mm were modified so as to accept a single sensor via a Lure lock connection in the lid. The bottles were partially filled with ~25 mm of the saturated salt solutions and then placed in a constant temperature water bath set at 25°C. The four salts used for calibration are listed in Table I, along with their associated RH at 25°C.[24] The RH inside the chambers was measured using a Sensirion Inc. SHT75 RH sensor with specified accuracy of ±1.8% RH. The Bragg wavelength shift of the FBG was detected using an optical interrogation unit (SM130 from Micron Optics, Inc., Atlanta, GA), with a specified wavelength resolution of 0.1 pm at a 10 Hz sampling rate.

The time response of the sensor was tested by moving it between two of the bottles containing different salt solutions, the act of which takes less than 2 s.

The RH calibration results for a 31.5 μm diameter fiber FBG with a 2.5 ± 0.5 μm Pyralin coating are shown in Fig. 3. The sensitivity to RH was 0.99 pm % RH^{-1} from the slope of the linear fit to the data. Although a saturated salt solution for a higher humidity level was not used, linear response for a Pyralin-coated FBG was shown up to 97% RH by Yeo et al. Furthermore, when the sensor was immersed in water, it measured 100 ± 2.0% RH and recovered quickly upon drying. For this fiber diameter and coating thickness, including their measured uncertainties, the calculated sensitivity based on Eq. 4 is 1.25 ± 0.25 pm % RH^{-1}, indicating a reasonable agreement between the model of Kronenberg et al. and this etched sensor design. The sensitivity measured here is more than 3 times higher than the value reported by Kronenberg et al. for a 3.6 ± 1 μm thick coating on an unetched fiber.

Figure 4 shows the sensor response to a step change in humidity from 43 and 84% RH. From this plot, the two conventionally defined response times are determined and given in the inset table. The 90% response time of 10 s is a vast improvement over the previous generation of unetched sensors reported in Ref. 20 and is suitable to measure transient phenomena inside a PEMFC. In fact, the 63%

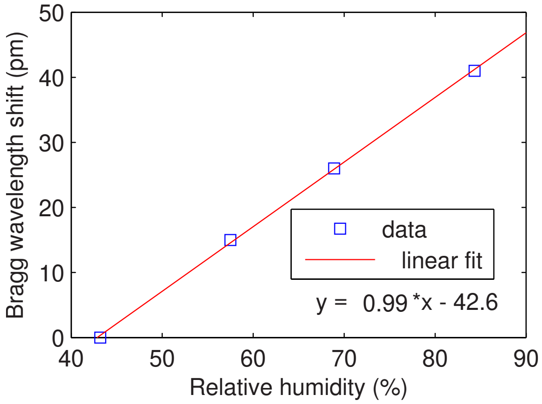

Figure 3. (Color online) RH calibration data for a 34 μm RH sensor acquired using humidity fixed point chambers containing saturated salt solutions.

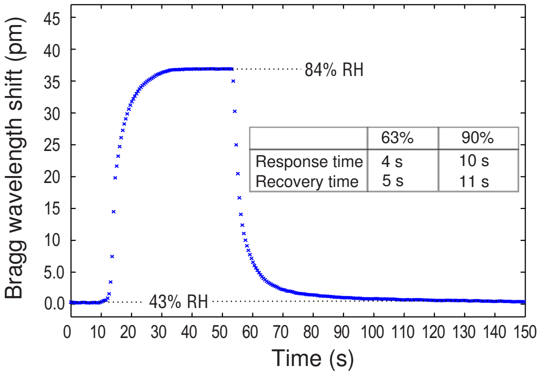

	63%	90%
Response time	4 s	10 s
Recovery time	5 s	11 s

Figure 4. (Color online) Response of the etched sensor with coating thickness of 2.5 ± 0.5 μm to a step change in RH. Conventionally defined response times for the sensor are shown in the table.

response time is half that specified for the commercial sensors used in Ref. 25. Also notable in the response data is that upon returning to the low humidity state, the Bragg wavelength settles back to the original value, indicating reversibility of the polymer expansion mechanism.

Temperature calibration was done with the sensors installed in the graphite fuel cell flow plate. Two miniature T-type thermocouples were installed into a blank graphite plate such that when it is used to cover the flow plate with the FBGs, the thermocouples and the FBGs are colocated. The single cell was assembled, with the blank plate used in place of the membrane electrode assembly (MEA) and the anode flow plate. Dry air was fed into the cathode flow field, and the temperature was increased using the water heating system and then allowed to cool to room temperature by natural convection.

Shown in Fig. 5 are temperature calibration data for each FBG acquired during slow thermal cycling of the sensors in situ under dry conditions. As indicated by the slopes of the linear fits to the data, the polymer coating on the RH-sensitive FBG has the effect of increasing its sensitivity to temperature by ~10%. This result is consistent with Eq. 3. Although the calibration was performed in the 25–80°C range, to cover the operating range of interest of the fuel cell, the sensor temperature range can be easily extended.[19]

With good linearity and reversibility in the RH and temperature calibration data, estimations of the accuracies of the etched FBG sensors fabricated in this work are ±2.0% RH and ±0.2°C. These values are based on the specifications of Sensirion SHT75 and the Omega thermocouple used as references for calibration. The absolute temperature uncertainty reported here is an order of magnitude improvement over that of the technique used by Basu et al. for their in situ measurements[13] and is adequate to investigate temperature differences between adjacent channels inside a single PEMFC.[13,17] Resolving differences in temperature and RH in situ is further improved by the high wavelength resolution of the Micron Optics SM130 used to interrogate the FBGs in the sensor. Based on this, the minimum detectable change in RH is 0.1% RH, assuming temperature compensation.

In Situ Experiments

Sensor installation.— A graphite flow plate for a single test cell of an active area of 30.25 cm^2 was machined with a serpentine flow field and instrumented with two of the previously discussed FBG RH sensors. The schematic in Fig. 6a shows the location of one of the installed sensors in the flow plate and where it sits relative to the main PEMFC components. The design challenges in embedding the FBG sensor in an operating fuel cell were discussed in Ref. 17. To avoid interference with the flow in the gas channel, the sensor was installed in a groove at the bottom of the flow channel, as shown in Fig. 6b. Underneath the sensor is a recess in the groove to ensure that the entire surface of the sensor is in contact with the air in the channel. Clearly, from the figure, with this installation and with the small diameter of the sensor, there is minimal impact on the active area of the PEMFC.

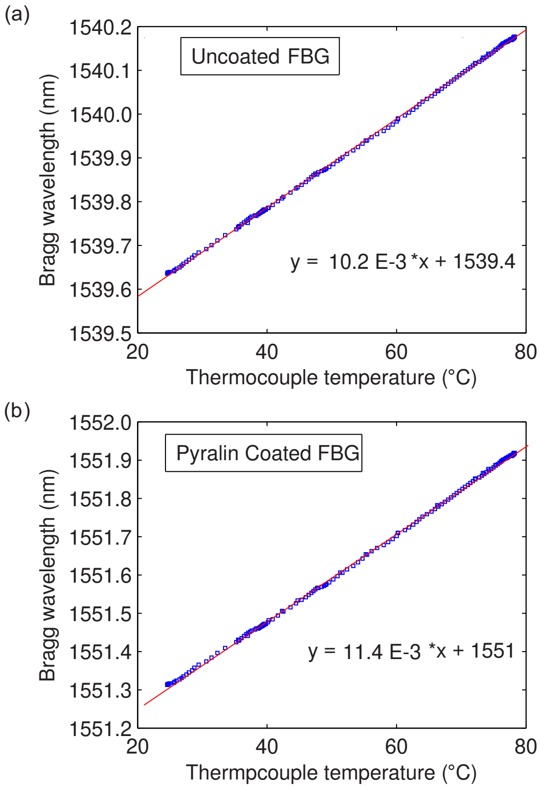

Figure 5. (Color online) Calibration data for the RH sensor with respect to temperature acquired under dry conditions. (a) 125 μm uncoated FBG used for temperature compensation. (b) 34 μm Pyralin-coated FBG.

Proper sealing of the installation is also important to minimize the impact on performance. Cyanoacrylate adhesive was used to fix the fiber in place and to seal the angled hole where it enters the flow channel. This provides strain relief to ensure that only the changes in RH and temperature within the sensing region are detected rather than mechanical strain transmitted from the exterior. Another important feature of the design shown in Fig. 6b is the curve in the fiber as it enters the sensing region from outside the cell. Excessive bending results in loss of optical power transmitted to and from the sensor, and bends therefore should be limited to about 1 cm in radius.

Figure 7 shows the locations of the two sensors along the flow field in the graphite flow plate. The plate is used on the cathode side of the test cell, and air flows over sensors 1 and 2 from the inlet to the outlet, respectively.

Test cell.— The instrumented graphite plate described above was sized to fit into a pre-existing fuel cell test assembly. The assembly consists of gold-plated current collector plates, and stainless steel manifolds for gas distribution and water circulation for the cell heating system. This assembly can be seen in Fig. 8, where the fiber optics is also shown entering the cathode plate.

MEAs for the test cell were fabricated at the National Research Council Institute for Fuel Cell Innovation, Vancouver, Canada. An active area of 30.25 cm^2, with platinum loading of 0.4 mg/cm^2, was achieved by masking and spray deposition of a carbon catalyst ink onto Nafion 115 membrane. The gas diffusion layer used for the

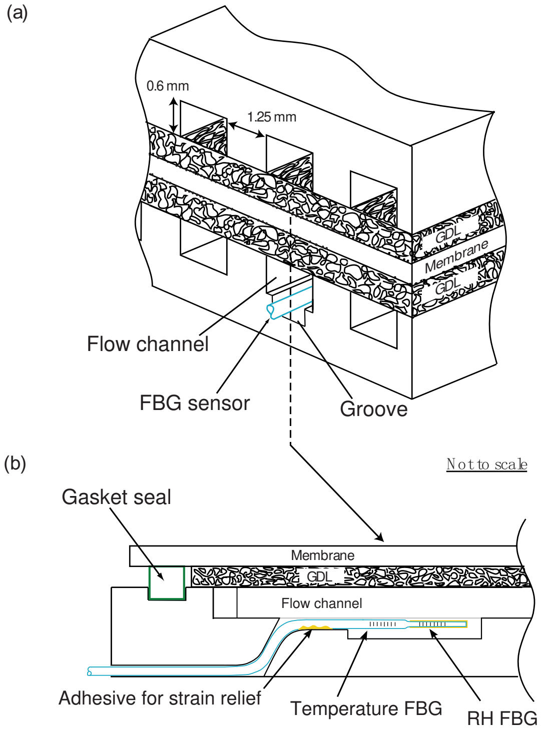

Figure 6. (Color online) Schematic of the in situ FBG sensor located in the bottom of the flow channel of the graphite flow plate (a). The side view schematic in (b) shows how the sensors were installed into the flow plate.

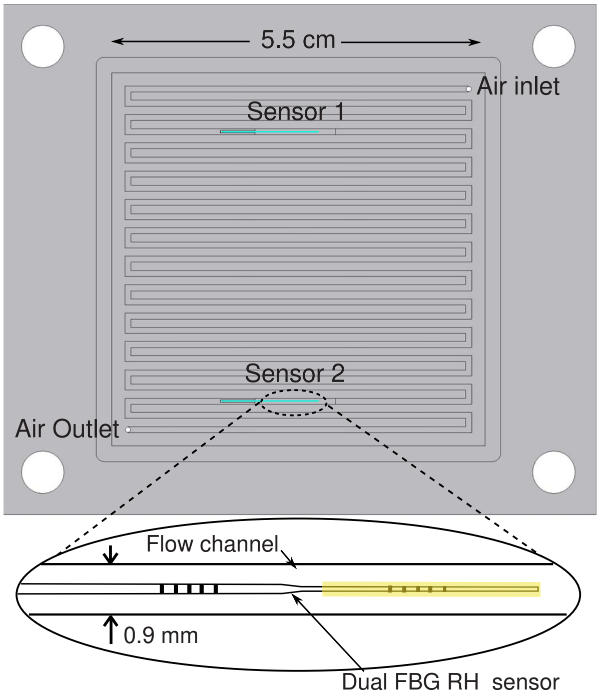

Figure 7. (Color online) Schematic of the cathode flow plate showing the locations of the two etched FBG RH sensors. Inset drawing is of a single sensor embedded in the flow channel.

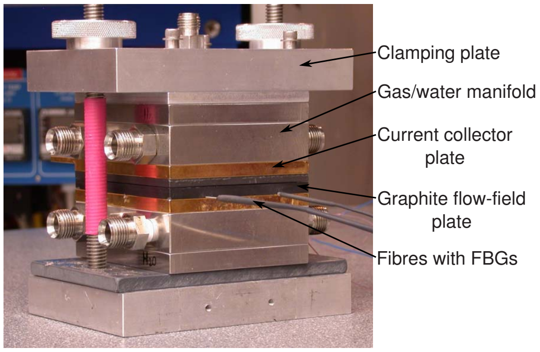

Figure 8. (Color online) Photograph of the single test cell assembly. The cell temperature is set by circulating deionized water from a temperature controlled bath in the test station through the stainless steel plates on either side of the cell.

MEAs was Toray paper with 10% polytetrafluoroethylene content, and that for the MEAs used in this study was not hot-pressed onto the carbon catalyst layer.

The test cell was operated using a Ballard 3 kW fuel cell test station, which enabled control of the fuel and oxidant flow rates, and a cell temperature with a water heating system. The current density of the fuel cell was varied using an electronic load bank (Dynaload Inc., MCL488, Hackettstown, NJ) that was connected via copper leads to the gold-plated collector plates on either side of the single cell. The cell voltage was measured using analog inputs on a 16 bit data acquisition device (National Instruments Inc.).

In situ testing conditions.— For in situ testing of the sensors, the cell was run in the coflow mode with the temperature set to 40°C. Water tanks for the gas humidifier were also set to 40°C, but because the tubing from these tanks to the test cell was not heated, the inlet gas streams were underhumidified. A standard PEMFC test is to vary the cell current with the load and to acquire a polarization curve by measuring the corresponding cell voltages. By performing this test with the sensors installed, steady-state and transient behaviors are observed in the cell voltage as well as in the RH and temperature within the cell. Data from the sensors were acquired at a sampling rate of 1 kHz and presented with 1000 averages to improve the resolution. Before carrying out the current sweeps for polarization tests, the MEA was conditioned by running the cell at 0.3 A cm^{-2} for ~30 min.

Results and Discussion

To obtain a polarization curve quasi-statically, the cell current was incremented from 0 to 15 A and back down to 0 in steps of 3 A, allowing the cell voltage to reach steady state between each step. The flow rates for the air and hydrogen streams were set to 1.25 and 0.75 slpm. This overstoichiometry was used to prevent water accumulation in the flow channels. Because the etched fiber sensor is free at one end in this installation, the fine fiber can be easily deflected due to the surface tension of water accumulated around it. The resulting strain on the FBGs perturbs the sensor measurements significantly. Such perturbations were observed at low oxidant flow rates and higher currents.

Results from incrementally increasing the cell current from 0 to 15 A are shown in Fig. 9 with the cell voltage data and the sensor measurements. In Fig. 9b, the RH near the outlet climbs higher than the inlet RH after the first step in cell current. The following two steps in current, to 6 and 9 A, are also marked with increases in RH near the outlet. Subsequent steps in current result in smaller increments in RH near the outlet until a maximum of around 90% RH is reached.

In contrast to the large changes in RH near the outlet, the inlet RH increases in smaller steps. These steps continue throughout the

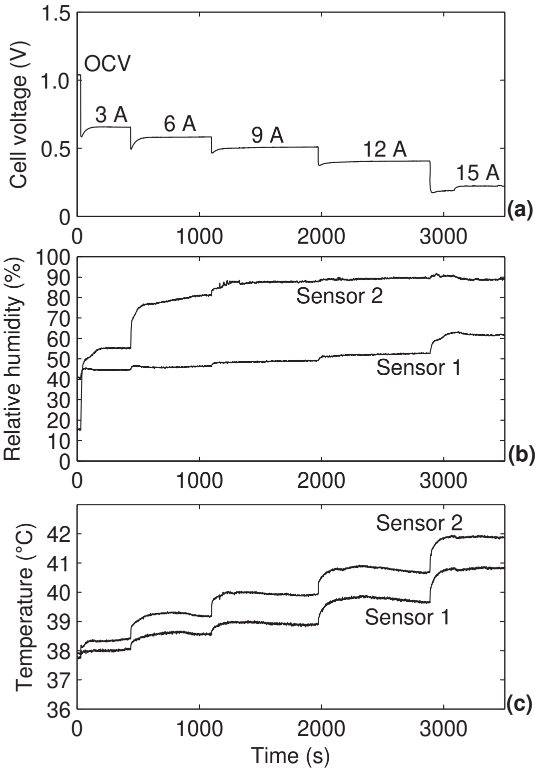

Figure 9. (a) Voltage, (b) RH, and (c) temperature data taken while incrementing cell current for obtaining a polarization curve. The flow rates for the air and hydrogen were 1.25 and 0.75 slpm, respectively.

range of currents with no plateau, as is the case for the outlet RH. The higher RH measured near the outlet on the cathode side for all cell currents above zero is to be expected; water produced in the catalyst layer during cell operation acts to increasingly humidify the air as it flows from the inlet to the outlet. Sensor 1 is only a few channels downstream from the inlet and, therefore, measures air that has a limited interaction with product water and has thus generally lower RH.

Shown in Fig. 10 is the transient response of sensor 2 following a step change in current from 0 to 3 A, with the cell voltage response plotted for comparison. There is an initial rise in RH of more than 30% in ∼30 s after the step change. This is followed by a smaller and slower increase in RH, after which it reaches steady state at a time comparable to the cell voltage ($t = \sim 180$ s). The response of the cell voltage and the RH agrees with measurements of Hinds et al. and is consistent with the time scale of water sorption into the Nafion membrane, which is of the order of hundreds of seconds.[26] This result demonstrates that RH transients inside a PEMFC exist on a time scale approaching the sensor response time and that the sensor could provide information on the dynamics of water transport in the MEA.

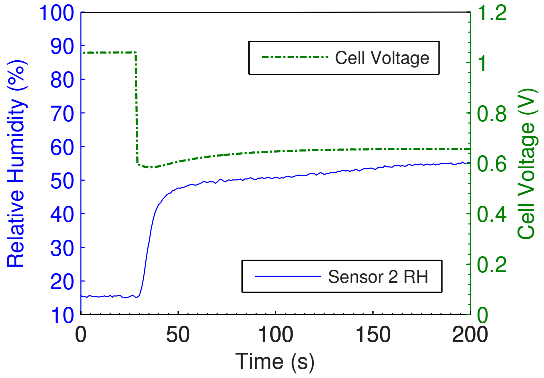

Figure 10. (Color online) Transient response of sensor 2 following a step change in current density from 0 to 3 A at time $t = 28$ s. The cell voltage response is also shown for comparison.

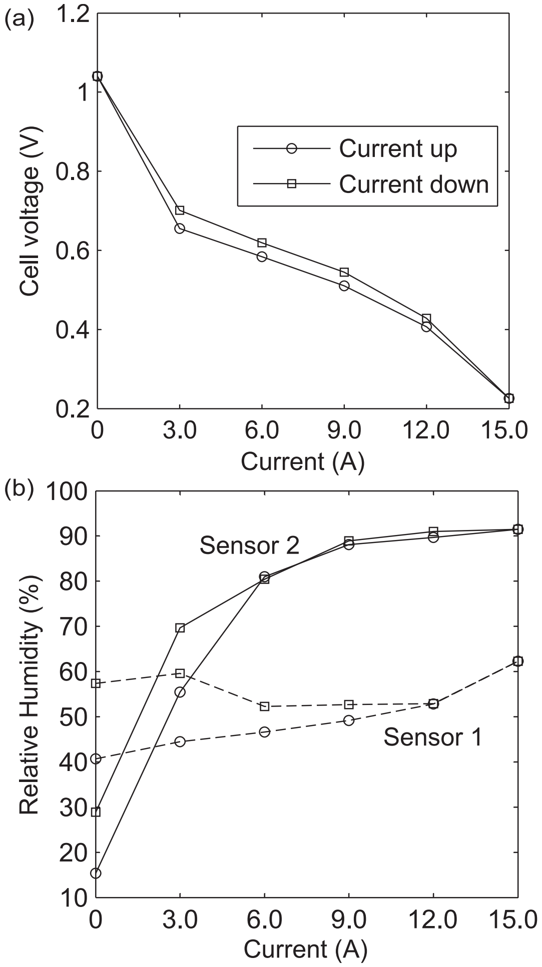

Figure 11. (a) Steady-state polarization data for increasing and decreasing currents with cell temperature set to 40°C. (b) Corresponding steady-state RH measurements of sensors 1 and 2.

Temperature differences, reaching up to ∼1.5°C, were also measured in the flow field between the inlet and the outlet, as shown in Fig. 9c. These are expected as a result of higher membrane hydration toward the outlet, leading to higher current densities and more ohmic losses. Gradients in temperature such as this have also been reported in other studies.[17,27,28]

The steady-state polarization results for the test described are shown in Fig. 11. The cell voltage measured for decremented current is higher than that for the incremented current, indicating hysteresis in performance. The corresponding steady-state measurements of RH are shown in Fig. 11b, which also show hysteresis and likely contribute to the hysteresis in the polarization curve.

Conclusions

An etched fiber, polymer-coated FBG sensor for a fast response, high sensitivity measurement of RH and temperature has been demonstrated. Two of the sensors were embedded directly into the cathode flow channels of a single test cell and were used to make real-time measurements of RH and temperature during cell operation.

Results show that for an increased current density, much larger increases in RH occur near the outlet than near the inlet, a trend that has been reported in other studies. From the results, it was also determined that RH transients inside a PEMFC exist on a time scale approaching the sensor response time, proving that the sensor could provide information on the dynamics of water transport in the MEA.

The small size of the sensor implemented here and its accurate, high resolution measurement capabilities combine to address key limitations of other techniques used for in situ PEMFC measurements. In the interest of improved cell design, particularly with regard to humidification and thermal and water management schemes, this relatively inexpensive technique could prove useful as a noninvasive in situ diagnostic tool.

Further improvements of the technique involve the multiplexing of several temperature-compensated FBG RH sensors on a single fiber. This increases the number of measurement points from 4 to 10, resulting in truly distributed RH and temperature data within an operating fuel cell. This naturally lends itself to a sensor installation that is fixed on both ends and, therefore, to measurements that are unperturbed by liquid water. Furthermore, with the minimal invasiveness of the optical fibers into the fuel cell flow plate, the technique could be extended for use in bipolar plates for multipoint monitoring of complete stacks.

Acknowledgments

This work was funded by the Natural Sciences and Engineering Research Council (NSERC) of Canada and the Canada Research Chairs program. The authors also acknowledge the valuable input of Dr. Matt Moffit on coating techniques.

University of Victoria assisted in meeting the publication costs of this article.

References

1. J. Lariminie and A. Dicks, *Fuel Cell Systems Explained*, John Wiley & Sons, New York (2000).
2. M. M. Mench, Q. L. Dong, and C. Y. Wang, *J. Power Sources*, **124**, 90 (2003).
3. Q. G. Yan, H. Toghiani, and J. X. Wu, *J. Power Sources*, **158**, 316 (2006).
4. A. Z. Weber and J. Newman, *J. Electrochem. Soc.*, **153**, A2205 (2006).
5. S. Kim and M. M. Mench, *J. Electrochem. Soc.*, **156**, B353 (2009).
6. C. Chen and T. F. Fuller, *Polym. Degrad. Stab.*, **94**, 1436 (2009).
7. N. Djilali and D. Lu, *Int. J. Therm. Sci.*, **41**, 29 (2002).
8. T. Berning and N. Djilali, *J. Electrochem. Soc.*, **150**, A1589 (2003).
9. S. Kjelstrup and A. Rosjorde, *J. Phys. Chem. B*, **109**, 9020 (2005).
10. M. Meiler, D. Andre, O. Schmid, and E. P. Hofer, *J. Power Sources*, **190**, 56 (2009).
11. A. A. Shah, G. S. Kim, P. C. Sui, and D. Harvey, *J. Power Sources*, **163**, 793 (2007).
12. C.-Y. Lee, G.-W. Wu, and C.-L. Hsieh, *J. Power Sources*, **172**, 363 (2007).
13. S. Basu, M. W. Renfro, and B. M. Cetegen, *J. Power Sources*, **162**, 286 (2006).
14. W. P. Partridge, T. J. Toops, J. B. Green, and T. R. Armstrong, *J. Power Sources*, **160**, 454 (2006).
15. G. Hinds, M. Stevens, J. Wilkinson, M. de Posta, and S. Bell, *J. Power Sources*, **186**, 52 (2009).
16. K. Inman, X. Wang, and B. Sangeorzan, *J. Power Sources*, **195**, 4753 (2010).
17. N. A. David, P. M. Wild, J. Hu, and N. Djilali, *J. Power Sources*, **192**, 376 (2009).
18. Y.-J. Rao, *Meas. Sci. Technol.*, **8**, 355 (1997).
19. P. Kronenberg, P. K. Rastogi, P. Giaccari, and H. G. Limberger, *Opt. Lett.*, **27**, 1385 (2002).
20. T. L. Yeo, T. Sun, K. T. V. Grattan, D. Parry, R. Lade, and B. D. Powell, *Sens. Actuators B*, **110**, 148 (2005).
21. X. F. Huang, D. R. Sheng, K. F. Cen, and H. Zhou, *Sens. Actuators B*, **127**, 518 (2007).
22. S. Shimpalee, W.-k. Lee, J. Van Zee, and H. Naseri-Neshat, *J. Power Sources*, **156**, 355 (2006).
23. American Society for Testing and Materials, E104-02 (2007).
24. L. Greenspan, *J. Res. Natl. Bur. Stand., Sect. A*, **81A**, 1 (1977).
25. SHT7x Datasheet, Sensirion Inc., Zurich, Switzerland, http://www.sensirion.com, last accessed 2009.
26. P. Majsztrik, M. Satterfield, A. Bocarsly, and J. Benziger, *J. Membr. Sci.*, **301**, 93 (2007).
27. M. Wang, H. Guo, and C. Ma, *J. Power Sources*, **157**, 181 (2006).
28. P. T. Nguyen, T. Berning, and N. Djilali, *J. Power Sources*, **130**, 149 (2004).

Appendix D

Fiber Bragg Grating Sensor for Two-Phase Flow in Microchannels

Noname manuscript No.
(will be inserted by the editor)

Fiber-Bragg Grating Sensor for Two-Phase Flow in Microchannels

Nigel David · Ned Djilali · Peter Wild

Received: date / Accepted: date

Abstract A new non-intrusive measurement technique for two-phase flow in microchannels is presented. The development of an evanescent field based optical fibre Bragg grating sensor is described, and experiments coupled with flow visualization demonstrating the performance of this sensor are presented. Two adjacent 1 mm FBGs in etched D-shaped fibre are embedded into the surface of a PDMS microchannel. Experiments are conducted in both droplet and slug flow regimes and high speed digital video are captured synchronously with the sensor data. The FBGs exhibit an on-off type response to the passage droplets which is shown to correlate precisely with the passage of the liquid phase. This correlation enables the measurement of droplet average velocity and size using only the sensor data. In addition to the use of both FBG signals for the purpose of measuring droplet speed and size, it is shown that for droplets larger than the FBG length, a single FBG can be used to estimate the convection velocity and size of fast moving droplets. This sensing method is potentially useful for monitoring two-phase

---

N. David · N.Djilali · P. Wild
Department of Mechanical Engineering, University of Victoria, PO Box 3055, STN CSC, Victoria, BC, V8W 3P6, Canada
Tel.: +250-721-8940
Fax: +250-721-6323
E-mail: nadavid@uvic.ca

N. Djilali
E-mail: ndjilali@uvic.ca

flow in fuel cells and microfluidic applications such as micro-heat exchangers and lab-on-a-chip systems.

Keywords Multiphase flow · Liquid water · Fiber-optics · PEM Fue cell · Water management

1 Introduction

Two phase flows in microchannels occur in numerous applications. These include heat sinks that rely on the phase transition of boiling refrigerants to cool integrated circuits and electronic devices [1,2]; microfluidic devices used in microchemical microelectromechanical and lab-on-chip systems [3,4]; and fuel cells used to convert chemical energy into electricity[5]. In spite of the progress in general understanding of microchannel two-phase flow phenomena, the development of broadly applicable predictive models is still lagging. Two phase flow regimes in microchannels differ significantly [6–8] from those encountered in more classical systems, and there is a need for improved experimental techniques [9] to further fundamental understanding of flow dynamics, bubble and/or film sizes, pressure drop, wettability etc. in order to inform improved design and control of the flow and associated transport processes. In polymer electrolyte membrane (PEM) fuel cells, which are the primary motivation for the work presented here, liquid water management in the gas flow microchannels is a critical problem that leads to numerous performance and material degradation issues [10,11]. In microfluidic devices that are increasingly designed for an array of complex processes including mixing, assays and chemical reactions, more precise understanding of the dynamics of immiscible fluid phases is needed to achieve precise control [12].

Experimental methods currently available for characterizing the dynamics and mixing of two-phase flows in microchannels and micro-reactors are reviewed in [13]. These include visualization techniques tracking directly interfaces or in conjunction with fluorescent dyes or reactive species; micro particle image velocimetry; and non-intrusive sensors. Visualization techniques have also been extensively used to visualize liquid water in operating fuel cells [10] specifically designed to allow optical access; the techniques include NMR imaging, neutron imaging, synchrotron X-ray imaging, microtomography and optical photography. Visualization-based techniques have proven extremely valuable but typically require expensive equipment, and are limited to optically accessible systems. Investigation of multi-layered microfluidic devices is for example difficult, and optical access in commercial fuel cell stacks is not possible without compromising the design.

Micro-sensors are an obvious alternative to address the needs for monitoring and measurements. Non-intrusive sensors that rely on infrared absorption or refractive index detection have been developed for microfluidic devices and microreactors, however these still require optical access [12]. The only micro-sensor demonstrated to date for measurement of two-phase flow in fuel cells is reported by Conteau *et al.*[14]. The sensor was based on an impedance measurement between two electrodes on either side of a graphite micro-channel used to simulate experimentally two phase flows relevant to fuel cells. Correlation of the sensor data with high-speed digital images showed the capabilities of the sensor in detecting small and fast water droplets injected into the microchannel.

Electrode-based sensors, such as the one developed by Conteau *et al.*, will require special attention to electrical isolation, which, inside of an electrochemically active fuel cell, can prove difficult. For distributed measurements using these sensors, multiplexing will require several electrically isolated leads, which poses another significant instrumentation challenge.

Fiber optics is an approach to PEMFC diagnostics that is free from the constraints of electronic sensors. Important advantages of optical fiber sensors are that they are inherently small, electrochemically inert, and there is potential for multiplexing several sensors along a single optical fiber.

The fiber Bragg grating (FBG) sensor, for instance, can be multiplexed easily, and can be used to measure multiple parameters. As a result, there are growing number of applications for which FBGs are being used. FBG sensors were recently developed and used to measure temperature and humidity in operating PEM fuel cells[15,16]. Humidity sensitivity is achieved by adding a hygroscopic polymer coating to the cladding of fiber.

Temperature and humidity are important parameters inside a PEMFC, but the measurement of liquid water is paramount. It has been shown that by removing the glass cladding around an FBG, it becomes sensitive to the surrounding refractive index [17–19]. These types of sensors, known as evanescent field sensors are sensitive along the length of the FBG, which makes them ideal for multiplexed implementation into fuel cell plates. Such sensors have not yet, however, been demonstrated to measure the difference of refractive index between air and water inside of a PEMFC.

In this paper, a proof-of-concept study of an FBG-based evanescent field sensor for detecting water droplets in a microchannel is presented. Validation of the design was carried out by correlations between high-speed digital video footage and the sensor response under various two-phase flow conditions.

2 Sensing principle

An FBG typically consists of a short segment of single mode optical fiber with a photo-induced periodically modulated index of refraction in the core of the fiber. When the grating is illuminated with broadband light, the reflected spectrum has a peak at the Bragg wavelength given by

$$\lambda_B = 2\Lambda n_{eff}, \tag{1}$$

where n_{eff} is the effective index of refraction of the modified core and Λ is the grating pitch. Both n_{eff} and Λ are dependent on strain and temperature, which enables the FBG to be used for sensing parameters such as temperature, strain, pressure and humidity, for example.

When the cladding of the fiber is removed around the Bragg grating, n_{eff} becomes influenced by the refractive index of the surrounding medium. For constant temperature and strain conditions, small variations in the Bragg wavelength due to changes in the effective refractive can be simply expressed by

$$\Delta\lambda_B = 2\Delta n_{eff}(n_s)\Lambda \tag{2}$$

where n_{eff} is written as a function of n_s, the refractive index of the surrounding medium.

The refractive index sensitivity of etched cladding FBGs written in standard single mode fiber with a core of 8.3 μm was determined numerically and experimentally by Iadicicco *et al.* [17]. A non linear dependence of λ_B on n_s was reported with increased sensitivity as the surrounding refractive index approached that of glass. The study showed that for a sensor with cladding diameter of 8.5 μm, measurement resolutions of 10^{-5} and 10^{-4} were possible for the outer refractive index of 1.45 and 1.33, respectively, when using an FBG interrogator with 1pm resolution.

Iadicicco *et al.* cite the reason for higher sensitivity for higher refractive index surroundings is the penetration depth of the evanescent field. For lower external refractive indexes, like air (1.0) and water (1.33) the light is well confined within the core, leading to a weak dependence on n_s. However, for higher indexes approaching that of the fiber core (n=1.46), the fundamental mode is less confined to the core region, leading to increased interaction with the surrounding medium.

Etching standard single mode optical fiber to a diameter of ~8 μm makes it difficult to handle and to package into a sensor, particularly when embedding into a surface to detect liquid water. Alternative solutions to gain access to the evanescent field about an FBG without sacrificing its mechanical integrity were demonstrated by Schroeder *et al.* [18] and Meltz *et al.* [19]. Schroeder *et al.* used side polishing on a pre-embedded standard single mode fiber to construct a sensor that was sensitive to the refractive index change induced by the presence of hydrogen on the surface.

Meltz *et al.* used a specialty D-shaped fiber supplied by KVH Industries, Inc. with minimal etching to demonstrate a highly sensitive refractive index sensor. This was the approach taken for the development of the liquid water surface sensor described in this paper.

3 Materials and Methods

Based on the sensing principle described in the previous section, a liquid water sensor consisting of a D-shaped fiber embedded into the surface of a polymer was constructed. Two adjacent FBGs were used so that the size and speed of a droplet could be measured as it passes along the length of the fiber. See Fig.1. To test and evaluate performance, the sensor was embedded in a microfluidic platform allowing optical access and controlled generation of two phase flow (air-water). The sensor fabrication and testing methods are discussed in the following sections.

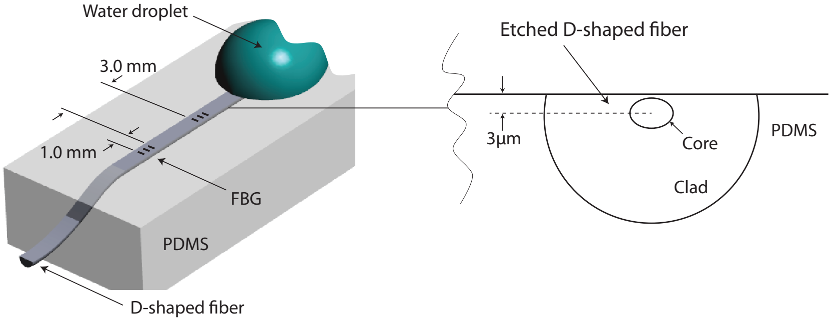

Fig. 1 Schematic of the liquid water sensor.

3.1 Sensor fabrication

Polydimethylsiloxane (PDMS) polymer was used as a substrate material for the sensor prototype because it has good adhesion to glass, and, like the graphite composite used for fuel cell plates, it is hydrophobic. In addition to these properties, PDMS is commonly used in prototyping microfluidic devices and, therefore, could be used for the transparent microchannel to test the sensor.

D-fiber has a roughly semi circular cross section with the light carrying core lying just beneath the flat surface. It requires only minimal etching to access the evanescent field near the core of the fiber, leaving a fiber that is substantially easier to work with during the fabrication steps following the etching. The D-fiber used for the sensors in this study was supplied by KVH industries, Inc.

Two adjacent FBGs were written into the D-fiber by Technica SA, Inc., China. They were specified to be one millimetre in length with centre wavelengths of 1547 and 1552 nm and spaced apart at the inside edges by 3 mm. See Fig. 1. Using a hot wire technique to locate the FBGs, the centre-to-centre grating spacing was verified to be 4 mm.

To detect the refractive index change above the flat side of the D-fiber, the fiber was etched with hydrofluoric acid (HF). Using a 48% HF solution at room temperature, the etch rate for the flat to the round dimension was determined to be 2.75 μm/min. A length of 1.5 cm of the D-fiber containing the two FBGs at the distal end of the fiber was immersed in the HF solution and etched for 8 minutes.

According to the D-fiber specifications provided be KVH, Inc. the core diameter is 5 μm, and the distance from the centre of the core to the flat side is nominally $\sim$14 μm. After etching the D-fiber in HF for 8 minutes this distance becomes 3 μm, leaving a cladding thickness of $\sim$0.5 μm above the core.

The spectra of the FBGs were measured prior to and after etching with a Smart Scan FBG interrogator (Smartfibers, Inc., Bracknell, UK). Wavelength resolution of the Smartscan is $\sim$1 pm. The full etching caused a blue shift of 800 pm of the Bragg wavelengths when exposed to the air, with no difference in peak amplitude. This effect has been observed before, and is attributed to residual strain relaxation in the core of the fiber [17]. Upon submerging the etched FBGs in water, the Bragg wavelengths of the two FBGs increased by $\sim$400 pm, indicating a clear response to the change in surrounding refractive index. See Fig.2

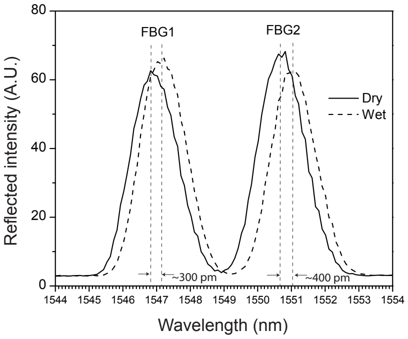

Fig. 2 Sensor response to liquid water.

Subsequent to etching the D-fiber, it was cast into PDMS using a mold made from Poly(methyl methacrylate) (PMMA). PMMA has a flat, shiny surface to which PDMS does not bond.

Using a fiber rotator, and a stereo microscope, the D-fiber was oriented in the mold such that the flat side of the fiber was parallel to the PMMA surface. A 1 cm length of the fiber containing the two FBGs was pressed against the PMMA surface with two small PDMS blocks that were weighted down. This was to ensure the FBGs would be exposed at the surface of the sensor once released from the mold.

The PDMS used for the sensor was the two part Sylgard 184 silicone elastomer kit from Dow Corning, Inc. A 5:1 by weight ratio of pre-polymer to curing agent was used to obtain a stiffer cured material. After thoroughly mixing the PDMS, it was degassed under vacuum for 20 minutes, and then poured into the mold over top of the FBGs to a depth of $\sim$7 mm. The PDMS was allowed to cure for 24 hrs.

With the FBGs located at its center, a rectangle approximately 30 mm x 60 mm was cut into the cured PDMS with a scalpel. The rectangular slab containing the FBGs was carefully released from the PMMA mold. Inspection under a microscope revealed a thin layer of PDMS on top of the fiber that inhibited the sensor response to liquid water. This thin layer was removed mechanically with a soft tool, and the sensitivity to surface droplets was established.

3.2 Sensor testing setup

A schematic of the setup for sensor testing is shown in Fig. 3. A microchannel made from PDMS was placed on top of the sensor allowing controlled generation of both droplet and slug two-phase flow. The cross sectional area of the microchannel as well as the range of air and water injection rates used in the tests are representative of fuel cell conditions. The sensors performance was validated by correlating high speed digital video of the two-phase flow with the sensor data, which was acquired synchronously.

The digital video was taken with a Vision Research, Inc. (Phantom, Miro 4) camera at a frame rate of 1000 frames per second. The FBG data was acquired at 2 kHz using the Smartscan interrogation unit.

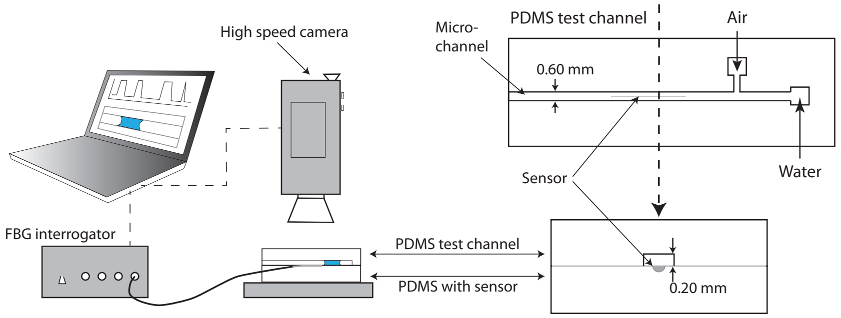

Fig. 3 Schematic of the sensor test setup.

The microchannels used for the tests were fabricated out of PDMS using standard soft photolithography techniques and incorporated air and water injection ports connected to syringe pumps controlled to create the desired flow regime. The dimensions of the microchannel are shown in Fig. 3. The air and water injection ports were fed with syringe pumps to create segmented flow within the channel.

With air and water injection rates set to 90 and 45 μlmin^{-1} respectively, short segments of water, or slugs, spaced apart by longer segments of air passed through the channel and over the embedded FBGs. A small amount of red dye was mixed into the water as a contrast to enable better visualization of the water.

To test the sensor response to fast moving droplets, a 1 mm wide PDMS channel was created with side walls and no cover. Individual droplets were deposited at the entrance to the channel. Forced air was blown through the widened entrance to the channel causing the small droplet to convect through the channel at a high speed. Care was taken to ensure the droplet remained intact without touching the side walls as it passed over the FBGs.

4 Results and discussion

Tests were carried out to validate the sensor in the slug and droplet flow regimes that are relevant to the fuel cell two-phase flows that motivated this work [20].

4.1 Slug flow regime

Shown in Fig. 4 are sample results from the slug flow regime tests. The slugs passed through the channel in the direction from FBG1 to FBG2. The sensor data plotted in Fig. 4(a) was taken over a 25 second time period during which 4 slugs passed across the sensor. It is clear that each FBG exhibits an on-off type response to the passing slugs with the response of FBG1 leading that of FBG2, which is consistent with the relative locations of the gratings. The Bragg wavelength shifts are consistent with the initial tests carried out after etching. See Fig.2.

The sensor response to the passage of a single slug is shown in Fig. 4(b). Selected video frames, at particular times of interest on the response plot are shown in Fig. 4(c) for comparison. Comparison of the video frames to the sensor data is important for validating the sensor performance. The locations of the FBGs have been highlighted since they are normally transparent.

At time t_1, both sensors are reading the low Bragg wavelength indicating a dry state. Looking at the first video frame this is indeed the case, as the slug has not yet reached FBG1. At time t_2, FBG1 is starting to respond with an increasing Bragg wavelength, indicating that it is entering into the wet state. The video frame corresponding to t_2 agrees with the data, showing the front of the slug just reaching the edge of FBG1. A short time later, at t_3, the FBG response becomes saturated, indicating that it is fully covered by water. This is confirmed in the corresponding video frame, which shows the slug covering FBG1. The same correlation for wetting is seen for FBG2 at t_5 and t_6.

The wet to dry transition for FBG2, between times t_8 and t_9 shows an immediate recovery as soon as the trailing edge of the slug reaches the edge of the FBGs. This is an indication that there is no film of water left on the fiber behind the slug, despite a difference in wetting characteristics between the PDMS and the glass.

After validating the FBGs responses to the passing slug using visualization, it was clear that the data could be used to reliably calculate the average velocity of the slug as it passes over the sensor. The spacing between FBG1 and FBG2 (4.0 mm) was divided by the time interval between the leading edges of the response curves of Fig. 4(b) , i.e. times t_2 for FBG1 and t_5 for FBG2. For this slug, the average velocity was 3.0 cm/s. The slug length can then be computed by multiplying the residence time on one FBG by the average velocity. The residence time, at FBG2 for example, is taken to be t_8-t_5 = 0.2 s. With this, the size of the passing slug is estimated to be 6.0 mm. Using the scale on the images, the slug measures closer to 5.0 mm. The longer residence time at FBG2 compared to FBG1, however, indicates the slug velocity is not constant as it passes over the sensor, highlighting the limitation of this post-processing technique. The use of a third grating could however overcome this limitation and yield more accurate velocity and size date for accelerating and decelerating slugs.

For a more instantaneous measure of the slug velocity, the response of a single FBG was also analyzed. The velocity of the front passing FBG1 can be measured by dividing the FBG length by the time taken to cover it (t_3-t_2=0.03s). Using an

FBG length of 0.8mm the velocity is 2.7 cm/s, and the size is estimated to be 4 mm. These values are in reasonable agreement with those calculated using the spacing between two FBGs, indicating that a single FBG can be used to estimate the speed and size of a slug passing through a microchannel. The can only be done, however, if the exact length of the FBG is known.

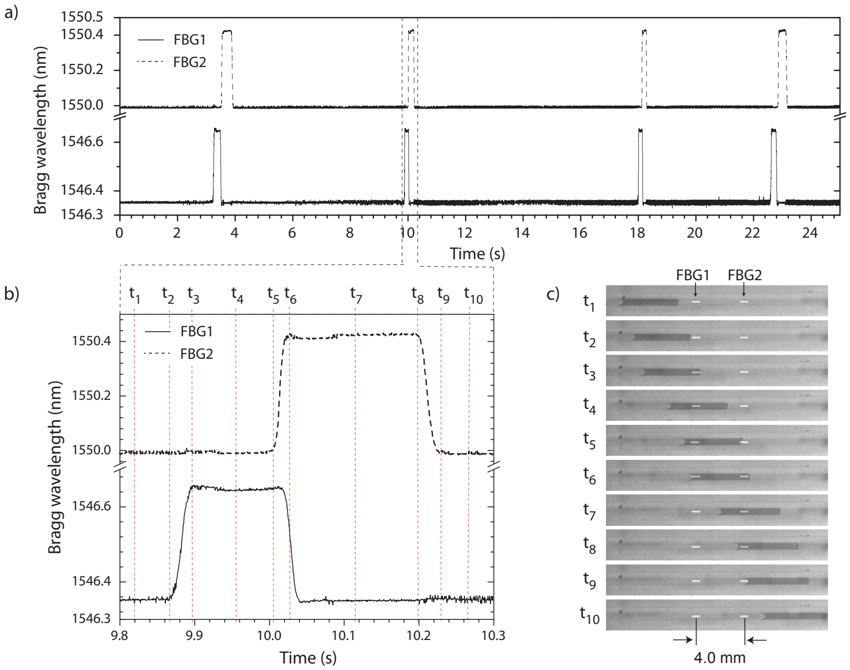

Fig. 4 Results from sensor validation test in the slug flow regime. (a) Response of sensor to passing slugs of water flowing through microchannel. (b) Bragg wavelength shifts of FBG1 and FBG2 as a result of a single slug. (c) Frames from high speed camera corresponding to the times shown in the sensor data from plot (b). Locations of FBGs have been highlighted in the images.

4.2 Droplet flow regime

Representative results from the passage of a single droplet over the sensor are shown in Fig. 5. As with the slug results, the response data for the droplet correlated well with the synchronized video images. The response curve of FBG1 has features that are not present in the response of FBG2. Upon closer analysis of the high speed video, these features in the data can be attributed to the droplet front's shape changing as it passes over FBG1. This is likely due to a combination of fluctuation from the forced air entering the open-top flow channel and imperfect homogeneity of the surface.

Using the FBG spacing, and the time interval between t_2 and t_7 the average velocity of the droplet shown in Fig. 5 is calculated to be 25 cm/s. It is clear, however, from the response curves that the droplet speeds up between FBG1 and FBG2. Using the response of only FBG2, the velocity is calculated to be 53.0 cm/s, more than double the average velocity. With this, the size of the droplet is estimated to be 2.3 mm. This is in good agreement with the video frame corresponding to t_{10}.

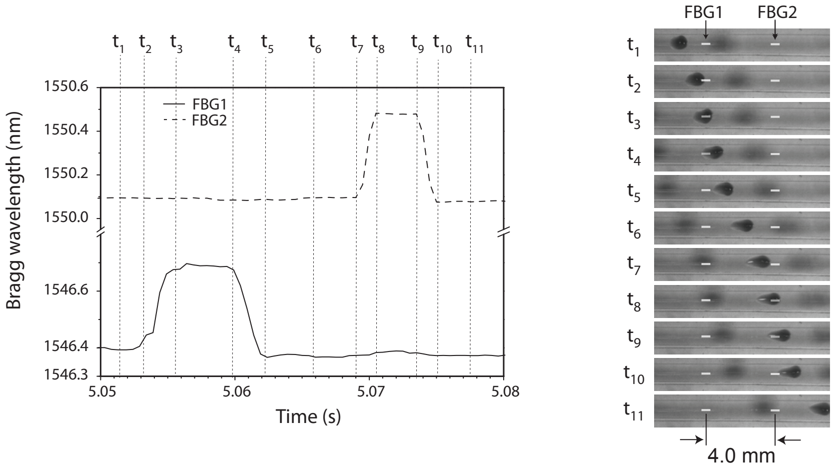

Fig. 5 (a) Sensor data from single fast droplet test. (b) Selected frames from the high speed video, corresponding to times shown in (a). Locations of FBGs have been highlighted in the images.

5 Conclusions

The concept of a surface embedded FBG sensor for the measurement of two-phase flow dynamics has been demonstrated and validated. It was shown that with minimal etching, FBGs written into a D-shaped fiber respond to the presence of liquid water due to a change in the surrounding refractive index. Such a strong response precludes the need for temperature compensation for a sensor design based on this principle.

A sensor consisting of a D-fiber with two adjacent FBGs embedded into the surface of a polymer was constructed. The polymer substrate with embedded sensor was used as a wall in a microchannel. High speed digital video of the droplet flow was captured synchronously with the sensor data acquisition. The FBGs exhibited an on-off type response to the passage droplets, which correlated precisely with liquid water flowing over the FBG locations. This correlation enabled the measurement of droplet average velocity and size using only the sensor data. In addition to the use of both FBG signals for the purpose of measuring droplet speed and size, it was shown that for droplets larger than the FBG length, a single FBG can be used to estimate the speed and size of a fast moving droplet.

The study presented here suggest that an evanescent field FBG sensor based on this concept could be adapted for use in the flow-channel of a PEMFC to investigate droplet and flooding phenomena. This sensing concept is not, however, limited to fuel cells. It could be applied, for example, to microfluidic devices or to the detection of condensation.

6 Acknowledgments

This research was funded through a Strategic Research grant from the Natural Sciences and Engineering Research Council (NSERC) of Canada. The D-fiber used for the sensors in this study was kindly provided by KVH industries Inc.

References

1. G. Hetsroni, A. Mosyak, Z.e.a. Segal, International Journal of Heat and Mass Transfer **45**, 3275 (2002)
2. L. Zhang, J.M. Koo, L.e.a. Jiang, Journal of Microelectromechanical Systems **11**, 12 (2002)

3. A. Gunther, S. Khan, M. Thalman, F. Trachsel, K. Jensen, Lab Chip **4**, 278 (2004)
4. D. Funfschilling, Y. Ma, H.Z. Li, Microfluidics and Nanofluidics **8**, 467 (2010)
5. X. Zhu, P.C. Sui, N. Djilali, Microfluidics and Nanofluidics **4**, 1613 (2008)
6. A.E. Bergles, S.G. Kandlikar, Journal of Heat Transfer **127**, 101 (2005)
7. W.S. von Rohr Philipp Rudolf, International Journal of Multiphase Flow **32**, 791 (2006)
8. P.S. Zhu, X., N. Djilali, Journal of Power Sources **181**, 101 (2008)
9. G.R. B. Tibiri, F. J. do Nascimento, Experimental Thermal and Fluid Science **34**, 463 (2010)
10. A. Bazylak, International Journal of Hydrogen Energy **34**, 3845 (2009)
11. H. Li, Y. Tang, Z. Wang, Z. Shi, S. Wu, D. Song, J. Zhang, K. Faith, J. Zhang, H. Wang, Z. Liu, R. Abouatallah, A. Mazza, Journal of Power Sources **178**, 103 (2008)
12. M.B. F. Schembri, Microfluid Nanofluid **11**, 189 (2011)
13. R.G. C. King, E. Walsh, Microfluid Nanofluid **3**, 463 (2007)
14. D. Conteau, C. Bonnet, D. Funfschilling, M. Weber, S. Didierjean, F. Lapicque, Fuel Cells **4**, 520 (2010)
15. N.A. David, P.M. Wild, J. Hu, N. Djilali, Journal of Power Sources **192**, 376 (2009). DOI 10.1016/j.jpowsour.2009.03.021
16. N.A. David, P.M. Wild, J. Jensen, T. Navessin, N. Djilali, Journal of The Electrochemical Society **157**(8), B1173 (2010). DOI 10.1149/1.3436652
17. A. Iadicicco, A. Cusano, A. Cutolo, R. Bernini, M. Giordano, IEEE Photo **16**, 1149 (2004)
18. K. Schroeder, W. Ecke, R. Willsch, Optics and Lasers in Engineering **47**, 1018 (2009)
19. G. Meltz, S.J. Hewlett, J.D. Love, in *Proceedings of SPIE Vol. 2836 Chemical, Biochemical, and Environmental Fiber Sensors VIII, pp. 342-350* (1996)
20. T.C. Wu, N. Djilali, Submittted to the Journal of Power Sources